ORTA DOĞU TEKNİK ÜNİVERSİTESİ
FEN BİLİMLERİ ENSTİTÜSÜ MÜDÜRLÜĞÜ

TEZ ŞABLONU ONAY FORMU
THESIS TEMPLATE CONFIRMATION FORM

1. Şablonda verilen yerleşim ve boşluklar değiştirilmemelidir.
2. **Jüri tarihi** Başlık Sayfası, İmza Sayfası, Abstract ve Öz'de ilgili yerlere yazılmalıdır.
3. İmza sayfasında jüri üyelerinin unvanları doğru olarak yazılmalıdır. Tüm imzalar **mavi pilot kalemle** atılmalıdır.
4. **Disiplinlerarası** programlarda görevlendirilen öğretim üyeleri için jüri üyeleri kısmında tam zamanlı olarak çalıştıkları anabilim dalı başkanlığının ismi yazılmalıdır. Örneğin: bir öğretim üyesi Biyoteknoloji programında görev yapıyor ve biyoloji bölümünde tam zamanlı çalışıyorsa, İmza sayfasına biyoloji bölümü yazılmalıdır. İstisnai olarak, disiplinler arası program başkanı ve tez danışmanı için disiplinlerarası program adı yazılmalıdır.
5. Tezin **son sayfasının sayfa** numarası Abstract ve Öz'de ilgili yerlere yazılmalıdır.
6. Bütün chapterlar, referanslar, ekler ve CV sağ sayfada başlamalıdır. Bunun için **kesmeler** kullanılmıştır. **Kesmelerin kayması** fazladan boş sayfaların oluşmasına sebep olabilir. Bu gibi durumlarda paragraf (¶) işaretine tıklayarak kesmeleri görünür hale getirin ve yerlerini **kontrol edin**.
7. Figürler ve tablolar kenar boşluklarına taşmamalıdır.
8. Şablonda yorum olarak eklenen uyarılar dikkatle okunmalı ve uygulanmalıdır.
9. Tez yazdırılmadan önce PDF olarak kaydedilmelidir. Şablonda yorum olarak eklenen uyarılar PDF dokümanında yer almamalıdır.
10. Tez taslaklarının kontrol işlemleri tamamlandığında, bu durum öğrencilere METU uzantılı öğrenci e-posta adresleri aracılığıyla duyurulacaktır.
11. Tez yazım süreci ile ilgili herhangi bir sıkıntı yaşarsanız, Sıkça Sorulan Sorular (SSS) sayfamızı ziyaret ederek yaşadığınız sıkıntıyla ilgili bir çözüm bulabilirsiniz.

1. Do not change the spacing and placement in the template.
2. Write **defense date** to the related places given on Title page, Approval page, Abstract and Öz.
3. Write the titles of the examining committee members correctly on Approval Page. **Blue ink** must be used for all signatures.
4. For faculty members working in **interdisciplinary programs**, the name of the department that they work full-time should be written on the Approval page. For example, if a faculty member staffs in the biotechnology program and works full-time in the biology department, the department of biology should be written on the approval page. Exceptionally, for the interdisciplinary program chair and your thesis supervisor, the interdisciplinary program name should be written.
5. Write **the page number of the last page** in the related places given on Abstract and Öz pages.
6. All chapters, references, appendices and CV must be started on the right page. **Section Breaks** were used for this. **Change in the placement** of section breaks can result in extra blank pages. In such cases, make the section breaks visible by clicking paragraph (¶) mark and **check their position.**
7. All figures and tables must be given inside the page. Nothing must appear in the margins.
8. All the warnings given on the comments section through the thesis template must be read and applied.
9. Save your thesis as pdf and Disable all the comments before taking the printout.
10. This will be announced to the students via their METU students e-mail addresses when the control of the thesis drafts has been completed.
11. If you have any problems with the thesis writing process, you may visit our Frequently Asked Questions (FAQ) page and find a solution to your problem.

☒ **Yukarıda bulunan tüm maddeleri okudum, anladım ve kabul ediyorum. / I have read, understand and accept all of the items above.**

Name :
Surname :
E-Mail :
Date :
Signature : _____

pH and TEMPERATURE RESPONSIVE MULTIPLE DRUG RELEASE from LAYER-by-LAYER MODIFIED MICROPARTICLES

A THESIS SUBMITTED TO
THE GRADUATE SCHOOL OF NATURAL AND APPLIED SCIENCES
OF
MIDDLE EAST TECHNICAL UNIVERSITY

BY

ESMA UĞUR

IN PARTIAL FULFILLMENT OF THE REQUIREMENTS
FOR
THE DEGREE OF MASTER OF SCIENCE
IN
CHEMISTRY

AUGUST 2022

Approval of the thesis:

pH and TEMPERATURE RESPONSIVE MULTIPLE DRUG RELEASE from LAYER-by-LAYER MODIFIED MICROPARTICLES

submitted by **ESMA UĞUR** in partial fulfillment of the requirements for the degree of **Master of Science** i**n Chemistry, Middle East Technical University** by,

Prof. Dr. Halil Kalıpçılar
Dean, Graduate School of **Natural and Applied Sciences** _____

Prof. Dr. Özdemir Doğan
Head of the Department, **Chemistry** _____

Prof. Dr. İrem Erel Göktepe
Supervisor, **Chemistry, METU** _____

Examining Committee Members:

Prof. Dr. Ayşen Yılmaz
Chemistry, METU _____

Prof. Dr. İrem Erel Göktepe
Chemistry, METU _____

Prof. Dr. Sreeparna Banerjee
Biology, METU _____

Assoc. Prof. Dr. Zeynep Çulfaz
Chemical Engineering, METU _____

Asst.Prof. Dr. Cemal Merih Şengönül
Manufacturing Engineering, Atılım University _____

Date: 10.08.2022

I hereby declare that all information in this document has been obtained and presented in accordance with academic rules and ethical conduct. I also declare that, as required by these rules and conduct, I have fully cited and referenced all material and results that are not original to this work.

Esma Uğur :

Signature :

ABSTRACT

pH and TEMPERATURE RESPONSIVE MULTIPLE DRUG RELEASE from LAYER-by-LAYER MODIFIED MICROPARTICLES

Uğur, Esma
Master of Science, Chemistry
Supervisor : Prof. Dr. İrem Erel Göktepe

August 2022, 105 pages

This thesis study reports on preparation of layer-by-layer (LbL)-modified microparticles based on temperature responsive poly(2-isopropyl-2-oxazoline) (PIPOX) and pH-responsive Tannic Acid (TA), displaying dual responsive multiple drug release. PIPOX, exhibiting lower critical solution temperature (LCST)-type phase behavior, was synthesized through cationic ring opening polymerization (CROP). PIPOX was then partially hydrolyzed in concentrated acid medium, resulting in poly(2-isopropyl-2-oxazoline-r-polyethylene imine) (PIPOX-PEI). Multilayer films of PIPOX-PEI and TA were produced using LbL self-assembly method through hydrogen bonding interactions between carbonyl groups of PIPOX and phenolic hydroxyl groups of TA together with electrostatic interactions between secondary amine groups of PEI and phenolate groups of TA. Covalent crosslinks were introduced between the layers upon treatment with $NaIO_4$ solution. Stability of noncross-linked and cross-linked multilayers were contrasted with respect to stability at physiologically related pH and temperature conditions. Stability and water uptake of non-crosslinked PIPOX-PEI and TA multilayers were found to depend on pH and temperature. The highest water uptake was recorded at pH 7.4 and 37°C when hydrogen bonding interactions between PIPOX-PEI and TA was partially disrupted due to ionization of TA and conformational transition of PIPOX occured above its critical temperature. On the contrary, crosslinked PIPOX-PEI and TA multilayers did not show water uptake under similar conditions. On the other

hand, stability of cross-linked multilayers was remarkably higher at basic conditions compared to noncross-linked films. The fundamental information generated on LbL films constructed on 2D substrates has formed a basis to construct multilayers on 3D colloidal microparticles. Two different $CaCO_3$ microparticles were used, i.e. bare and Curcumin (CUR) loaded. Bare $CaCO_3$ microparticles were LbL-modified using TA and PIPOX-PEI, cross-linked using $NaIO_4$ and made hollow by dissolving the $CaCO_3$ core using EDTA solution. The hollow interior and the capsule wall were used for CUR and Doxorubicin (DOX) loading. CUR-loaded microparticles were LbL-modified using TA and PIPOX-PEI and post-loaded with DOX. Two different microparticles were contrasted with respect to drug loading and release properties. In addition, the effects of pH and temperature on release of CUR and DOX from both types of microparticles were examined. Finally, preliminary results on synergistic effect of CUR and DOX and potential of these LbL particles for anticancer applications were demonstrated.

Keywords: Poly(2-isopropyl-2-oxazoline), Tannic Acid, Temperature Responsive, pH Responsive, Multiple Drug Release

ÖZ

KATMAN-KATMAN YÜZEYİ DEĞİŞTİRİLMİŞ MİKROPARÇACIKLARDAN pH ve SICAKLIK DUYARLI ÇOKLU İLAÇ SALIMI

Uğur, Esma
Yüksek Lisans, Kimya
Tez Yöneticisi: Prof. Dr. İrem Erel Göktepe

Ağustos 2022, 105 sayfa

Bu tez çalışması, sıcaklığa duyarlı poli(2-izopropil-2-oksazolin) (PIPOX) ve pH'a duyarlı Tannik Asit (TA)'den oluşan çift duyarlı ve birden fazla ilaç salabilen katman-katman (LbL) modifiye edilmiş mikropartiküllerin hazırlanmasını konu almaktadır. Alt kritik çözelti sıcaklığı (LCST) tipi faz davranışı sergileyen PIPOX, katyonik halka açılma polimerizasyonu (CROP) yoluyla sentezlendi. PIPOX daha sonra konsantre asit ortamında kısmen hidrolize edildi ve poli (2-izopropil-2-oksazolin-r-polietilen imin) (PIPOX-PEI) elde edildi. PIPOX-PEI ve TA'dan oluşmuş çok katmanlı filmler, PIPOX'un karbonil grupları ile TA'nın fenolik hidroksil grupları arasındaki hidrojen bağı etkileşimleri ve PEI'nin ikincil amin grupları ve TA'nın fenolat grupları arasındaki elektrostatik etkileşimler sayesinde LbL kendiliğinden yapılanma yöntemiyle üretildi. $NaIO_4$ çözeltisi ile muamele sonrasında katmanlar arasına kovalent çapraz bağlar eklendi. Çapraz bağlı olmayan ve çapraz bağlı çok-katmanlı filmlerin kararlılıkları, fizyolojik pH ve sıcaklık ile ilişkili koşullarda karşılaştırıldı. Çapraz bağlanmamış PIPOX-PEI ve TA çok-katmanlı filmlerinin kararlılık ve su alım özelliklerinin pH ve sıcaklığa bağlı olduğu bulundu. En yüksek su alımı TA'nın iyonlaşması nedeniyle PIPOX-PEI ve TA arasındaki hidrojen bağı etkileşimlerinin kısmen bozulduğu ve PIPOX'un kritik sıcaklık değerinin üzerinde konformasyonal değişime uğradığı pH 7.4

ve 37°C koşulunda gözlendi. Aksine, çapraz bağlı PIPOX-PEI ve TA çoklu katmanlar, benzer koşullar altında su alımı göstermedi. Bunun yanısıra, bazik koşullarda çapraz bağlı çok-katmanlı filmlerin kararlılıkları çapraz bağlı olmayan filmlere kıyasla oldukça yüksek bulundu. 2D substratlar üzerinde büyütülen LbL filmler hakkında üretilen bilgi, 3D kolloidal mikropartiküller üzerinde TA/PIPOX-PEI katmanlarının biriktirilmesi için temel oluşturdu. Yalın ve Kurkumin (CUR) yüklü olmak üzere iki farklı $CaCO_3$ mikropartikülleri sentezlendi. Yalın $CaCO_3$ mikropartikülleri, TA ve PIPOX-PEI kullanılarak LbL-modifiye edildi, $NaIO_4$ kullanılarak çapraz bağlandı ve EDTA çözeltisi kullanılarak $CaCO_3$ çözülerek içi boş hale getirildi. İçi boş kapsüllerin iç kısmı ve kapsül duvarı, CUR ve Doksorubisin (DOX) yüklemesi için kullanıldı. Buna karşın, CUR yüklü mikropartiküller, TA ve PIPOX-PEI kullanılarak LbL-modifiye edildi ve sonrasında DOX ile yüklendi. Her iki tip LbL-modifiye mikropartiküllerin ilaç yükleme ve salım özellikleri karşılaştırıldı. Ayrıca, CUR ve DOX salımı üzerine pH ve sıcaklığın etkileri incelendi. Son olarak, CUR ve DOX'un sinerjistik etkisi ve bu tür LbL partiküllerinin antikanser uygulamaları için potansiyeline dair ön sonuçlar sunuldu.

Anahtar Kelimeler: Poli(2-izopropil-2-oksazolin), Tanik Asit, Sıcaklık Duyarlı, pH Duyarlı, Çoklu ilaç salımı

To live in paradise which is in our dream…

ACKNOWLEDGMENTS

I would like to express my deep and sincere gratitude to my research supervisor, Prof.Dr. İrem Erel Göktepe for giving me the opportunity to do research and providing invaluable guidance throughout this research. Her dynamism, vision, sincerity, and motivation have deeply inspired me. It was a great privilege and honor to work and study under her guidance.

I am extremely grateful to my parents for their love, prayers, caring and sacrifices for educating me and preparing me for my future.

I would like to say thanks to my friends and research colleagues Dilara Gündoğdu, Çağrı Turan, Gökçe Tidim, Umut Aydemir, Cemre Alemdar for their constant encouragement.

This thesis study has been financially supported by METU Scientific Research Projects (GAP-103-2020-10125). I would also like to acknowledge the scholarship provided by METU Scientific Research Projects (GAP-103-2020-10125).

I would like thanks to Prof. Dr. Sreeparna Banerjee and her students for valuable advises about biological experiments and giving us opportunity to use their research facilities.

Finally, my thanks go to all the people who have supported me to complete the research work directly or indirectly.

TABLE OF CONTENTS

LIST OF TABLES

TABLES

LIST OF FIGURES

FIGURES

LIST OF ABBREVIATIONS

ABBREVIATIONS

PAOX	Poly (2-alkyl-2-oxazoline)
TA	Tannic Acid
PEOX	Poly(2-ethyl-2-oxazoline)
PMEOX	Poly(2-methyl-2-oxazoline)
PIPOX	Poly(2-isopropyl-2-oxazoline)
PnPrOX	Poly(2-n-propyl-2-oxazoline)
PSS	Poly(sodium 4-styrene sulfonate)
$CaCO_3$	Calcium carbonate
UCST	Upper Critical Solution Temperature
LCST	Lower Critical Solution Temperature
PNIPAM	Poly (N-isopropylacrylamide)
PEG	Poly(ethylene oxide)
LbL	Layer-by-Layer
PEI	Poly(ethylene imine)

CHAPTER 1

INTRODUCTION

1.1 Poly (2-alkyl-2-oxazoline)s

Poly(2-alkyl-2-oxazoline) s (PAOXs) are a class of synthetic polyamides. PAOXs were first synthesized by four different research groups in 1966 through cationic ring opening polymerization (CROP) of 2-oxazolines [1]. The resulting polymer has a tertiary amide structure with the nitrogen atom being on the backbone and the carbonyl unit on the side chain. Figure 1.1 represents the chemical structure of PAOXs.

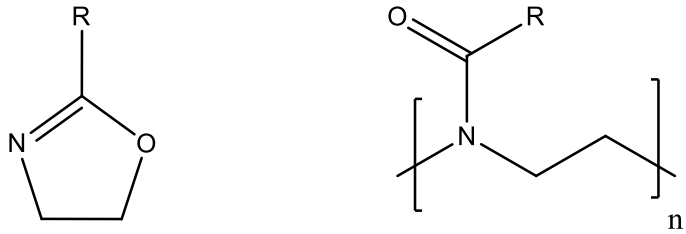

A B

R= alkyl, aryl

Figure 1.1. Chemical structure of A) 2-Oxazoline B) poly (2-alkyl/aryl-oxazoline).

Chemical structures of PAOXs resemble to those of polypeptides. Because of this structural similarity, PAOXs are called “pseudopeptides”, and they are considered as bioinspired polymers[2]. Importantly, different from polypeptides, PAOXs have tertiary amide groups. Tertiary amides cannot be hydrolyzed or recognized by enzymes. Therefore, PAOXs are more stable than polypeptides in biological environment[2].Additionally, polymer backbone cannot be hydrolyzed because tertiary amides are in the side chain rather than on the backbone [2].

The properties of PAOXs can be tuned by changing the side chain groups. For example, side groups such as methyl, ethyl, and propyl provide hydrophilic and/or thermoresponsive behavior to PAOXs. Side groups composed of aryl and large aliphatic groups lead to formation of hydrophobic polymers[2]. Furthermore, by sequential adding methods, block copolymers can be synthesized, and amphiphilic PAOXs can be obtained[2]. Figure 1.2 represents examples of PAOXs of varying chemical structures.

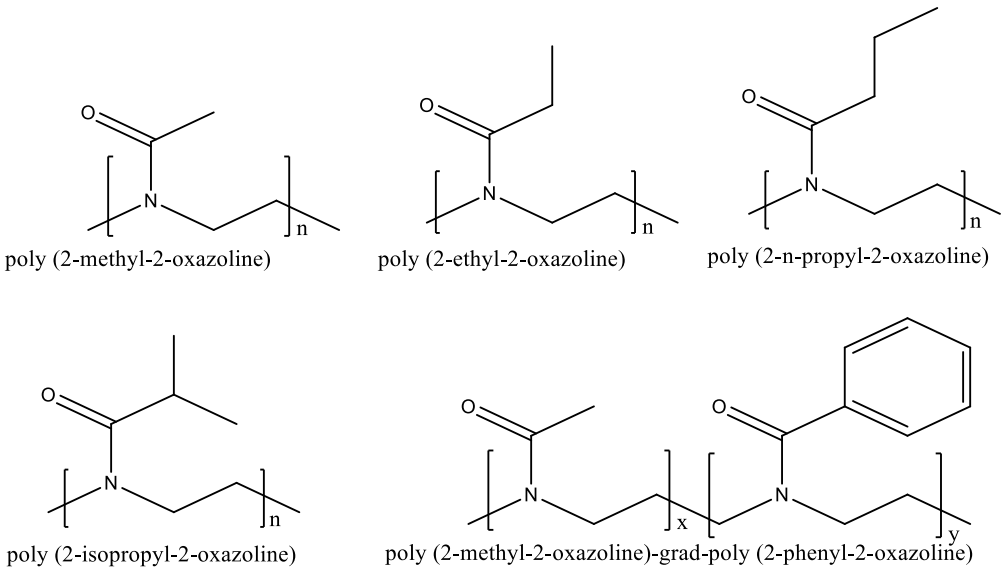

Figure 1.2. Examples of chemical structure of poly (2-alkyl/aryl-2-oxazoline)s.

1.1.1 Cationic Ring Opening Polymerization of PAOXs

The cationic ring opening polymerization (CROP) is a typical chain growth polymerization. It involves initiation, propagation, and termination steps[3]. 2-oxazolines polymerize through living cationic ring opening polymerization. This means that undesired reactions such as termination or chain transfer reactions do not occur during polymerization under appropriate conditions [3,4].

In general, the polymerization reactions are entropically disfavored. The driving force for CROP of 2-oxazolines is the isomerization of the cyclic imino ether into a

more stable tertiary amide. This results in a spontaneous polymerization after the initiation step often at elevated temperatures. The enthalpic contribution to the polymerization from the release of the ring strain has also been mentioned in the literature. However, such a minor contribution was suggested to be negligible [3,5,6]

Initiation, propagation, and termination steps of 2-alkyl-oxazoline polymerization consist of electrophilic addition, nucleophilic substitution, and nucleophilic addition reactions, respectively. The general overview for the mechanism of polymerization is shown in Figure 1.3[3].

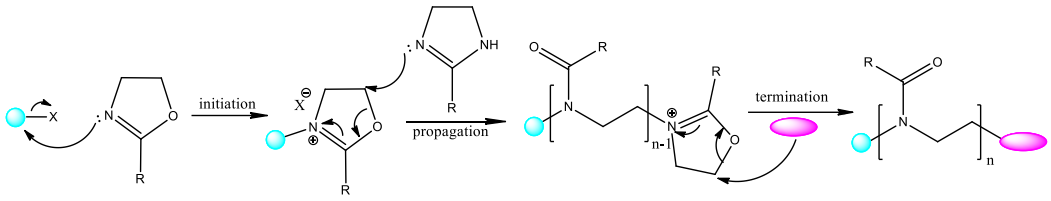

Figure 1.3. General overview for the mechanism of 2-oxazoline polymerization. (Modified from ref [3]).

In the initiation step, oxazolinium ion is formed by nucleophilic attacking of the cyclic imino ether to the electrophilic initiator[3]. Inorganic or organic species can be used as initiator. Examples of initiators are Lewis acids[7,8], acid halides[9], silyl halides[10], alkylating agents[11,3]. In the recent years, mostly tosylates, alkylhalides, and nosylates are used as initiators[1]. In the propagation step, nucleophilic attack of 2-oxazolines to oxazolinium ions provide formation of PAOX chain with oxazolinium end-group[1]. If the initiation step is fast and quantitative, there should be no chain transfer reaction. In this way, control in molecular weight and homogeneous molar mass distribution can be obtained[1]. In the termination step, two different terminating agents are used. These are categorized as softer and harder terminating agents. When a softer terminating agent, e.g., water is used, kinetically controlled nucleophilic attack occurs at 2-position of oxazolinium chain end and secondary amine or ester containing end groups are formed[3]. When a harder terminating agent such as nitrogen based terminating agent[12,13], carboxylates[14], or methanolic potassium hydroxide[15] is

used, thermodynamically controlled termination occurs at 5-position of oxazolinium species showed in Figure 1.4[3].

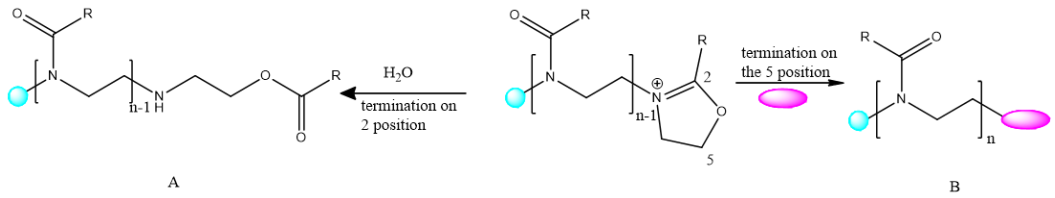

Figure 1.4. A) Kinetically driven termination B) Thermodynamically driven termination. (Modified from ref [3].)

Purity of the polymerization medium is important to synthesize polymers with low dispersity in CROP. An impurity with a nucleophilic character can interfere the polymerization and may terminate the polymerization at an undesired stage. Therefore, monomers and solvents should be pure and dry for an optimal polymerization reaction[3,7,8].

1.1.2 Temperature Responsive Behavior of Poly(2-alkyl-2-oxazoline)s in aqueous medium

When temperature-responsive polymers are dissolved in suitable solvents, they show phase separation at certain temperatures[16]. In other words, above or below a certain temperature, polymers change from being hydrophilic to hydrophobic[16]. If the polymer becomes hydrophobic above a certain temperature, this temperature is called as lower critical solution temperature (LCST). If the polymer becomes hydrophobic below a certain temperature, this temperature is called as upper critical solution temperature (UCST)[16]. In case of polymers exhibiting LCST-type phase behavior, polymers form hydrogen bonding with water molecules and adopt extended conformation below LCST. In other words, polymer-solvent interaction is dominant. Hydrogen bonding between the polymer and solvent weakens as the

temperature is increased and polymer-polymer interaction becomes dominant, resulting in formation of polymer aggregates above the critical temperature[16]. UCST-type phase transition is an enthalpically driven process, inter-/intra-chain interaction in polymer chains below the UCST is dominant. These interactions are weakened by heating of the solution and polymer becomes soluble above UCST[17].

Temperature-responsive behavior of poly(2-ethyl-2-oxazoline) (PEtOX) in aqueous solution was reported by Kwei et al. in 1988[18]. They demonstrated that thermo-responsive property depended on the concentration of the polymer solution and molecular weight of the polymer[2,18]. For example, LCST values of PEOX with molecular weights of 20,000, 50,000 and 500,000 kDa were determined to be 63.5 ^{o}C, 63 ^{o}C, and 61^{o}C, respectively. They also showed that addition of NaCl into polymer solutions decreased LCST. For example, adding NaCl into PEtOx solution at a concentration of 0.3 M and 0.5 M decreased LCST by 1-2 ^{o}C and 3-5 ^{o}C, respectively. On the contrary, LCST was found to increase by 5-10 ^{o}C when tetrabutylammonium bromide was added into PEtOx solution[2,18].

In 1992, Kobayashi et al. reported the thermo-responsive behavior of poly(2-isopropyl-2-oxazoline) (PIPOX) which has critical temperature between 36 ^{o}C – 39 ^{o}C [19]. LCST-type phase behavior of poly(2-n-propyl-2-oxazoline) (PnPrOx) was explored by Park et al. in 2007 and PnPrOx was found to have a critical temperature at 24 ^{o}C[20].

PIPOX and PnPrOX have especially drawn attention for biological applications because their LCST values are close to body temperature. For this reason, they have been considered as alternatives to poly(N-isopropylacrylamide) (PNIPAM), a widely used temperature-responsive polymer (LCST ~ 32 ^{o}C) for biological applications[2].

1.1.3 Comparison of Physical Properties of PIPOX and PNIPAM

PNIPAM, first synthesized in 1950s[21], is a temperature-responsive polymer, exhibiting LCST-type phase behavior at ~ 32 ^{o}C [22]. PNIPAM has widely been

explored for biomedical applications due its critical temperature which is close to body temperature. PIPOx is structural isomer of PNIPAM and exhibits LCST-type behavior with a critical temperature at ~ 36 ^{o}C[22]. PIPOX is also called as "thermoresponsive pseudopeptide" due to its temperature responsive behavior and structural similarity to polypeptides. Figure 1.5 presents the chemical structures of PIPOX and PNIPAM.

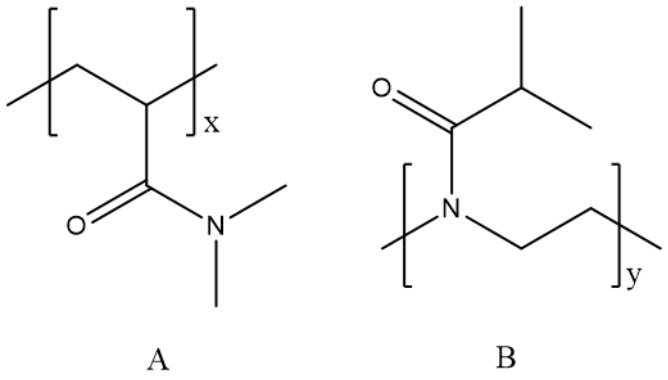

Figure 1.5. Chemical structure of A) PNIPAM B) PIPOX.

Despite the similarities in chemical structure and temperature-responsive behavior, they differ in the mechanism of phase transition, the presence of a hysteresis in the heating/cooling cycle and solubility property. Aqueous solution behavior of PIPOX has been reported in the literature[22]. Mechanism of LCST-type phase behavior of PIPOX can be summarized in the following way: PIPOX chains are in hydrated state in aqueous solution below LCST. The hydrogen bonding between PIPOX and water molecules weakens as the temperature was raised to 36 ^{o}C and this induces the liquid-liquid phase separation. Water molecules are expelled out of -C=O units of PIPOX when the temperature was further increased to 37 ^{o}C. This is accepted as the onset of conformational change of PIPOX towards an ordered and dehydrated state and formation of polymer aggregates. The phase transition process during heating and cooling were found to display good reversibility[23].

The mechanism of LCST-type phase behavior of PNIPAM is different than PIPOX. In case of PNIPAM, stable and compact globules are formed as the temperature was

raised above LCST. In other words, coil-to globule transition occurs rather than liquid- liquid phase separation as in the case of PIPOX. This difference was correlated with the strong intermolecular intra- and interchain hydrogen bonding between -C=O and -NH of amide groups [22,24]. In summary, PIPOX does not display hysteresis during phase transition. In contrast, PNIPAM shows a broad hysteresis at cooling step because of irreversible globular to coil transition[22,23].

Another difference between PNIPAM and PIPOX is the solubility properties. PNIPAM is soluble in water and methanol but not in the mixture of methanol/water (the phenomenon which is known as cononsolvency)[22]. On the other hand, PIPOX is soluble in water/methanol mixture and the amount of methanol in the mixture was found to be critical on the critical temperature. It has been reported that the critical temperature remained constant up to certain amount of methanol (20% v/v). However, further increasing methanol amount in the mixture increased the critical temperature of PIPOX[22].

1.1.4 Biological Properties of Poly(2-alkyl-2-oxazoline)s

Low protein adsorption and cell or bacteria adhesion, bioavailability, stealth behavior, low accumulation in tissue make PAOX a promising polymer class for biomedical applications. Taking advantage of these important biological properties of PAOX, polymer-protein conjugates, polymer drug, polymer peptide conjugates, polymeric micelles, aggregates, nanoparticles, hydrogels have been prepared and used as drug or gene carriers[4].

Protein adsorption, cell, or bacterial adhesion onto PMeOX, PEtOX, and poly(2-n-propyl-2-oxazoline) (PnPrOX) were studied by several groups. Protein adsorption and cell or bacterial adhesion onto hydrophilic PAOX's such as PEtOX, PMeOX were found to be relatively low compared to more hydrophobic PAOX such as PnPrOx[4,25–30]. PMeOx and PEtOx were considered as alternatives to PEG because of their nontoxicity, antifouling properties, and stealth effect. Of note, PEG is the

most used antifouling polymer in biomedical applications. PMeOx and PEtOx are also advantageous with respect to ease in synthesis, stability and lower viscosity compared to PEG[22]. A study by Textor and co-workers compared antifouling behavior of PMeOX and PEG. PMeOX coating was found to be more stable than PEG coating. Correspondingly, antifouling property of PMeOX was more stable over time while PEG coating degraded[4,31]. Another study reported on protein repellent properties of a triblock copolymer composed of PMeOX and PEO blocks, namely poly(2-methyl-2-oxazoline)-*b*-poly(ethyleneoxide)-*b*-poly(2-methyl-2-oxazoline) (PMeOX-*b*-PEO-*b*-PMeOX). However, the source of protein repellent property was ambiguous since both PMeOX and PEO exhibit antifouling behavior [32,33].

The biocompatibility of materials which interact with biological substances such as proteins, cell membranes through hydrophobic, electrostatic, or hydrogen bonding, is important in biological applications[4]. In general, taking cytotoxicity experiments performed with linear, hydrophilic, hydrophobic, amphiphilic and star-like PAOXs[34–36] and PAOX-based particles[37] in the literature as a basis, PAOXs are considered as biocompatible materials. Cytotoxicity of PAOXs were found to be low against human neural progenitor cells, Madin–Darby canine kidney cells, MCF7, HEP G2, and CATH cell lines[4].

The biocompatibility of poly(2-methyl-2-oxazoline) (PMeOX) was studied by Goddard et al. [33,38]. It was reported that ^{125}I-labeled PMeOXs excreted from mice without significant accumulation in organs. Nevertheless, some polymer was found in the skin and muscle tissue and attributed to high molecular weight polymers [33,38]. Jordan and co-workers also examined accumulation of PEtOX and PMeOX in tissue and rate of clearence from blood stream using radiolabeled polymers[33,39]. They concluded that PEtOX and PMeOX did not cause accumulation in tissue and showed rapid clearence from blood stream[33,39].

Another important property of PMeOX and PEtOX is the suppressed interactions of the polymer with proteins and immune systems, so called “stealth behavior”.

Zalipsky and co-workers reported on stealth behavior and biocompatibility of PMeOx and PEtOx based liposomes[33,40]. They have also reported increased blood circulation time with similar clearance rate to PEO based liposomes[33,40].

1.2 $CaCO_3$ Microparticles

1.2.1 Synthesis and Properties of $CaCO_3$ Microparticles

$CaCO_3$ is one of the most abundant minerals in nature. There are three different polymorphs of $CaCO_3$. The most thermodynamically stable and abundant form is rhomboidal calcite, the metastable phases are needle like aragonite and spherical vaterite form[1,41–43]. Since $CaCO_3$ microparticles have been used in drug delivery and biomedical applications, the synthesis of the microparticles was studied excessively in literature[44]. $CaCO_3$ microparticles are synthesized through four main methods. These are CO_2 bubbling, slow carbonation, reverse emulsion, and solution precipitation[45]. Among these methods, solution precipitation (also known as "mixing method"), which is based on mixing of CO_3^{2-} and Ca^{2+} salts with or without additives, is the simplest and quickest method of $CaCO_3$ synthesis [45].

$CaCO_3$ microparticles are considered as ideal templates for drug delivery applications due to properties such as biodegradability, nontoxicity, biocompatibility, high loading capacity, relatively easy synthesis, low-price mineral, pH-responsiveness [46,47]. The vaterite form have been used in biomedical application such as encapsulation of DNA, drugs, enzyme[46]. The vaterite form of $CaCO_3$ is usually colorless. It has spherical shape and porous inner structure. It is difficult to synthesize vaterite $CaCO_3$ since it is a metastable phase[41]. Among all polymorphs, the vaterite form is highly soluble and because of this reason, it easily transforms to other polymorphs. Vaterite formation can be promoted by controlling the experimental conditions, i.e., chemical nature of salts, pH of mixing solution, temperature, stirring time and speed, and type of additives [41,48,49].

1.2.2 Synthesis of $CaCO_3$ Microparticles by Mixing Method

$CaCO_3$ microparticle synthesis by mixing method is performed by direct mixing of $CaCl_2$ and Na_2CO_3 solution.

Figure 1.6 shows schematic representation of synthesis of $CaCO_3$ microparticles by mixing method.

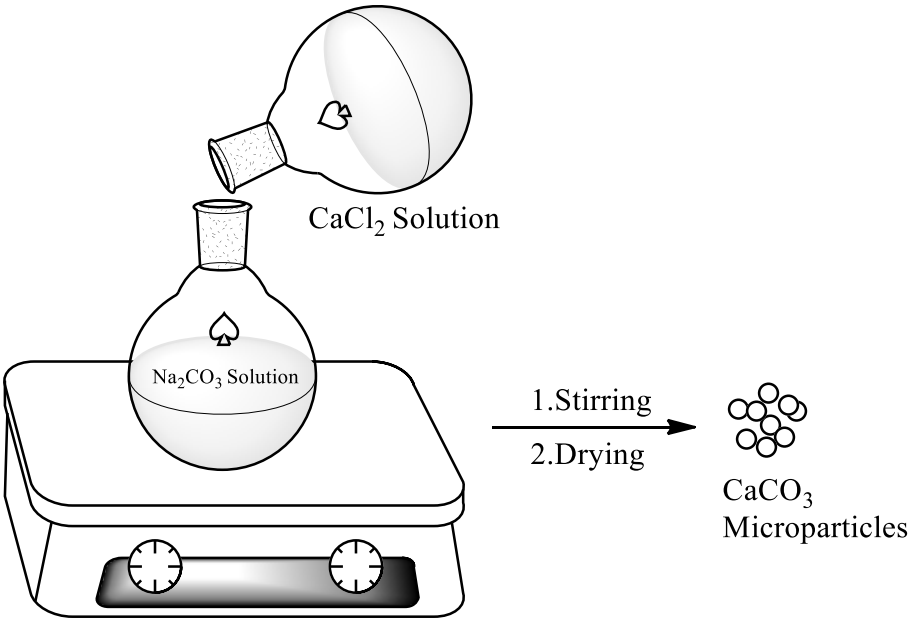

Figure 1.6. Synthesis of $CaCO_3$ microparticles by mixing method.

1.2.3 Factors Affecting Vaterite Formation

1.2.3.1 pH Effect

pH of synthesis medium mainly affects the CO_3^{2-} ion availability in the solution. Decreasing pH below 8 (pH≤8) results in protonation of the CO_3^{2-} ions which eventually decreases CO_3^{2-} ion concentration in the solution. This decreases the nucleation rate and affects crystallization morphology[46]. On the other hand, when the solution pH is highly basic (pH≥10), nucleation rate cannot be controlled, and a

homogeneous size distribution is not obtained[46]. Clifford Y. et al examined various experimental conditions and the authors showed that the vaterite form is mainly formed between pH 8.5-10 and at 24 ^{o}C[50].

1.2.3.2 Temperature Effect

Temperature is another important parameter affecting the morphology of $CaCO_3$ microparticles. The calcite phase is mainly formed at low temperatures (below 20 ^{o}C), whereas vaterite formation is induced between 30 ^{o}C and 40 ^{o}C and aragonite phase is obtained, above 70 ^{o}C[46,51]. Temperature affects not only the type of polymorph, but also the pore size of the particles. Feoktistova et al. demonstrated that pore size of microparticles increased as the temperature was increased [52].

1.2.3.3 Concentration of the Salts

Concentration of salts and ratio of $[CO_3^{2-}]$: $[Ca^{2+}]$ ions affect the morphology as well as size of the $CaCO_3$ microparticles[46]. According to a study by Kitamura, calcite phase is formed at low salt concentrations (0.05 M), while metastable phases (vaterite and aragonite) are formed at high salt concentration (0.2 M)[53]. It has been reported that when CO_3^{2-} ion concentration was higher than Ca^{2+} concentration, ellipsoidal form was dominant in a synthesis performed at high pH (11>). However, isotropic spherical formation was found to be dominant when CO_3^{2-} concentration was lower than Ca^{2+} concentration [44].

1.2.3.4 Speed and Time of the Mixing

Volodkin D.et al investigated the speed of mixing upon combination of $CaCl_2$ and Na_2CO_3 solutions at varying mixing times. They showed that increasing speed and time of mixing decreased the size of the particles[54]. This result was explained by the

formation of more nuclei at higher mixing times and speeds, leading to formation of smaller crystals.

1.2.3.5 Additives

Surfactants, inorganic compounds, biopolymers, synthetic polymers can be used as additives during $CaCO_3$ microparticle synthesis. Additives can affect the crystallization mechanism of microparticles, nucleation steps and promote the formation of one polymorph. PAA and PSS have been extensively used in $CaCO_3$ microparticle synthesis due to conservation of vaterite form of microparticles. BSA, starch, and dopamine have also been reported to form and stabilize the vaterite phase by changing surface energy and retarding transformation from vaterite to calcite form[46].

1.2.4 Biomedical Applications of $CaCO_3$ Microparticles

The potential of $CaCO_3$ microparticles as drug delivery vehicles for anticancer applications have been reported. For example, Kamba et al. demonstrated that $CaCO_3$ nanocrystals could be effectively loaded with DOX due to porous structure of nanocrystals. In addition to large loading capacity, such $CaCO_3$ nanocrystals were shown to exhibit enhanced DOX release at moderately acidic conditions, making them promise for controlled release of anti-cancer drugs[55].

In another study, Peng et al. studied loading/release of an anticancer drug, etoposide into/from mesoporous calcium carbonate nanospheres. They have also shown pH-responsive release from $CaCO_3$ nanospheres. Additionally, they showed that drug loaded nanocrystals had higher inhibition ratio at SGC-7901 cells. The apoptosis test showed that encapsulation of the anti-cancer drug increased the efficiency of drug delivery and suggested that effective drug delivery through $CaCO_3$ nanospheres provided enhanced inhibition of the cell growth[56].

$CaCO_3$ micro/nanoparticles have also been used for loading of antimicrobials[46]. For example, Isa et al. synthesized aragonite $CaCO_3$ microparticles and loaded ciprofloxacin into the particles. Anti-bacterial activity of ciprofloxacin loaded $CaCO_3$ microparticles was investigated against *Salmonella Typhimurium* ATCC 1402. Inhibition zones of ciprofloxacin loaded $CaCO_3$ microparticles was found to be larger than free ciprofloxacin, indicating enhanced anti-bacterial activity for ciprofloxacin loaded $CaCO_3$ microparticles[57]. Another example concerning the use of $CaCO_3$ microparticles for anti-bacterial applications was presented by Sahoo et al. silver nanoparticles loaded $CaCO_3$ microparticles were included into paint and the anti-bacterial activity of the paint was investigated against *Escherichia coli*, *Psychrobacter alimentarius*, and *Staphylococcus equorum*. While free paint did not show any antibacterial activity, it was observed that $CaCO_3$-AgNPs particles included paint showed antibacterial activity[58]. In another study, Ferreira et al. prepared PSS/PEI LbL coated $CaCO_3$ microparticles and loaded biocide benzyldimethyldodecylammonium chloride (BDMDAC) as the antibacterial agent. The antibacterial activity of LbL-coated $CaCO_3$ microparticles was examined against *Pseu-domonas fluorescens*. They reported that the anti-bacterial activity of BDMDAC agains *Pseu-domonas fluorescens* was not affected by the multilayer assembled $CaCO_3$ microparticles[59]. In another example Begum G. and coworkers studied tetracycline release from spherical $CaCO_3$ microparticles. They showed that tetracycline release was greater at acidic conditions and suggested that $CaCO_3$ microparticles could be used as carriers for stimuli-responsive drug release applications [60].

1.3 Layer-by-Layer Self Assembly and Preparation of Polymer Multilayers

Layer-by-layer (LbL) self-assembly technique is a bottom-up nanofabrication technique. It is inexpensive and practical compared to other thin film fabrication methods such as Langmuir-Blodgett (LB) technique, SAM technique[61]. This technique was first discovered in 1966 by Iller[52] in which silica and alumina particles

were deposited onto a glass substrate [62] . In 1991, Decher and coworkers applied this technique to oppositely charged polyelectrolytes to functionalize surfaces [61,63,64].

Ultrathin multilayers through LbL self-assembly technique are formed by alternating immersion of the substrate into oppositely charged polyelectrolyte solutions. Substrates are rinsed after deposition of each layer to get rid of the loosely bound polymers. This cycle is repeated until desired number of layers is deposited at the surface[51,59]. The driving force LbL deposition is not limited to electrostatic interactions. Metal coordination[65,66], hydrogen bonding[67,68], covalent bonding[69,70] have been reported for LbL deposition[71]. Figure 1.7 shows schematic representation of LbL self-assembly process.

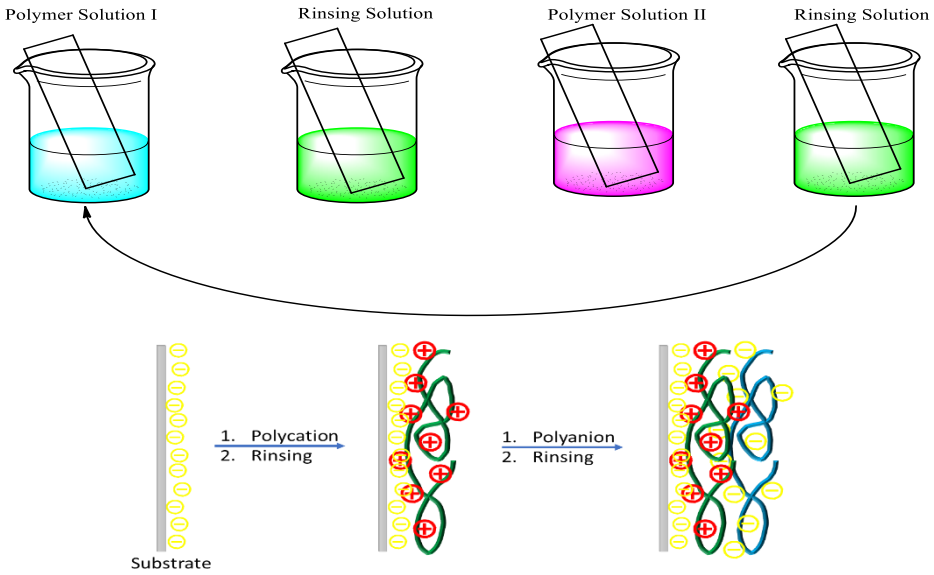

Figure 1.7. Schematic representation of LbL self-assembly process. (Modified from ref [62]).

LbL technique allows adsorption of materials of varying type, e.g. polyelectrolytes[72,73], proteins[74], inorganic substances[75] onto not only two-dimensional substrates but also three-dimensional substrates such as $CaCO_3$[76], silica[77], melamine formaldehyde[78], polystyrene particles[79] .

The nano/microparticles are dispersed in the polymer solution. The polymer is expected to be adsorbed on the surface for a certain period. After the coating of the polymer on the surface is completed, the particles are precipitated, and the rinsing step is carried out. After the rinsing is finished, the precipitated particles are dispersed in the second polymer solution and waited for a while. After the second coating is completed, the rinsing process is performed, and these steps are repeated according to the desired number of layers. After the desired number of layers is coated, the core can be dissolved to obtain a hollow capsule. Figure 1.8 shows schematic representation of LbL microparticles and hollow capsule preparation.

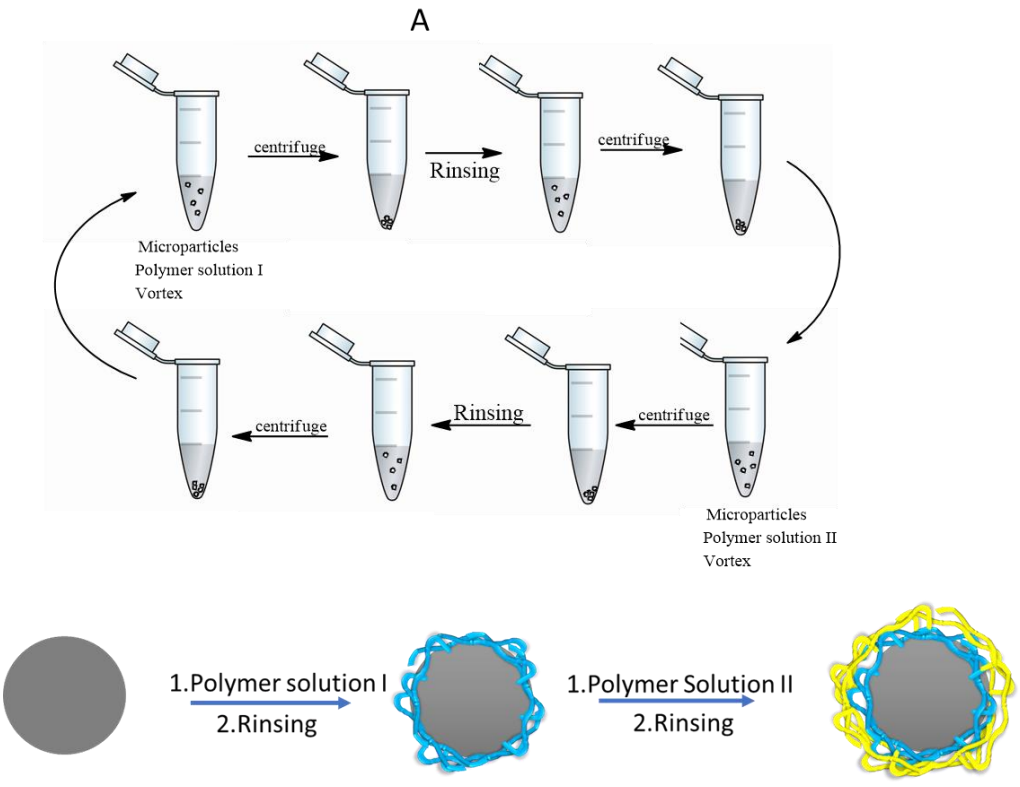

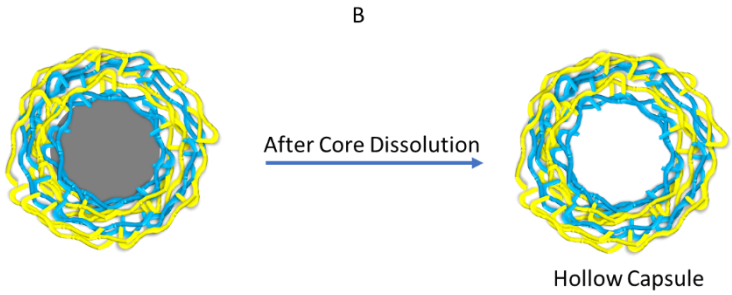

Figure 1.8. A) Schematic representation of fabrication of LbL Microparticles B) Schematic representation of preparation of hollow capsule. (Modified from ref[3]).

1.4 LbL Films as Drug Delivery Platforms

Among various drug carriers, thin films have been of interest for site-specific drug delivery applications compared to conventional tablets which are brittle and require special packaging[80,81] , liquid drug formulations with poor stability[82] and patches which may sometimes cause skin irritation[83,84] . Advantages of thin films for drug delivery applications can be summarized as:

i) faster disintegration of thin films than conventional drug products, providing fast drug action,

ii) reduced dose frequency,

iii) reduced side effects,

iv) release of drugs in a controlled manner, providing improved drug efficacy[85–87].

LbL self-assembly is a practical and a relatively inexpensive technique to prepare thin films. In addition, it allows control in film properties during self-assembly and post-assembly steps. Moreover, this technique does not display any restrictions for the size and shape of the substrates. Considering all these advantages, LbL thin films are advantageous for drug-delivery applications. Drug molecules can be incorporated into the multilayers during either deposition or post-deposition steps. On the other hand, drug molecules can be released from the multilayers through self-diffusion, film dissolution or film degradation.

There are various factors to be considered prior to incorporation of the drugs into the multilayers. These are:

1) Choosing appropriate thin film materials to provide interaction with the specific drug molecules;
2) Chemical and physical stability of multilayers;
3) Ensuring the drug molecules to reach the targeting site (generally accomplished through constructing the multilayers using stimuli-responsive polymers which undergo structural changes and release drug molecules in response to external stimuli, e.g., pH, ionic strength and/or temperature[88].
4) Controlling the drug release kinetics.

There are several methods to incorporate drugs into multilayers. The simplest method is based on loading drug molecules into multilayers at the post-assembly step. Drug molecules can be loaded into pre-fabricated multilayers by immersing the films into drug solution and simple adsorption of the drug molecules onto polymer layers through hydrogen bonding, electrostatic, hydrophobic or van der Waals interactions. The loading amount has been controlled by the thickness of the multilayers as well as the concentration of the drug solution[89]. For example, the amount of paclitaxel release from polylysine/hyaluronic acid (PLL/HA) multilayers which were post-loaded with paclitaxel was found to be tuned with the film thickness and concentration of paclitaxel solution[90].

Another method, commonly used for incorporating drug molecules into LbL films is to use the drug molecules as building blocks for multilayer construction. For example, gentamicin could be used as a building block and incorporated into LbL films composed of hyaluronic acid and poly (β-amino ester) as the polyanion and polycation, respectively. They reported more robust film growth when relatively high molecular weight of poly (β-amino ester) was used. However, the amount of drug per film thickness, so called "density of drug incorporation" was lower compared to multilayers produced at low molecular weight poly (β-amino ester)[91] . Another study based on poly(β-amino ester)-based multilayers was prepared by constructing poly(β-amino ester) and vancomycin together with either dextran

sulfate, chondroitin sulfate or alginate. Such multilayers have been shown to degrade and release vancomycin in a controlled manner and present activity against *S.aureus* [92].

Another way to load drug molecules into multilayers is to load drug molecules into cargo materials such as block copolymer micelles and use the drug loaded cargo materials as building blocks during LbL self-assembly[89]. This way of film preparation is advantageous when protection of the drug against decomposition is required until the target site is reached. In addition, loading capacity of multilayers for hydrophobic molecules can also be increased owing to hydrophobic micellar cores. Note that, LbL films are composed of water soluble, hydrophilic polymers and loading capacity of polymer multilayers for hydrophobic drug molecules is relatively low. Thus, use of block copolymer micelles not only provides protection of the drug molecules but also increases the hydrophobic drug loading capacity of the multilayers. An example to block copolymer micelle containing multilayers was built up by LbL deposition of Coumarin-6 loaded block copolymer micelles of PS-*b*-PAA and graphene oxide. These films were found to release Coumarin-6 in response to pH changes[93].

Drugs can also be incorporated into multilayers through covalent coupling of the drug to polymers *via* responsive bonds and use polymer-drug conjugates as building blocks in LbL assembly. Such multilayers were shown to provide stimuli-responsive drug delivery[94]. For example, Christopher et al. conjugated DOX with poly(Lglutamic acid) (PGA_{Alk}) via amide bond formation. DOX conjugated PGA_{Alk} and poly(N-vinyl pyrrolidone) (PVPON) assembled onto silica particles via hydrogen bonding. PVPON was released into multilayers by manipulating pH and DOX conjugated PGA_{Alk} stabilized with cross-linker agent. They investigated DOX conjugated PGA_{Alk} capsules cell viability, and they reported that the covalently bound drug-polymer conjugated capsules decreased the cell viability[95].

LbL assembly has also been applied to coat inorganic micro-/nano particles which can absorb both hydrophilic and hydrophobic drug molecules in their pores. In other

words, drug containing inorganic particles are used as substrates for LbL deposition. Multilayers have been reported to control the drug release from the interior region. For example, DOX encapsulated silica microparticles, LbL modified using bis-aminated poly (glycerol methacrylate)s (BA-PGOHMAs) and cucurbit[7]uril (CB[7]), were shown to release DOX in response to pH or presence of competitive agents such as adamantaneamine hydrochloride (AH) [96] . Dissolution of the core material upon LbL deposition resulting in formation of hollow capsules was also shown in the literature for encapsulation of functional molecules in the interior region. For example, Volodkin et al. prepared PAH/PSS coated $CaCO_3$ microparticles in a LbL fashion, followed by core dissolution. The resulting hollow LbL capsules could be loaded with Bovine Serum Albumin (BSA) and dextran without losing activity of the biological molecules[97]. Similar hollow capsules were also prepared by Zhao et al. [91]. DOX and daunorubicin (DNR) loaded hollow capsules were found to exhibit diffusion-controlled drug release [98].

Liu et al. constructed multilayer film system with PAH/PSS deposited onto melamine formaldehyde (MF) colloidal particles. Hollow polyelectrolyte hollow capsule was obtained by dissolving core particles at acidic conditions. Daunorubicin (DNR) was loaded into hollow capsules. The loading amount of DNR was found to be controlled with concentration of drug, concentration of salt and temperature [99].

In another study Andalib et al. deposited chitosan (CS) and poly (ethylene glycol dimethacrylate-co-methacrylic acid) (EM) onto $CaCO_3$ microparticles. After $CaCO_3$ core dissolution with EDTA, anticancer drugs of gemcitabine (Gem) and curcumin (Cur) were loaded into the hollow capsules. They reported that Gem and Cur loaded hollow capsules showed high toxicity on HCT-116 colorectal carcinoma cells depending on the concentration of hollow capsules[100].

Wang et.al. modified $CaCO_3$ microparticles through LbL deposition using poly-L-ornithine (PLO) and fucoidan was deposited onto $CaCO_3$ microparticles. DOX was loaded into LbL-coated microparticles, and such particles were shown to display significant cell inhibition on MCF-7 cells[101].

LbL modification of $CaCO_3$ microparticles using sodium poly (styrene sulfonate) (PSS) and aliphatic poly(urethane-amine) (PUA) was reported to prevent burst release of DOX from $CaCO_3$ microparticles. Additionally, DOX release was found to be increased with increasing temperature and decreasing pH due to core dissolution and [102].

1.5 Layer-by-Layer Assemblies of Poly(2-alkyl-2-oxazoline)s

Multilayers of PAOXs, constructed onto both 2D and 3D substrates have been reported in the literature.

1.5.1 PAOX-based multilayers constructed onto 2D-subtrates

Thickness dependent antifouling behavior of thermally crosslinked PAA and partially hydrolyzed PEOX multilayers (deposited onto silicon wafers) was demonstrated by Jiang et.al. Multilayers were found to be resistant against attachment of bovine serum albumin (BSA), fibroblasts, gram-positive (S.aureus) and gram-negative (E.coli) bacteria. They found that increasing multilayer thickness adversely affected the anti-adhesiveness against protein attachment.[103]

Thermally crosslinked multilayers of partially hydrolyzed PEtOX (7%) and PAA displayed antifouling property against bacterial attachment when incubated with gram positive *B.subtils* and gram negative bacteria *E.coli* for 6 hours. The authors also examined healability of the same multilayers and found that healability decreased as the crosslinking degree due to restriction of polymer chain mobility[104].

In another study, Antunes et.al. examined LbL deposition of temperature responsive PnPrOX and TA onto gold coated quartz chip below and above LCST of the PnPropOX. Their findings showed that deposition temperature was critical on the multilayer growth mechanism. Deposition above LCST resulted in high change in resonance frequency (Δf) due to dehydration of PnPropOX leading to more globular

conformation. On the other hand, LbL deposition below LCST provided low change in resonance frequency (Δf) due to more extended conformation of PnPropOX [105].

LbL deposition of PiPOX and water-soluble complexes of TA and DOX was reported by Haktanıyan et.al. They found that DOX release from multilayers was greater at acidic conditions than neutral pH. pH-responsive release was explained by protonation of TA as the pH decreased resulting in disruption of electrostatic association among DOX and TA, providing greater amount of DOX release from multilayers [106].

Hendessi et.al demonstrated that functionalization of coating Ag nanoparticles with PEOX enhanced stability of the particles and molecular weight of PEOX together with the pH of the solution were both critical on the stability. In the same study, PEOX stabilized Ag nanoparticles were co-assembled with TA onto quartz and silicon wafer substrates. Such multilayers were shown to display pH-responsive Ag^+ release, providing antibacterial activity to the surfaces[107] .

A contrastive study on surface morphology, stability, wettability, stimuli-responsive drug release properties, anti-adhesive and antibacterial properties of PEOX/TA and PIPOX/TA was reported by
Çağlı et.al. Wettability of multilayers was found to be critical on the resistivity against Bovine Serum Albumin (BSA) adsorption and were more effective to reduce adherence of *E. coli*. Both PEOX/TA and PIPOX/TA multilayers did not display antiadhesiveness against *S. aureus*. Although PIPOX/TA multilayers released greater amount of CIP especially at acidic pH and 37 °C, PAOX-multilayers showed similar antibacterial activity against *E. coli* under all conditions. On the other hand, antibacterial activity of the films against *S. aureus* was in good agreement with the amounts of CIP released from multilayers[108] [ref].

1.5.2 PAOX-based multilayers constructed onto 3D-subtrates

LbL coating of super magnetic iron oxide nanoparticles by TA and PiPrOx was demonstrated by Erel and co-workers. DOX was post-loaded into the particles via electrostatic and hydrogen bonding interactions between DOX and TA[109]. DOX release was triggered by both pH and temperature at physiologically related conditions[109].

Mathivanan et al. prepared hollow capsules by LbL modifying $CaCO_3$ microparticles using temperature sensitive poly(2-n-propyl-2-oxazoline) (PnPropOx) and TA through hydrogen bonding interactions. $CaCO_3$ microparticle template was then dissolved using EDTA resulting in PnPropOx/TA hollow capsules. pH-dependent stability of hollow capsules was examined through confocal laser scanning microscopy (CLSM) using TRITC-dextran and FITC-dextran as fluorescence probes. PnPropOx/TA hollow capsules were found to be stable between pH 3 and 8.5. They observed that the capsules shrunk at pH 9, swelled below pH 3 and completely dissolved at pH 2. The permability of capsule walls was examined using 4 different fluorescent dyes, i.e., FITC-dextran, TRITC-dextran, rhodamine, and carboxyfluorescein. Capsules were permeable to all these fluorescence molecules between pH 2 and 5. At pH 7, capsules were permeable to all the dyes except FITC-dextran. This was explained with the decreasing pore size within the PnPropOx/TA multilayers, making capsule walls impermeable to FITC-dextran with relatively big size. The electrostatic repulsion between FITC-dextran and TA or PSS in the capsule interior could have also contributed to impermeability of the wall towards FITC-dextran. On the contrary, relatively small molecules such as rhodamine and carboxyfluorescein were found to diffuse into the capsules even above pH 8.5 when the pores were closed [110].

LbL capsules composed of TA and poly(2-n-propyl-2-oxazoline)s (PnPrOX) with LCST-type phase behavior were prepared by Paramasivam et. al. The effect of temperature on the morphological changes of the capsule wall was investigated[111]. Their findings showed that pores were formed on the capsule wall beyond LCST of

PnPrOX and these pores could be opened or closed below or above the critical temperature of PnPrOX, which may be promising for temperature-controlled drug delivery[111].

Kempe and co-workers synthesized both linear- and brush-like PEOX. LbL deposition of these PEOX onto silica particles was achieved using poly (methacrylic acid) (PMA). Stabilization of linear PEOX with alkene functionality and PMA multilayers was assured through thiol-ene chemistry, whereas for brush-like PEOX with alkyne moieties, copper-catalyzed azide-alkyne cycloaddition reaction was performed. Hollow capsules obtained after removal of the silica particles using hydrofluoric acid were shown to exhibit low-fouling behavior[112]. Same authors also reported on LbL deposition of thiol-containing poly(2-ethyl-2-oxazoline) and PMA which were crosslinked through disulfide bond formation. Redox-responsive behavior of the capsules arising from disulfide crosslinking introduced degradability to the capsules under simulated intracellular conditions (pH 5.9- and 5-mM glutathione). Capsule degradation was also observed after incubation with dendritic JAWS II cells[113].

1.6 Aim of Thesis

Poly(2-oxazoline)s (PAOXs) have attracted increasing attention in the recent years especially due to their important biological properties such as biocompatibility, non-toxicity and anti-fouling[33,114]. Although there are several studies concerning functionalization of surfaces using PAOXs through LbL self-assembly technique[104,107,108,112], still there are challenges to address in the use of PAOX-based LbL films for biomedical applications. For example, PAOXs are neutral polymers and their LbL films are constructed through physical interactions such as hydrogen bonding. This sometimes brings together long-term stability problems in biomedical applications since hydrogen bonding is sensitive to the pH, ionic strength and temperature of the environment. There are only two studies, reporting on thermal crosslinking of partially hydrolyzed poly(2-ethyl-2-oxazoline) (PEOX-PEI) and

polyacrylic acid multilayers through amide bond formation. Note that this crosslinking is only possible when the counterpart polymer in the LbL self-assembly is a polycarboxylic acid.

In this context, this thesis study first aimed to investigate a new crosslinking chemistry for LbL films composed of a PAOX, namely poly(2-isopropyl-2-oxazoline) and a polyphenol, TA and then contrast the physicochemical properties of crosslinked and noncross-linked PIPOX-PEI and TA with respect to stability at physiologically related pH and temperature conditions. The second aim was to transfer the knowledge generated on 2D studies to prepare LbL-modified microparticles and LbL hollow capsules. The third aim of the study was to explore different routes for loading hydrophobic drug molecules into LbL microparticles and hollow capsules. The fourth and last aim was to demonstrate dual responsive (pH and temperature) release of multiple drug molecules from the particles and the synergistic effect of the two drug molecules to assess their potential for anticancer applications.

CHAPTER 2

EXPERIMENTAL

2.1 Materials

Phosphate buffer saline (PBS) (tablet), calcium chloride ($CaCl_2$, anhydrous, granular), sodium carbonate (Na_2CO_3) (powder, ≥ 99.5%, ACS reagent), Curcumin (CUR) and poly(sodium 4-styrenesulfonate) (PSS) (70,000 g/mol) were purchased from SigmaAldrich Chemical Co. Sodium dihydrogen phosphate dihydrate ($NaH_2PO_4.2H_2O$), Tannic Acid (TA, Mw 1701). sodium hydroxide (NaOH) (pellet), SpectroPor7 regenerated cellulose dialysis membrane (molecular weight cut off: 3.5 kDa) and Spectra/Por Float-A-Lyzer G2 Dialysis device were purchased from Merck Chemicals. Deionized (DI) H_2O was purified by passage through a Milli-Q system (Millipore) at 18.2 MΩ. Sodium dodecyl sulphate (SDS) was purchased from BioShop® Canada Inc.. Ethanol (≥ 99.9%) was purchased from Isolab® Chemicals. Ethanolamine(>99%), cadminum acetate dihydrate (98%), α-bromoisobutyrl bromide (98%), acetonitrile (>99.9%), 2-butanol (>99%).

2.2 Methods

2.2.1 Synthesis of IPOX

Cadmium acetate dihydrate (1.08 mmol, 0.29 g) was added to ethanolamine (0.052 mol, 3.52 mL) and isobutyronitrile (0.043 mol, 3.9 ml) under argon atmosphere. This mixture was refluxed at 130°C for 20 hours. The product was distilled under low

pressure at 50°C and separated from unreacted ethanolamine and isobutyronitrile. It was dried with CaH_2 and distilled again.

2.2.2 Synthesis of PIPOX

IPOX and acetonitrile were dried with CaH_2. 41 mmol of iPOX was dissolved in 5.35 mL of acetonitrile (ACN) in an inert atmosphere. 0.4 mmol of α-bromoisobutyryl bromide was added to the solution. After mixing, the reaction vessel was placed in an oil bath at 80°C. After 72 hours, the mixture was cooled to room temperature. Polymerization was terminated by adding 1.2 mmol of 2-butanol and the reaction solution was stirred at 80°C for another 2 days. Afterwards, the solvent was removed in the rotavap. The product was dissolved in deionized water and dialyzed against deionized water for 2 days. Finally, the solution was freeze-dried.

2.2.3 Synthesis of Poly (2-isopropyl-2-oxazoline-*r*-polyethylene imine)

0.16 g of PIPOX was dissolved in 3 mL of concentrated HCl solution. This solution was stirred at 500 rpm at 100 °C for 6 hours. Afterwards, the solution was cooled to room temperature.15 mL of 6 M NaOH was added to the polymer solution until it became basic. The basic polymer solution was dialyzed against deionized water for 2 days and freeze-dried.

2.2.4 Synthesis of $CaCO_3$ Microparticles

20 mg of PSS was added to 10 mL of 0.3 M Na_2CO_3 solution and mixed at 1000 rpm for 1 hour. 0.3 M $CaCl_2$ solution was prepared in a separate beaker. 10 mL of 0.3 M $CaCl_2$ solution was added onto 10 mL of 0.3 M Na_2CO_3 solution containing PSS and mixed at 1000 rpm for 30 seconds. $CaCO_3$ microparticles were separated by vacuum filtration, washed with 50 mL of DI water and dried in an oven at 60 °C for 1 hour.

2.2.5 Synthesis of Curcumin (CUR) Loaded $CaCO_3$ Microparticles

25 mg of CUR was dissolved in 5 mL of ethanol. 50 mg of SDS and 50 mg of PVP were added into this solution and mixed on a magnetic stirrer at 1000 rpm for 1 hour. 10 mg of PSS was added to 5 mL of 0.3 M Na_2CO_3 solution and stirred for 1 hour at 1000 rpm. SDS/PVP/CUR solution in ethanol was added to 5 ml of 0.3 M Na_2CO_3 solution containing PSS and mixed at 1000 rpm for 5 minutes. 5 mL of 0.3 M $CaCl_2$ solution was added to this mixture in a controlled manner for 40 seconds and then mixed for 2 minutes. CUR-loaded $CaCO_3$ microparticles were separated by vacuum filtration, washed with 50 mL of DI water and dried in an oven at 60 °C for 1 hour.

2.2.6 Calculation of Loading amount of Curcumin in $CaCO_3$ Microparticles:

25 µl of 15 mL filtrate obtained after the filtration of $CaCO_3$ microparticles was added onto 4 mL of 60% v/v PBS-EtOH solution. Then, 100 µl of this solution was taken and diluted to 2 mL with 60% v/v PBS-EtOH solution. The fluorescence intensity of CUR in the obtained solution was measured and the amount of CUR was determined using calibration curves prepared under similar conditions. The reason for dilution was the high fluorescence intensity of CUR in the solution which lied outside the linear range. The amount of CUR in 15 mL filtrate was calculated. To calculate the amount of CUR loaded into the $CaCO_3$ microparticles, the amount of CUR in the filtrate was subtracted from the amount of CUR (25 mg) added during particle synthesis. The values obtained after the calculations for 4 different samples are summarized in the table below and the amount of CUR loaded into 0.13195 ± 0.00225 $CaCO_3$ microparticles was accepted as $\sim 8.2 \pm 1.1$ mg.

Table 1. Loading amount of Curcumin in $CaCO_3$ Microparticles.

	Amount of $CaCO_3$ Microparticles	**Loading amount of loaded Curcumin**
Sample 1	0.13 g	8.30 mg
Sample 2	0.13 g	9.70 mg
Sample 3	0.13 g	7.90 mg
Sample 4	0.13 g	7.00 mg

2.2.7 Fabrication of TA/PIPOX-PEI Multilayers onto Silicon Wafer

To clean the surfaces of the silicon wafers, the wafers were first immersed in concentrated sulfuric acid for 85 minutes and then rinsed with DI water. Then, the surfaces were immersed into 0.25 M NaOH solution for 10 minutes and rinsed with DI water. A layer of branched polyethyleneimine (BPEI) was deposited on the surface of silicon wafers to improve the adhesion of subsequent layers. For this, the cleaned wafers were dipped into 0.5 mg/mL BPEI solution (pH 5.5, prepared in 10 mM phosphate buffer solution), waited for 30 minutes and then rinsed for 1 minute in 10 mM phosphate buffer solution (pH 5.5).

0.2 mg/mL (pH 6.5) TA solution and 0.2 mg/mL (pH 6) PIPOX-PEI solution were prepared by dissolving TA and PIPOX-PEI in 10 mM phosphate buffer. The cleaned and BPEI coated silicon wafers were first immersed in the TA solution for 15 minutes. Afterwards, the silicon wafers were washed twice, for 1 min each, by immersion in 10 mM phosphate buffer solution (pH 6.5). In the second step, these wafers were immersed in the PIPOX-PEI solution for 15 minutes. Afterwards, the

silicon wafers were washed twice by immersion in 10 mM phosphate buffer solution (pH 6) for 1 minute each. This cycle was continued until the desired number of layers were deposited on the surface. Film thickness was measured after each layer using a spectroscopic ellipsometer.

2.2.8 Fabrication of covalently crosslinked TA/PIPOX-PEI Multilayers

14-layer PIPOX-PEI/TA films were prepared as described in section 2.9. The films were incubated in 1 mM $NaIO_4$ solution (prepared in pH 5, 10 mM phosphate buffer solution) for 5 minutes. Afterwards, the films were rinsed by immersing into 10 mM phosphate buffer solution (pH 5) for 1 min. Crosslinking was indirectly confirmed through exposing multilayers to PBS at either decreasing or increasing pH values for 30 minutes at 25 °C and following the fraction retained at the surface at each pH value. Fractions were calculated by dividing the thickness at each pH to the initial thickness of the film.

2.2.9 Stability of Multilayers in PBS at neutral and acidic pH

The stability of the 14-layer non-crosslinked or covalently cross-linked PIPOX-PEI/TA films was examined in phosphate buffer saline (PBS) at pH 5.5/25°C; pH 7.4/25°C; pH 5.5/37°C and pH 7.4/37°C. Films were exposed to PBS solution, waited for certain time, dried and the thickness was measured. Fraction retained at the surface was followed as a function of time. Fractions were calculated by dividing the thickness of multilayers to the initial thickness. Similar experiment was also carried out for non- crosslinked films in PBS containing 20% by volume of ethanol under the above-mentioned conditions.

2.2.10 Deposition of TA/PIPOX-PEI onto $CaCO_3$ Microparticles

LbL deposition onto bare and CUR-loaded $CaCO_3$ microparticles was performed as explained in the following paragraph:

10 mg of $CaCO_3$ microparticles were placed in an eppendorf centrifuge tube and dispersed in 2 mL of 10 mM phosphate buffer solution (pH 6) for 2 hours using a vortex shaker. Microparticles were precipitated by centrifugation at 3500 rpm for 1 minute. The precipitate was dispersed for 20 minutes in 2 mL of 2 mg/ml TA solution (prepared in pH 6.5, 10 mM phosphate buffer solution) with the vortex shaker. Microparticles were precipitated by centrifugation at 3500 rpm for 1 minute. For rinsing, the precipitate was dispersed for 1 minute in 10 mM phosphate buffer solution (pH 6.5) and precipitated again for 1 minute at 3500 rpm. The rinsing process was repeated 2 times. For the second layer, the precipitated $CaCO_3$ microparticles were dispersed in 2 mL of 0.5 mg/mL PIPOX-PEI solution (prepared in pH 6, 10 mM phosphate buffer solution) for 15 minutes using a vortex shaker. Microparticles were precipitated by centrifugation at 3500 rpm for 1 minute. For rinsing, the precipitate was dispersed in 10 mM phosphate buffer solution (pH 6) for 1 min and precipitated again at 3500 rpm for 1 min. The rinsing process was repeated 2 times. This cycle continued until 5 layers were deposited on the $CaCO_3$ microparticles. All layers except the first one was deposited for 15 minutes. 1 mg/mL TA solution was used for the 2nd and 3rd TA layers. The order of the layers deposited on the surface is as follows: 1st layer: TA; 2nd layer: PIPOX-PEI; 3rd layer: TA; 4th layer: PIPOX-PEI; 5th layer: TA.

2.2.11 CUR Release from LbL-coated $CaCO_3$ Microparticles

5 mg of LbL-coated $CaCO_3$ microparticles were dispersed in 4 mL of 80% PBS-EtOH solution and mixed on a vortex shaker at 100 rpm. After a certain time, the capsules were precipitated and the amount of CUR in the supernatant was determined by fluorescence spectroscopy method. Fresh 4 mL of 80% PBS-EtOH solution was

added on the precipitated LbL capsules and CUR release was continued. CUR was excited at 425 nm (excitation wavelength) and fluorescence intensity was followed at 525 nm. Since the amount of CUR in the supernatant solution obtained at the end of the 1st and 3rd hours was high, it was determined that the obtained fluorescence intensity was outside the linear region. Therefore, 200 μL of the supernatant solution obtained at the end of the 1st and 3rd hours was taken, completed to 1 ml with 20% v/v EtOH-PBS solution, and then 1 mL of pure EtOH was added to the measurement. In summary, the amount of EtOH in the mixture was 60% by volume prior to fluorescence intensity measurements. The concentration of released CUR was calculated with the help of calibration curve. The amounts of CUR released at the end of the 5th, 7th and 24th hours were low compared to the first and third hours. For this reason, dilution with 20% v/v EtOH-PBS mixture was not performed before the fluorescence intensity measurement. Instead, 1 mL of pure EtOH was added to 1 mL of sample taken from the supernatant and the % EtOH ratio in the solution was similarly increased to 60%. Since the supernatant was discarded after each measurement and replaced with fresh 20% v/v EtOH-PBS, the concentration values shown in Figure 3.17 are cumulative concentration values.

2.2.12 CUR Loading into Crosslinked and Non-Crosslinked Hollow Capsules

CUR loading into crosslinked and non-crosslinked hollow capsules was performed at pH 5. Crosslinked and non-crosslinked hollow capsules were dispersed in 2 mL of 0.2 mg/mL CUR solution (prepared in 20% EtOH-10 mM phosphate buffer) and mixed using a vortex shaker for 4 hours at room temperature. The amount of CUR loaded into crosslinked and non-crosslinked hollow capsules were calculated by measuring the fluorescence intensity of CUR at 525 nm, then quantifying the amount of CUR in the supernatant, and finally subtracting the amount in the supernatant from the amount of CUR in the loading solution. The amount of CUR loaded into non-

crosslinked and crosslinked were ~ 240μM ± 7.5 for both crosslinked and noncross-linked hollow capsules.

2.2.13 CUR Release from Hollow Capsule

TA/PIPOX-PEI crosslinked and non-crosslinked hollow capsules were dispersed in 2 mL of 80% PBS-EtOH solution and mixed on a vortex shaker at 100 rpm. After a certain time, the capsules were precipitated and the amount of CUR in the supernatant was determined by fluorescence spectroscopy method. Fresh 2 mL of 80% PBS-EtOH solution was added on the precipitated crosslinked and non-crosslinked hollow capsules and CUR release was continued. CUR was excited at 425 nm (excitation wavelength) and fluorescence intensity was followed at 525 nm. Since the amount of CUR in the supernatant solution obtained at the end of the 1st, 3rd and 5th hours were high, it was determined that the obtained fluorescence intensity was outside the linear region. Therefore, 10 μL of the supernatant solution obtained at the end of the 1st, 3rd, 5th hours were taken, completed to 1 ml with 20% v/v EtOH-PBS solution, and then 1 mL of pure EtOH was added to the measurement. In summary, the amount of EtOH in the mixture was 60% by volume prior to fluorescence intensity measurements. The concentration of released CUR was calculated with the help of calibration curve presented in Appendix 3 and 4. Since the supernatant was discarded after each measurement and replaced with fresh 20% v/v EtOH-PBS.

2.2.14 Doxorubicin (DOX) Loading into LbL-coated $CaCO_3$ Microparticles

2 mg of $CaCO_3$ microparticles coated with 5-layers of PIPOX-PEI/TA multilayer films were dispersed in 1 mL of 0.1 mg/ml DOX solution (prepared in pH 7.4, 10 mM phosphate buffer solution) and stirred at 1200 rpm for 1 hour using a vortex shaker. As explained in more detail in section 2.15, CUR-free (bare) $CaCO_3$

microparticles were used for DOX loading and release studies. The particles, which were precipitated by centrifugation at 3500 rpm for 1 minute, were dispersed again in pH 7.4, 10 mM phosphate buffer solution to get rid of weakly attached DOX molecules. Supernatants were collected and the amount of DOX was calculated with the help of calibration curves. The amount of DOX loaded into LbL-coated $CaCO_3$ microparticles was approximated by subtracting the DOX amount in the supernatant from the amount of DOX in the loading solution. The amount of DOX loaded on 2 mg LbL coated $CaCO_3$ microparticles was calculated to be approximately 0.045 ± 0.006 mg.

2.2.15 Doxorubicin (DOX) Loading into Crosslinked and Non-Crosslinked Hollow Capsules

DOX loading into crosslinked and non-crosslinked hollow capsules were performed at pH 7.4 in 10 mM phosphate buffer. Crosslinked and non-crosslinked hollow capsules were dispersed in 1 mL of 0.1 mg/mL DOX solution (prepared in 10 mM phosphate buffer) and mixed using a vortex shaker for 1 hour at room temperature. The amount of DOX loaded into crosslinked and non-crosslinked hollow capsules were calculated by first measuring the fluorescence intensity of DOX at 555 nm, then quantifying the amount of DOX in the supernatant, and finally subtracting the amount in the supernatant from the amount of DOX in the loading solution. The amount of DOX loaded into non-crosslinked and crosslinked were ~ 70.3 µM ± 3.0 and 73.1 µM ± 2.9 respectively.

2.2.16 DOX Release from LbL-coated $CaCO_3$ Microparticles

Since DOX and CUR peaks overlap in the emission spectra, bare $CaCO_3$ microparticles were used for DOX release experiments. In addition to the overlap, the amount of CUR released was higher than DOX which made DOX peak undetectable. This is another reason why bare microparticles (no CUR loaded) were

used for DOX release experiments. 2 mg $CaCO_3$ microparticles coated with PIPOX-PEI/TA multilayer films and post-loaded with DOX were dispersed in 2 mL of PBS and mixed at 100 rpm on a magnetic stirrer. DOX release was followed at pH 5.5/25°C; pH 7.4/25°C; pH 5.5/37°C and pH 7.4/37°C. The pH and temperature of the PBS solution were adjusted before release was started. Particles were precipitated at certain time intervals and DOX release was followed by fluorescence spectroscopy (excited at 490 nm). Due to the high DOX concentration in the supernatant which did not lie in the linear region, 100 µL of the supernatant was taken and diluted by adding 900 µL of PBS. The intensity of the peak at 555 nm in the emission spectrum was monitored as a function of time. The amount of DOX released was calculated with the help of the calibration curves presented in Appendix 1 and 2.

2.2.17 DOX Release from Crosslinked and Non-crosslinked Hollow Capsules

DOX release was started by dispersing crosslinked and non-crosslinked hollow capsules into 2 mL of PBS which was then placed on a magnetic stirrer and stirred at 100 rpm. At determined time intervals, crosslinked and non-crosslinked hollow capsules were precipitated and the amount of DOX in the supernatant was calculated by measuring the intensity at 555 nm using fluorescence spectroscopy. After each measurement, 2 mL of fresh PBS solution was added onto precipitated the hollow capsules, and DOX release was continued. DOX was quantified using calibration curves prepared under release conditions.

The amount of DOX in the supernatant was too high and the fluorescence intensities lied outside of the linear range in the calibration curve. Therefore, the supernatants obtained at the end of the first and third hours were diluted with PBS solution with 1:19 ratio and fifth hours was diluted with 1:1.5 ratio. DOX release was quantified

using calibration curves presented in Appendix 1 and 2 Since the supernatant was discarded after each measurement and fresh PBS mixture was added instead.

2.3 Instrumentation

2.3.1 1H Nuclear Magnetic Resonance Spectroscopy

IPOX, PIPOX and PIPOX-PEI were characterized through NMR spectroscopy using a Brucker Spectrospin Avance DPX-400 Ultra shield instrument, operating at 400 MHz.

(Solvent: $CDCl_3$, D_2O).

2.3.2 Fourier Transform Infrared Spectroscopy

CUR loaded $CaCO_3$ and bare $CaCO_3$ were characterized using a Nicolet iS10 ATR-FTIR.

2.3.3 pH Meter

Ohaus Starter 3000 pH meter was used for pH adjustments.

2.3.4 X-ray Diffractometry

Rigaku X-ray Diffractometer with a miniflex goniometer operated at 30 kV and 15mA Cu-Kα line (α =1.54 Å) as the X-ray source was used for XRD measurements.

2.3.5 Scanning Electron Microscopy (SEM)

The morphology and size analysis of bare $CaCO_3$ and CUR loaded $CaCO_3$ microparticles were conducted using JSM-6400 Scanning Electron Microscope

(SEM) (JEOL, equipped with NORAN system 6 X-ray Micro-analysis system and semaphore digitizer, Westhorst, NL).

2.3.6 Dynamic Light Scattering and Zeta Potential Measurements

Zetasizer Nano-ZS equipment (Malvern Instruments Ltd., U.K.) was used for zeta potential measurements of $CaCO_3$ microparticles.

2.3.7 Fluorescence Spectroscopy

Release studies were conducted using a Perkin Elmer LS55 Fluorescence Spectrometer.

CHAPTER 3

RESULTS AND DISCUSSION

3.1 Synthesis of IPOX

2-isopropyl-2-oxazoline was synthesized as a result of the reaction between acetonitrile and ethanolamine under a Lewis acid catalysis. Schematic representation of IPOX synthesis and ^{1}H NMR spectrum of IPOX are shown in Figure 3.1. The peaks at 1.17 ppm and 1.19 ppm were correlated with methylene protons (d, 6H, -CH_3). The peak at 2.55 ppm (m, 1H -CH) was correlated with the proton on the tertiary carbon. The peak at 3.75 ppm was correlated with the protons on the carbon, neighbouring the nitrogen atom (t, 2H, =NCH_2). The peak at 4.25 ppm was related with the protons on the carbon atom, neighbouring the oxygen atom (t, 2H, -OCH_2). The ^{1}H NMR spectrum confirms successful synthesis of IPOX and the data is also in good agreement with the literature [115,116].

A

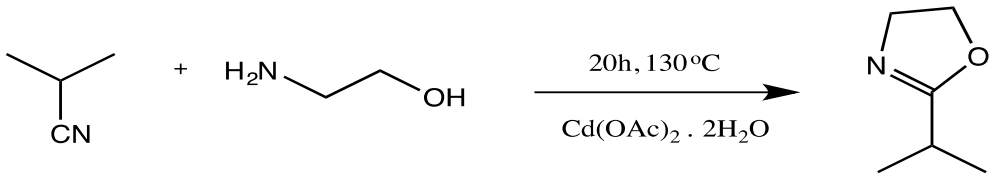

B

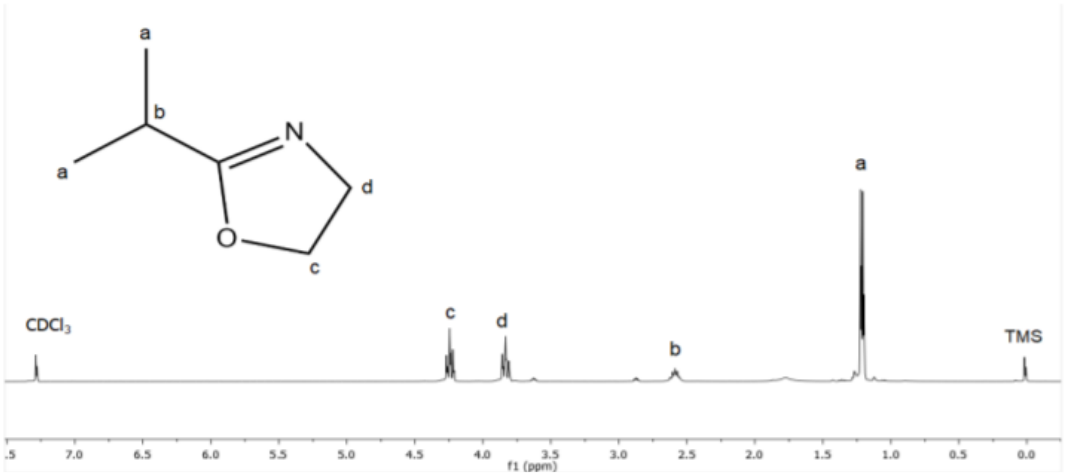

Figure 3.1. A) Schematic representation of IPOX synthesis and B) 1H-NMR spectrum of IPOX.

3.2 Synthesis of PIPOX

PIPOX was synthesized through cationic ring opening polymerization of 2-isopropyl-2-oxazoline in acetonitrile, using α-bromoisobutyrl bromide as the initiator. The mechanism for cationic ring-opening polymerization (CROP) of IPOX is represented in Figure 3.2A. The chemical structure of IPOX was identified by ^{1}H-NMR Spectroscopy (Figure 3.2B). The peak at 3.5 ppm, labelled as 'a' belongs to PIPOX backbone protons of -(CH_2-CH_2-N)- (s, 4H). The peaks at 2.9 and 2.7 ppm, labelled as 'b', belong to methine proton (-CH) (m, 1H) on the side group The peak at 1.12 ppm, labelled as 'd' was correlated with methylene protons (-CH_3) (s, 6H) on the side chain. The peaks observed in the ^{1}H NMR spectrum of PIPOX are in good agreement with the peaks reported for the same polymer in the literature[116]. The peak at 1.6 ppm was associated with the protons of the water molecules remaining after drying. Molecular weight of PIPOX was determined through Gel Permeation Chromatography (GPC). Figure 3.2C shows GPC chromatogram of PIPOX. The number average molecular weight of PIPOX was ~ 6100 g/mol, the weight average

molecular weight was ~ 7400, and the polydispersity index was 1.2. Since the polydispersity index was close to 1, it can be suggested that the controlled synthesis of PIPOX was achieved.

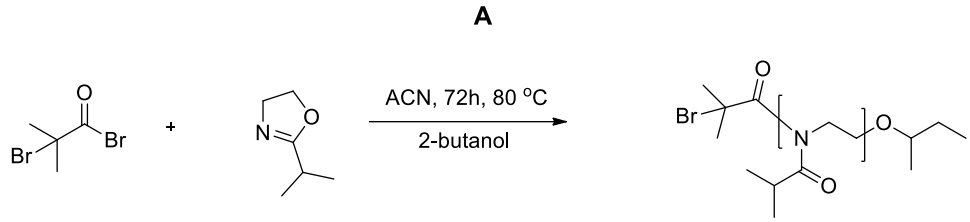

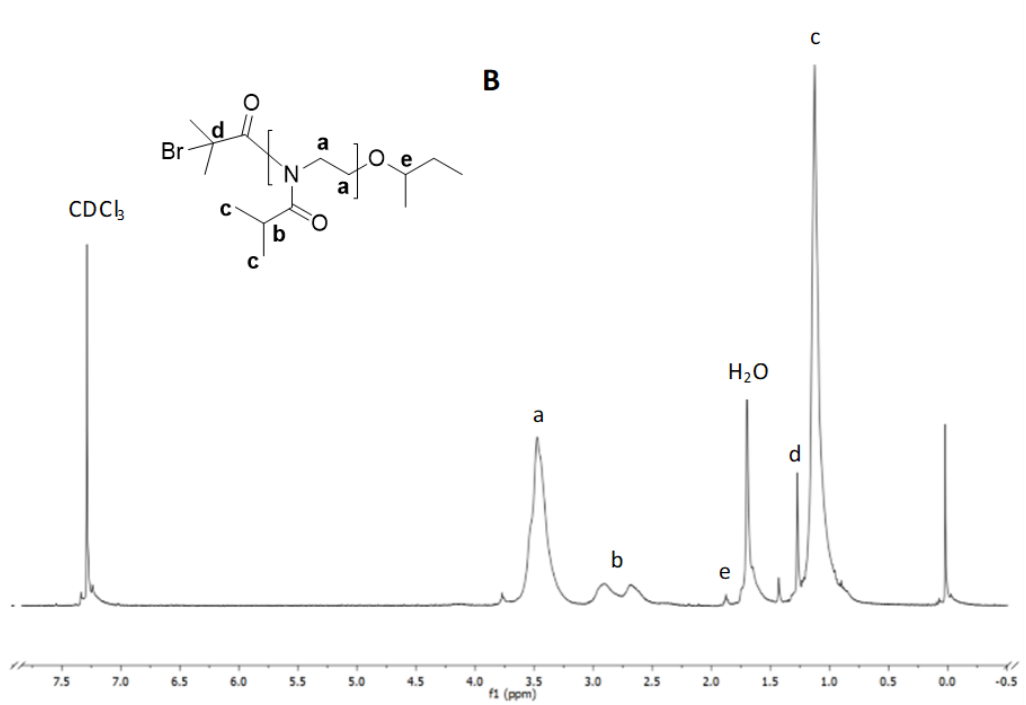

C

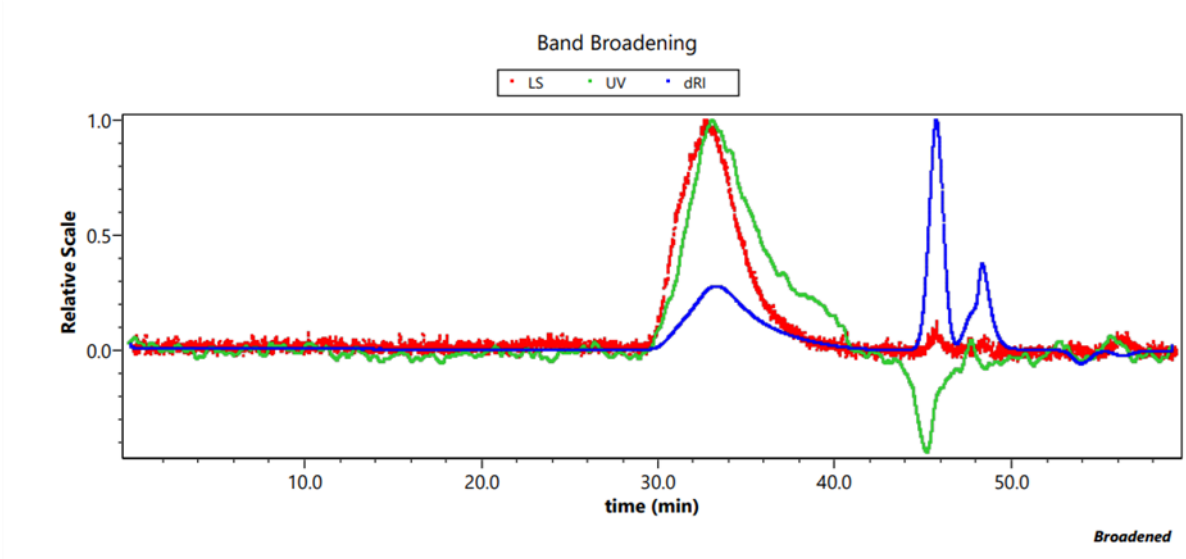

Peak Results

	Peak 1
Masses	
Calculated Mass (µg)	549.50
Mass Recovery (%)	100.0
Mass Fraction (%)	100.0
Molar mass moments (g/mol)	
Mn	6.125×10^3 (±7.655%)
Mp	7.730×10^3 (±5.243%)
Mv	n/a
Mw	7.429×10^3 (±5.798%)
Mz	9.175×10^3 (±16.495%)
Polydispersity	
Mw/Mn	1.213 (±9.603%)
Mz/Mn	1.498 (±18.185%)
rms radius moments (nm)	
rn	23.3 (±49.5%)
rw	24.6 (±37.7%)
rz	24.2 (±35.1%)

Figure 3.2. A) Schematic representation of mechanism of PIPOX synthesis, B) ^{1}H-NMR Spectrum of PIPOX and C) GPC Chromatogram of PIPOX.

3.3 Synthesis of PIPOX-PEI

Random copolymer of PIPOX and PEI was synthesized by time controlled partial hydrolysis of PIPOX in concentrated acid medium. In other words, PEI units were randomly introduced to PIPOX. The resulting polymer is denoted as PIPOX-PEI. Figure 3.3 shows hydrolysis reaction of PIPOX.

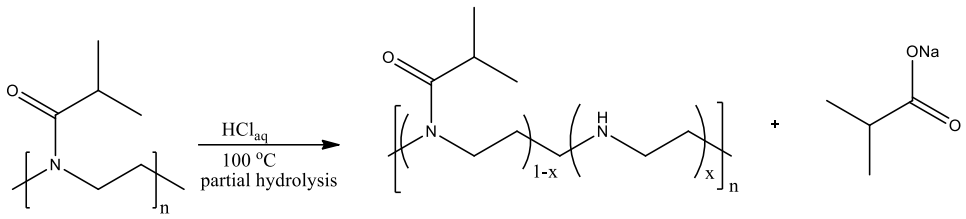

Figure 3.3. Synthesis of random copolymer of PIPOX-PEI.

Hydrolysis of PIPOX was confirmed using ^{1}H-NMR Spectroscopy (Figure 3.4). The peak at 2.94 ppm was correlated with protons which belong to ethyleneimine unit indicating successful hydrolysis of PIPOX. The percent (%) hydrolysis of PIPOX-PEI was calculated by dividing the area of the peak at 2.94 ppm, associated with the methylene protons of PEI (labelled as "d") by the sum of the areas of the peaks of methylene protons of PIPOX and PEI (labelled as "a" and "d", respectively) [117]. ^{1}H-NMR analysis program (Mestrelab) was used for peak integration. % hydrolysis was calculated as ~15%.

Degree of Hydrolysis = $\frac{Area\,(d)}{Area(d+a)} x100$

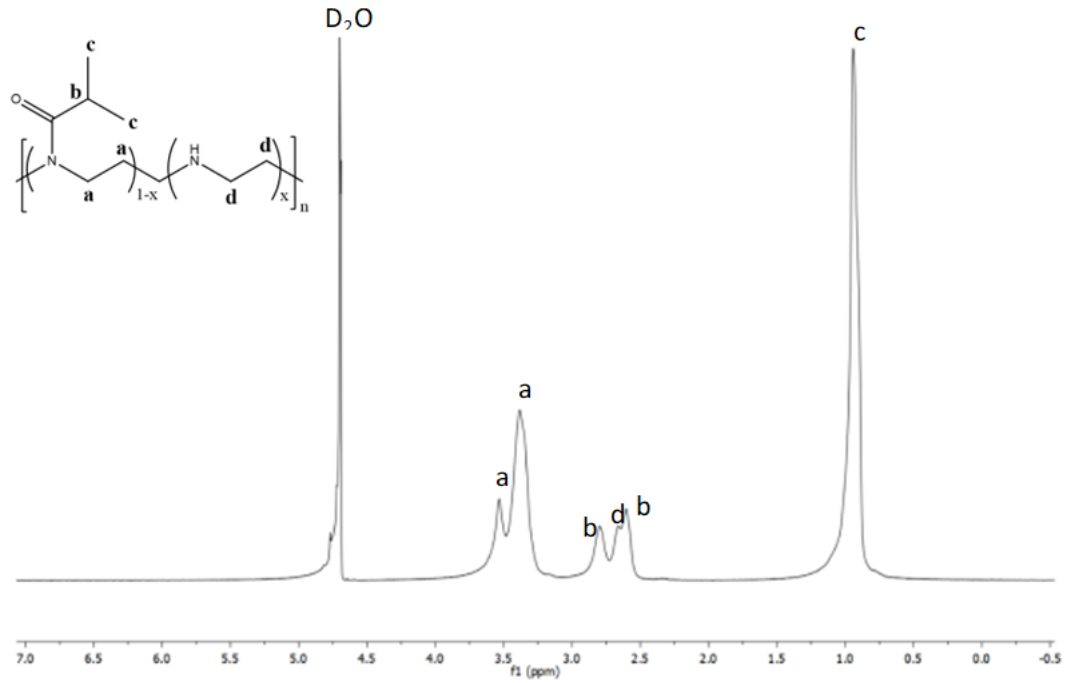

Figure 3.4. 1H-NMR spectrum of 15% hydrolyzed PIPOX-PEI.

3.4 Synthesis of $CaCO_3$

Two different types of $CaCO_3$ microparticles were synthesized using co-precipitation method. The first one, which will be denoted as "bare $CaCO_3$ microparticles" was synthesized using a procedure reported by Wang et.al. The second one, which will be denoted as "CUR loaded $CaCO_3$ microparticles" was synthesized by a procedure which was described earlier by Elbaz et al.

Infrared Spectroscopy has been used to distinguish calcium carbonate polymorphs. Absorption bands which are specific to the calcite polymorph of the carbonate ion are observed at 713 cm^{-1}, 848 cm^{-1}, and 1080 cm^{-1}, while the absorption bands of the vaterite form are recorded at 744 cm^{-1}, 876 cm^{-1}, and 1087 cm^{-1}. The peaks which belong to vibrations of CO_3^{2-} ion in vaterite form[48] are found at 744 cm^{-1} and 876 cm^{-1} and these peaks are usually used to distinguish the vaterite form. Figure 3.5 display

FTIR spectra of bare and CUR loaded $CaCO_3$ microparticles, respectively. Both particles present the characteristic peaks of the vaterite form.

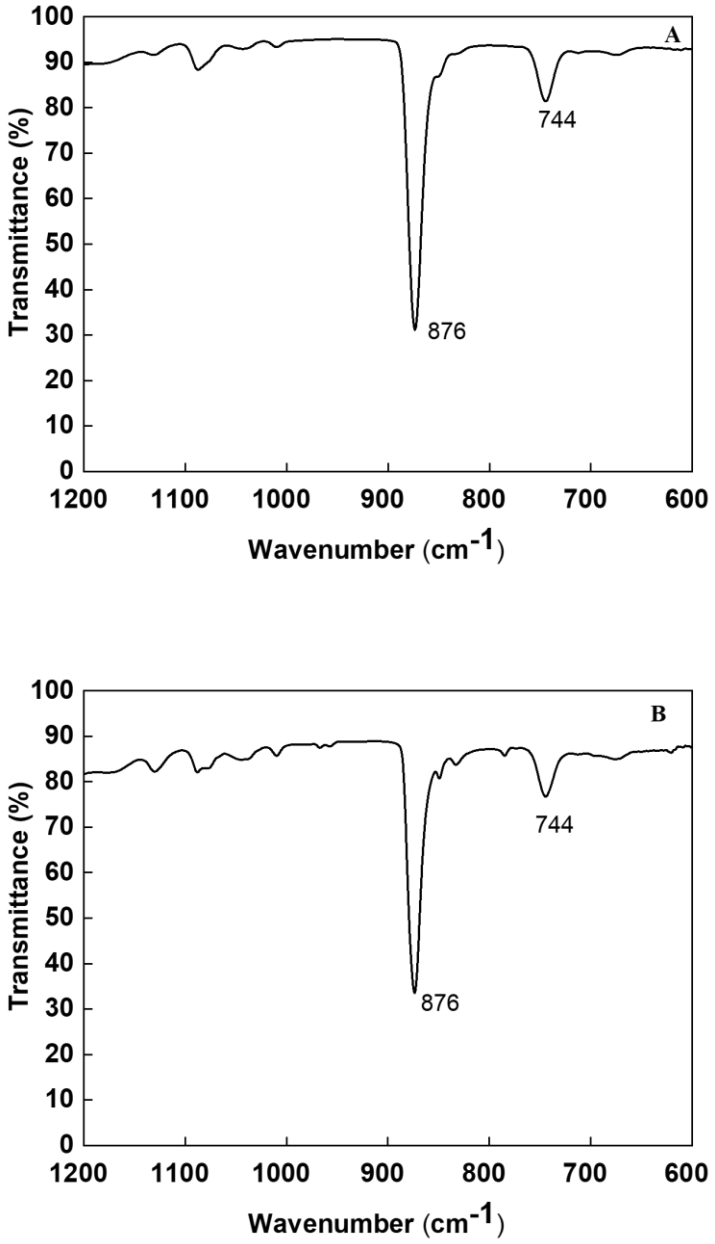

Figure 3.5. A) FTIR spectrum of $CaCO_3$ B) FTIR spectrum of CUR loaded $CaCO_3$.

The polymorph structure of $CaCO_3$ microparticles was further characterized by XRD analysis. XRD patterns of both microparticles (bare and CUR loaded) were

contrasted with X-ray diffraction standards reported in the literature[118]. Taking the peaks at 2 Θ = 21.004 º , 24.900 º , 27.047, 32.778 º , 42.759 º , 43.848º , 50.077 º , 55.805 º , 62.868º , 71.967º and 73.593 º, it was concluded that vaterite form was the predominance of the microparticles.

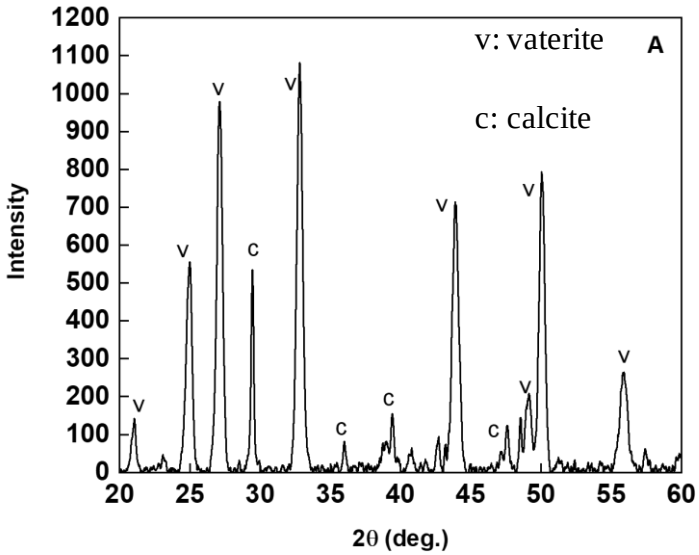

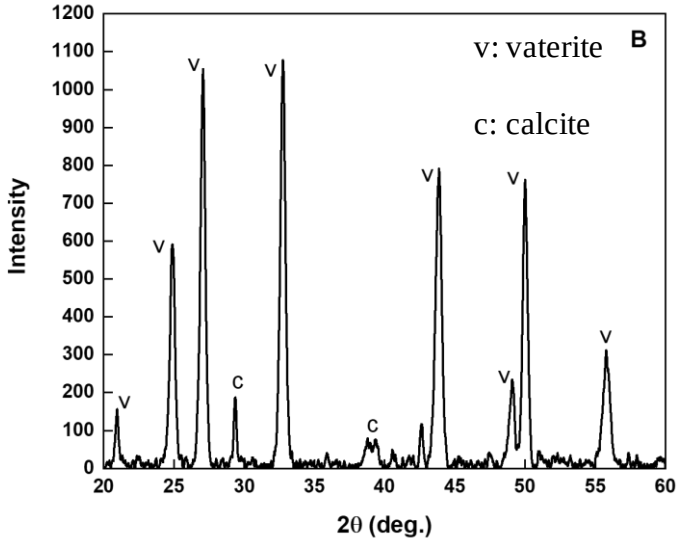

Figure 3.6. XRD patterns of A) Bare $CaCO_3$ Microparticles B) CUR loaded $CaCO_3$ Microparticles.

Morphology of $CaCO_3$ microparticles were characterized by Scanning Electron Microscopy (SEM) (Figure 3.7). Both bare and CUR loaded $CaCO_3$ microparticles were found to be spherical. The size of the particles ranged between 2.5-4 µm and 2.0 – 5.0 µm for bare and CUR loaded $CaCO_3$ microparticles, respectively.

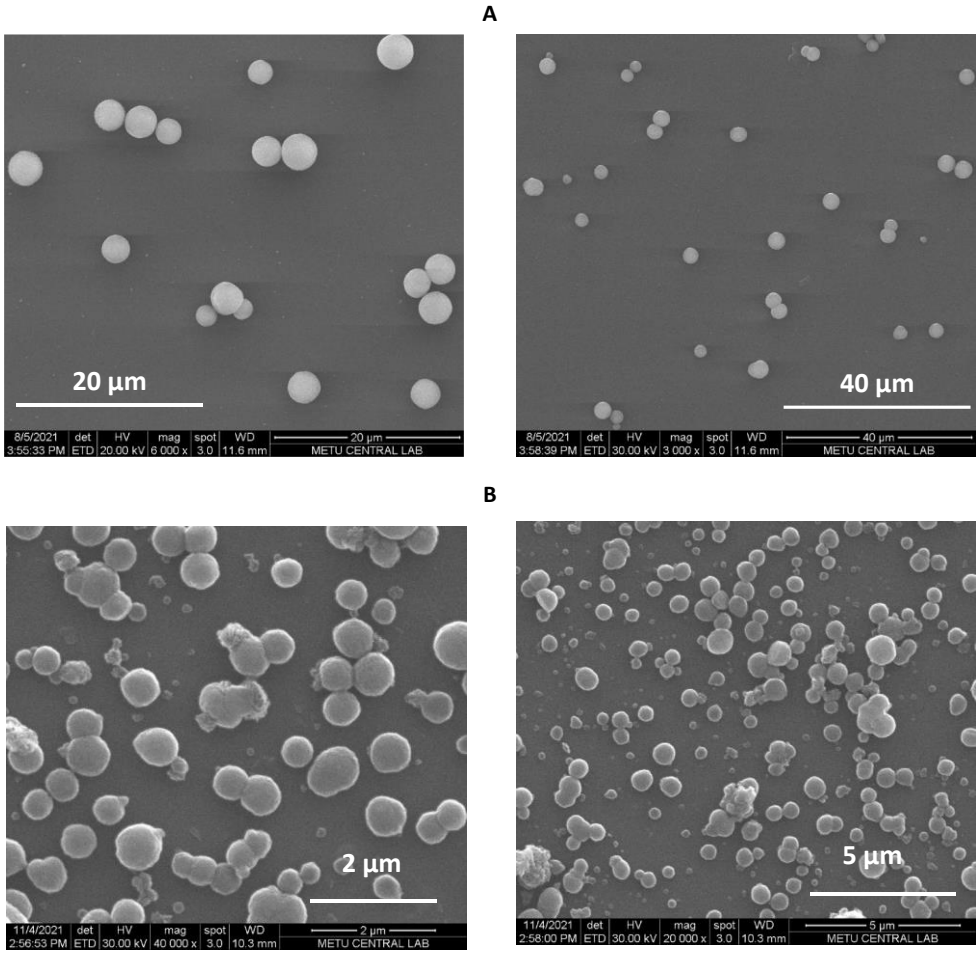

Figure 3.7. SEM image of A) Bare $CaCO_3$ microparticles B) CUR loaded $CaCO_3$ Microparticles.

Zeta potential of $CaCO_3$ microparticles is important for the design of the further surface modification. Therefore, finally, zeta potential measurements of $CaCO_3$ microparticles were conducted. As seen in Figure 3.8, both types of microparticles (bare and CUR loaded) have negative zeta potential which fall in the range of -27.3 ±1.97. mV and -29.1 ± 061 mV for bare and CUR loaded microparticles, respectively.

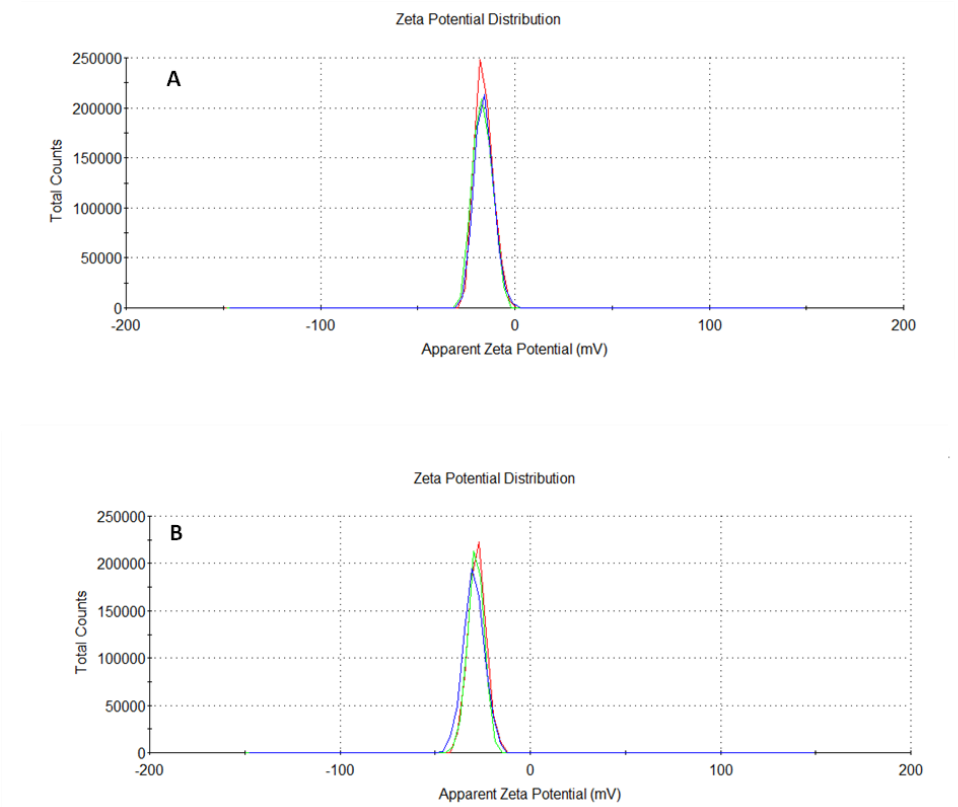

Figure 3.8. Zeta Potential Curve of A) Bare $CaCO_3$ microparticles B) CUR loaded $CaCO_3$ Microparticles.

3.5 LbL growth of TA and PIPOX-PEI on 2D substrate

Prior to LbL deposition onto $CaCO_3$ microparticles, LbL growth of TA and PIPOX-PEI was confirmed by depositing the polymer layers onto silicon wafers and measuring the dry thickness of the films after each layer construction. As seen in Figure 3.9, the film thickness increased linearly as the layer number increased, indicating successful LbL growth of TA and PIPOX-PEI. The thickness increment per bilayer was measured as ~4 nm. At pH 6.5, where TA layers are deposited, TA is partially ionized ($pK_{a,1}$ ~ 6.5 and $pK_{a,2}$ ~ 8)[106]. Therefore, both hydroxyl and phenolate groups were present on TA molecules. The pK_a for secondary amine groups is reported as ~ 8.5 in the literature [35]. At pH 6, where PIPOX-PEI layers were deposited, PEI units were expected to be positively charged. Therefore, the driving force for multilayer layer growth can be attributed to:

i) hydrogen bonding interactions between hydroxyl groups of TA and amide groups of PIPOX;
ii) electrostatic interactions between the phenolate groups of TA and the protonated secondary amine groups on the PEI units of PIPOX-PEI.

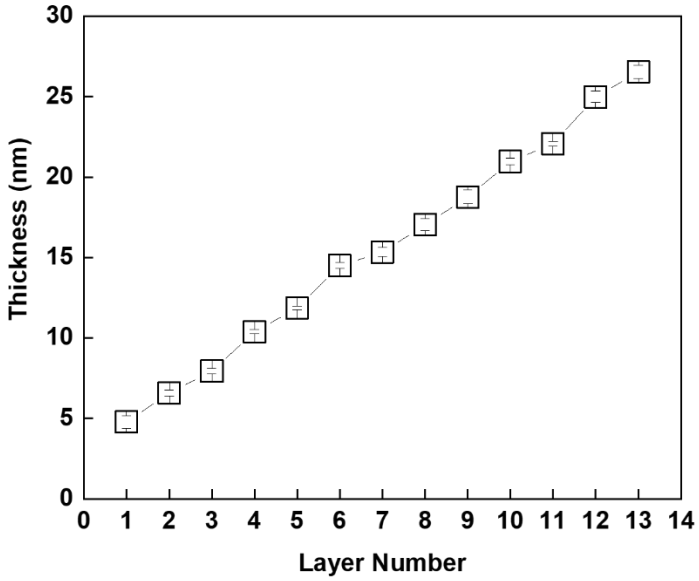

Figure 3.9. LbL growth of TA and PIPOX-PEI. Multilayers were deposited onto BPEI coated silicon wafers. The thickness of BPEI precursor layer was 3 nm and is included in the thickness values.

3.6 Covalent Crosslinking of TA/PIPOX-PEI Multilayers

Covalent crosslinking between PIPOX-PEI and TA was achieved using $NaIO_4$ as the crosslinking agent. 14-layer PIPOX-PEI/TA films were immersed into 10 mM $NaIO_4$ solution at pH 5 for 5 minutes. The covalent bond formation was expected to occur between PEI units of PIPOX-PEI and TA through oxidation of phenolic hydroxyl groups of TA to quinone groups by IO_4^- anions and the formation of covalent bonds between the quinone groups and the secondary amine groups of PEI units. As shown in Figure 3.10A, there are two possible mechanisms for the crosslinking reaction. One of them is Michael addition, suggesting formation of N-C bond. The other one is Schiff Base reaction, suggesting C=N bond formation. After treatment of the films with $NaIO_4$, ~10% loss in film thickness was recorded (Figure 3.10B)[119]. This decrease in film thickness has been attributed to stronger interaction among the layers and entrapment of less water molecules within the film structure.

Unfortunately, the covalent crosslinking between PIPOX-PEI and TA could not be confirmed through FTIR Spectroscopy. Formation of covalent crosslinks between the layers was indirectly verified through the difference in the stability of the crosslinked and non-crosslinked films. 14-layer PIPOX-PEI and TA films were prepared and exposed to PBS at either decreasing or increasing pH at 25°C. The starting point for the decreasing and increasing pH directions was 6.5 and 7.5, respectively. Figure 3.10C contrasts the thickness fraction retained at the surface at each pH value. Fractions were calculated by dividing the thickness to the initial film thickness. Both films showed increase in the fraction as the pH was decreased. Protonation of TA and loss of electrostatic interactions between TA and PIPOX-PEI led to weakening of the interactions within the multilayers and entrapment of water molecules, resulting in an increase in the fraction. When the films were exposed to increasing pH conditions, the onset of film disintegration for non-crosslinked films was observed at pH 9.5. Multilayers were totally erased from the surface at pH 10.5. The dissolution of the multilayers can be explained by ionization of TA and loss of hydrogen bonding interactions between PIPOX-PEI and TA. For crosslinked films, ~80 % of the film retained at the surface even at pH 11.5. The enhanced stability of crosslinked films was attributed to the formation of covalent crosslinks between the layers. In this way, $NaIO_4$ induced crosslinking was indirectly shown through stability experiments.

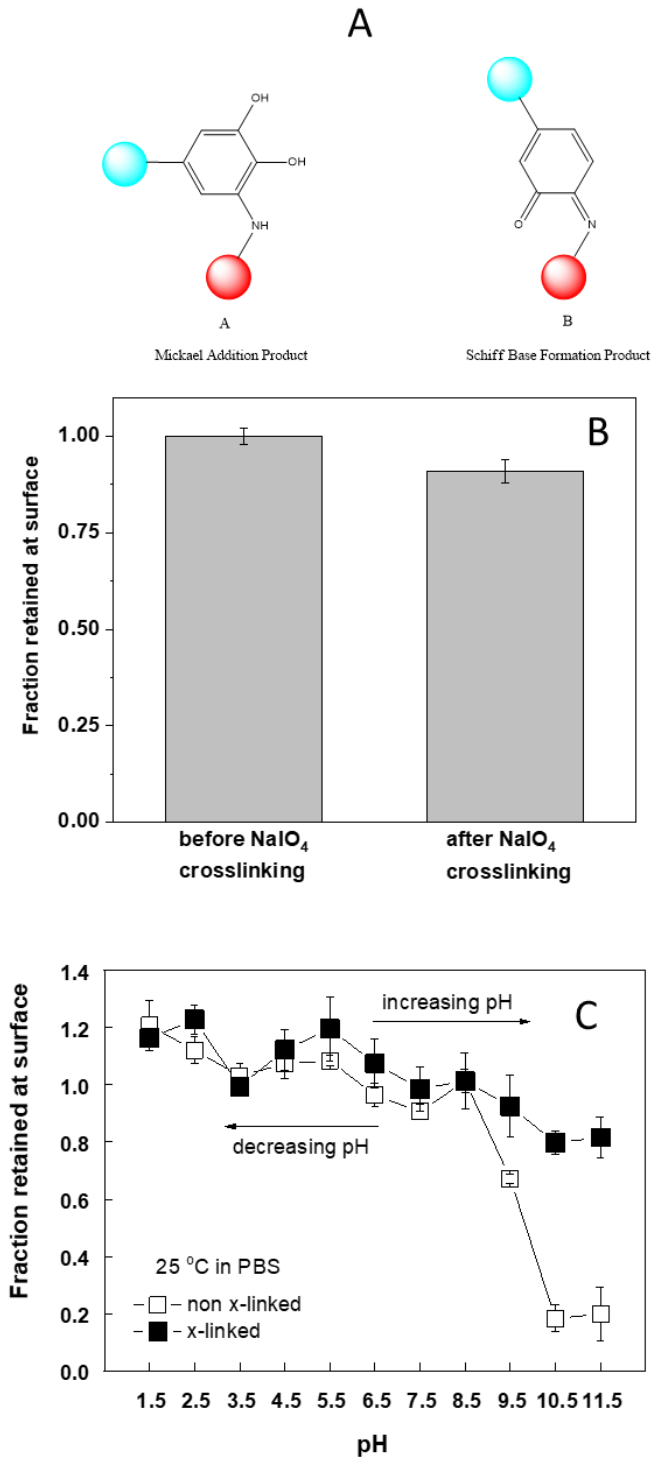

Figure 3.10. A) Schematic representation of possible mechanisms for the crosslinking reaction. (Modified from ref [119]) B) Fraction retained at the surface of the films after $NaIO_4$ treatment C) The thickness fraction retained at the surface

of crosslinked and noncross-linked multilayers upon exposure to PBS at either decreasing or increasing pH values at 25 °C.

3.7 Stability of TA/PIPOX-PEI Multilayers under drug release conditions

As will be discussed in the further sections, two different anticancer drugs will be encapsulated in the particles as well as in the multilayers. Considering the acidic nature of tumor tissues, release of both drugs will be investigated at both neutral and acidic environment. Therefore, prior to drug release studies, stability of multilayers was examined in PBS at both pH 7.4 and pH 5.5 at 37 °C. To understand the temperature-responsive behavior of the films, stability experiments was also conducted at 25 °C at both pH values.

Stability of TA/PIPOX-PEI multilayers in PBS at pH 7.4/37°C and pH 5.5/37°C was examined with respect to time. For comparison, similar stability experiments were also conducted at 25°C to understand the temperature-dependent physicochemical changes within the multilayers. First, 14-layer (non-crosslinked) films were prepared and separately immersed into PBS at the following conditions: i) pH 7.4/37°C; ii) pH 5.5/37°C; iii) 7.4/25°C; iv) 5.5/25°C. The films were removed from the solution at certain time intervals, followed by drying and thickness measurements. Figure 3.11A contrasts the thickness fraction retained at the surface at pH 7.4/37°C and pH 5.5/37°C. An increase in film thickness (~ 10 %) was recorded for both films in the first 4 hours. The increase in thickness was x4 times greater at pH 7.4/37°C than pH 5.5/37°C after hours of immersion in PBS. The increase in thickness was correlated with water molecules entrapped within the multilayers due to the following reasons:

i) Penetration of salt ions into the multilayers might have led to an increase in osmotic pressure, followed by diffusion of water molecules into the film[108]. At pH 7.4, TA is further ionized and the association between the layers weakened which might have facilitated the uptake of water molecules by the multilayers. It must be borne in mind that deposition pH was 6 and 6.5 for PIPOX and TA, respectively. At pH 5.5, the

hydrogen bonding driven association among the layers was greater, making multilayers more intense and uptaken water molecules less compared to pH 7.4.

ii) PIPOX exhibits LCST-type phase behavior between 36-40 °C depending on its molecular weight. PIPOX transforms from extended to coil conformation at 37°C. This conformational change was expected to be more possible within the multilayers at pH 7.4 where the layers associated relatively weak compared to pH 5.5. The more compact form of PIPOX possibly formed voids within the film which at the end resulted in greater amount of water uptake by the film at pH 7.4. To confirm that the swelling of multilayers originated from LCST-type phase behavior of PIPOX, similar experiments were conducted at 25°C (Figure 3.11B). The extent of increase in thickness was lower for both films compared to 37°C. Also, the extent of swelling was similar at pH 7.4 and pH 5.5. These results support the water uptake arising from temperature-responsive behavior of PIPOX.

The thickness of multilayers did not further increase at pH 5.5/37°C beyond 8 hours. On the other hand, ~40% decrease in thickness was recorded at pH 7.4/37°C, associated with the loss of layers from the surface. The extent of swelling at the end of 8 hours at pH 7.4/37°C could be reached at the end of 24 hours at pH 7.4/25°C.

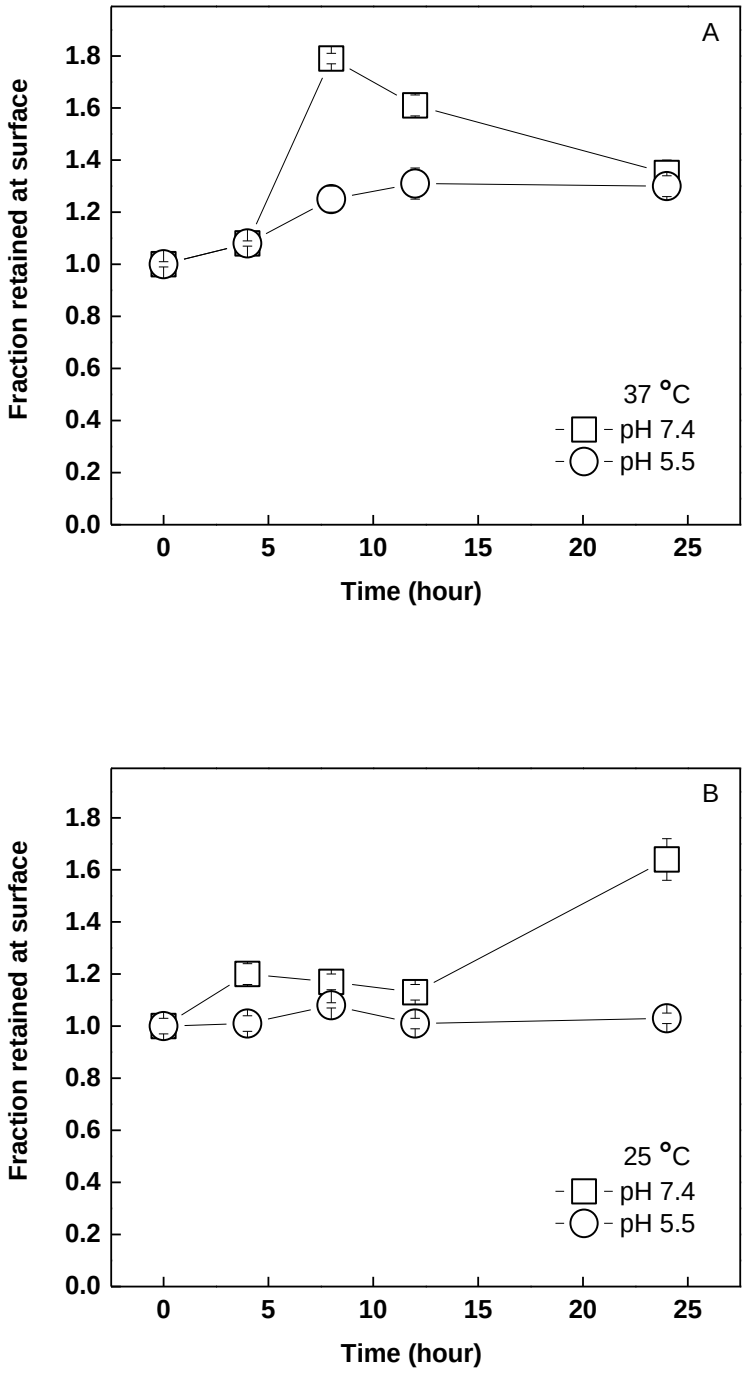

Figure 3.11. Fraction retained at surface as a function of time at A) 37 ^{o}C pH 7.4 and 5.5 B) 25 ^{o}C pH 7.4 and 5.5.

3.8 Stability of covalently cross-linked TA/PIPOX-PEI Multilayers under release conditions

Similar to the stability experiments discussed in the previous section, stability of covalently crosslinked TA/PIPOX-PEI multilayers were followed in PBS at pH 7.4/37°C; pH 7.4/25°C; pH 5.5/37°C and pH 5.5/25°C, Figure 3.12 presents the fraction retained at the surface of crosslinked films under various conditions. The data for non-crosslinked films was plotted for comparison. Importantly, the swelling observed in the non-crosslinked films at pH 7.4/37°C was not recorded for covalently crosslinked films. The swelling observed at 24th hours in non-crosslinked films at pH 7.4/25°C was also not observed in the crosslinked films. As mentioned earlier, the films show less swelling at pH 5.5, where the layers interact more strongly with each other. The extent of swelling was lower at pH 5.5/37°C compared to noncross-linked films. No swelling was observed for both crosslinked and non-crosslinked films at pH 5.5/25°C at all. In summary, crosslinking suppressed the swelling behavior of the films depending on pH, temperature, and salt concentration. This was most evident at pH 7.4 and 37°C, where the films swelled the most.

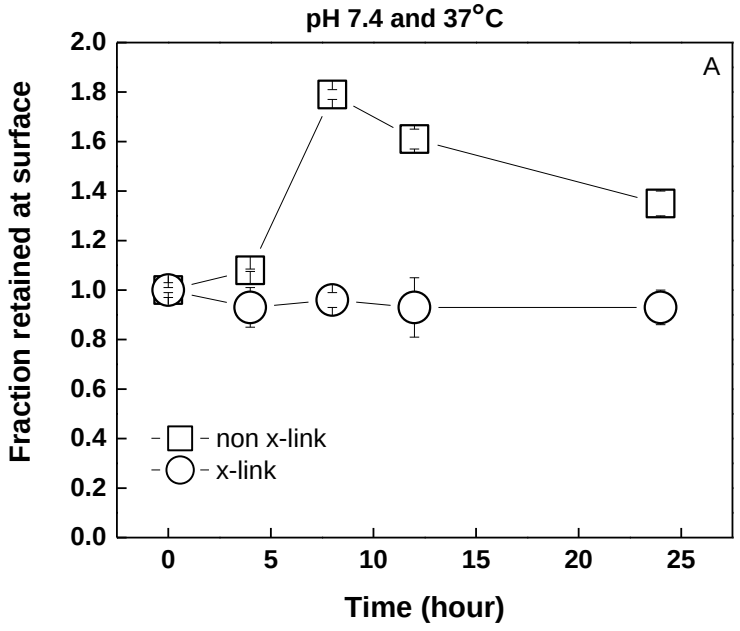

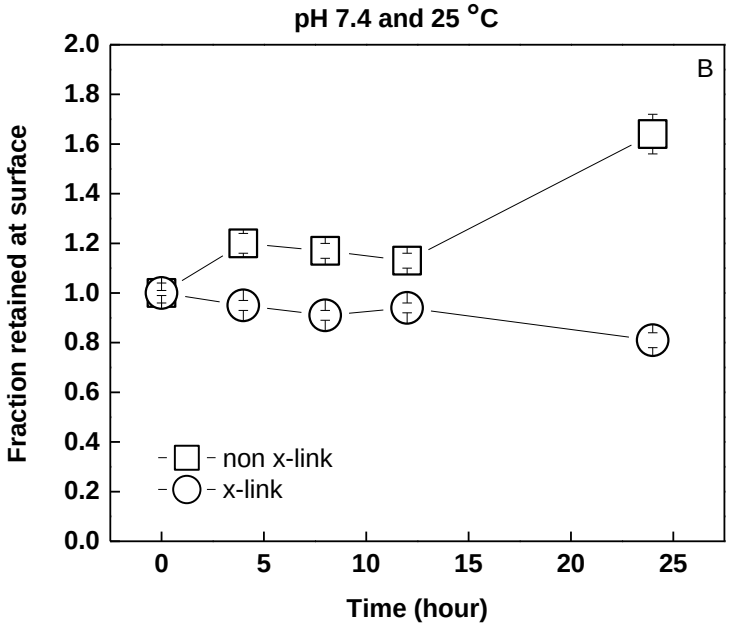
pH 7.4 and 25 °C
B
Fraction retained at surface
2.0
1.8
1.6
1.4
1.2
1.0
0.8
0.6
0.4
0.2
0.0
0
5
10
15
20
25
Time (hour)
non x-link
x-link

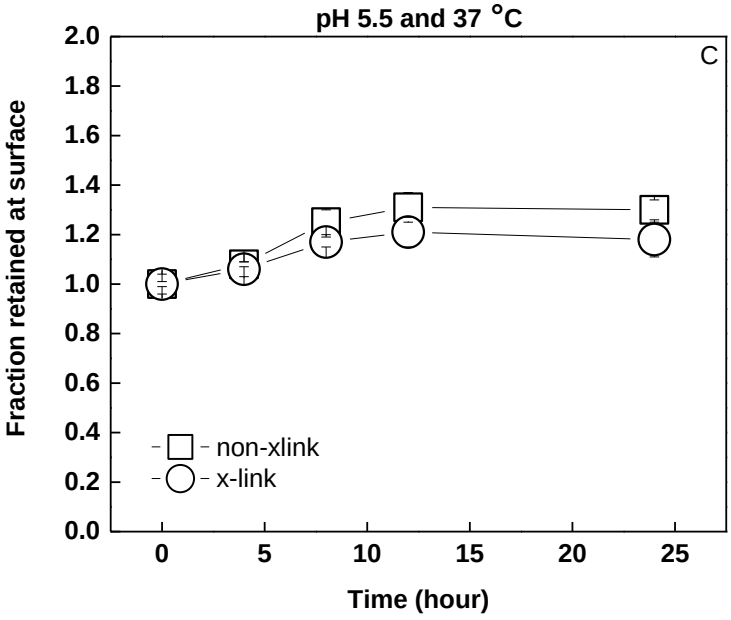
pH 5.5 and 37 °C
C
Fraction retained at surface
2.0
1.8
1.6
1.4
1.2
1.0
0.8
0.6
0.4
0.2
0.0
0
5
10
15
20
25
Time (hour)
non-xlink
x-link

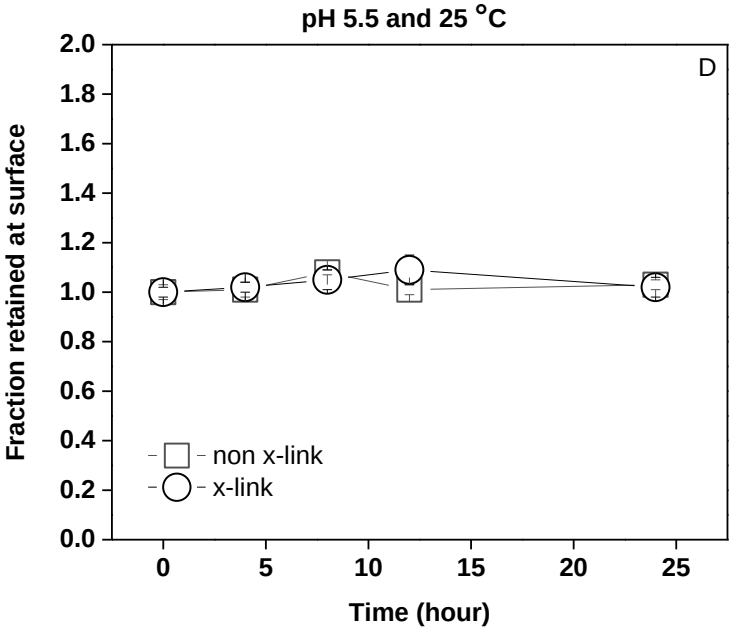

Figure 3.12. Time-dependent variation of the fraction retained at surface of crosslinked films in the presence of $NaIO_4$ immersed in PBS at (A) pH 7.4/37°C; (B) pH 7.4/25°C; (C) pH 5.5/37°C; (D) pH 5.5/25°C.

3.9 LbL Deposition of TA and PIPOX-PEI onto $CaCO_3$ microparticles

After assuring the LbL deposition on 2D substrates, TA and PIPOX-PEI layers were deposited onto both bare and CUR loaded $CaCO_3$ microparticles. LbL growth was followed by measuring the zeta potential of the microparticles after each layer deposition. The change in zeta potential was assumed as an indication of LbL growth. Figure 3.13A and 3.13B presents the the zeta potential measured after each layer for both particles. Both particles provided similar zeta potential values after deposition of each TA and PIPOX-PEI layer. The mean zeta potential value changed from -27.3 ± 1.97 mV to -31.8 ± 0.7 mV after the first TA layer deposition due to phenolate groups of TA ($pKa,_1 \sim 6.5$ and $pKa,_2 \sim 8$)[106]. The driving force for the adhesion of TA onto $CaCO_3$ microparticles was electrostatic interaction between Ca^{2+} and phenolate groups of TA together with the hydrogen bonds between the SO_3^{2-} units of PSS which are expected to be inside and on the surface of the $CaCO_3$

microparticles and the OH groups of TA. Besides, π-π stacking interactions between the aromatic rings of TA and the phenyl rings of PSS could have also contributed to the deposition of TA at the surface[110]. After the deposition of the second layer (PIPOX-PEI), the zeta potential value was recorded as ~-18.8 ± 0.6 mV. The shift of the zeta potential towards less negative value was due to the neutral units of PIPOX screening the negative charges on the microparticles. For the rest of the layers, the zeta potential changed to more negative values after each TA layer and to lower negative values after each PIPOX-PEI deposition. Figure 3.13C and 3.13D show the zeta potential distribution curve of the microparticles after each layer.

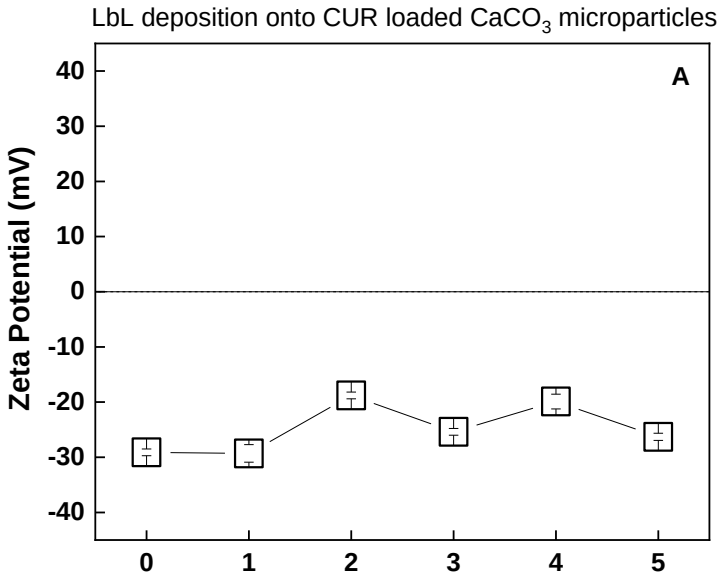

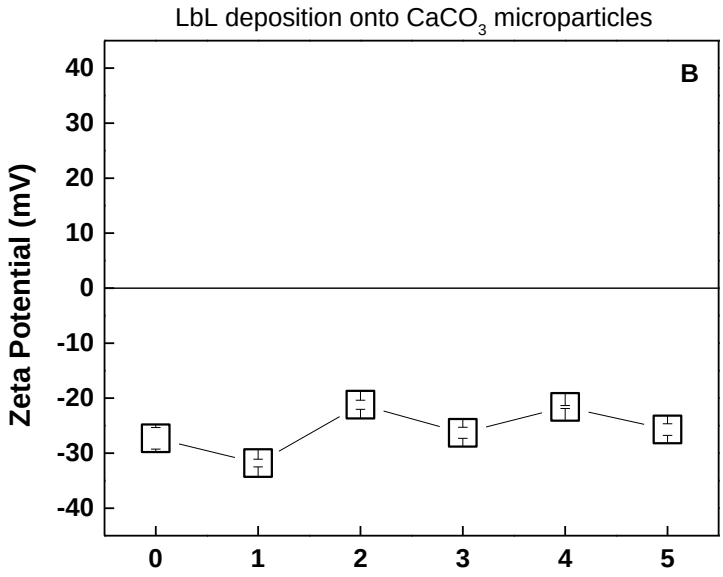
LbL deposition onto CaCO3 microparticles
B
Zeta Potential (mV)
40
30
20
10
0
-10
-20
-30
-40
0
1
2
3
4
5

c

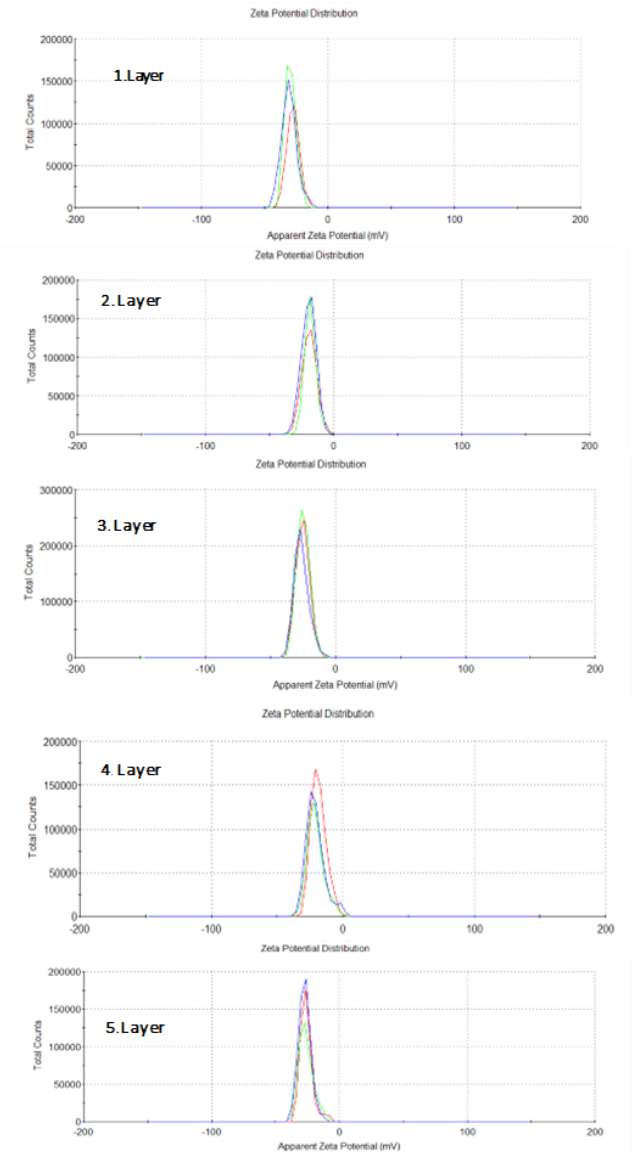
Zeta Potential Distribution
1.Layer
Total Counts
Apparent Zeta Potential (mV)
Zeta Potential Distribution
2.Layer
Total Counts
Zeta Potential Distribution
3.Layer
Total Counts
Apparent Zeta Potential (mV)
Zeta Potential Distribution
4.Layer
Total Counts
Zeta Potential Distribution
5.Layer
Total Counts
Apparent Zeta Potential (mV)

D

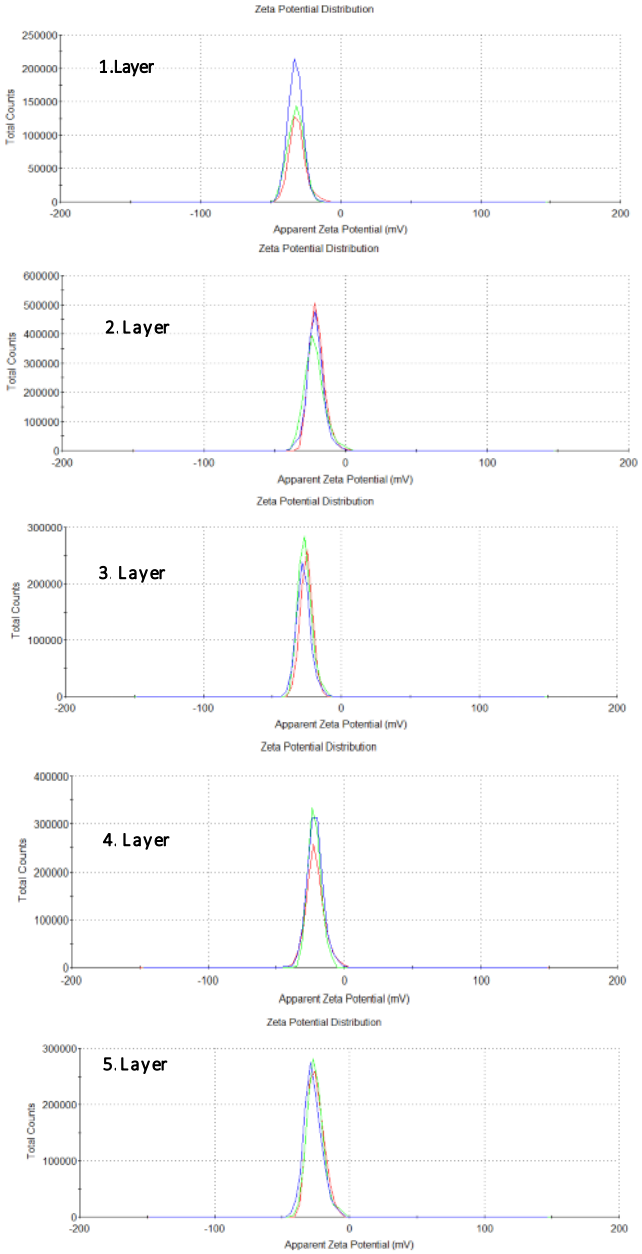

Figure 3.13. A) Change in zeta potential after each layer deposition on CUR-loaded $CaCO_3$ microparticles. B) Change in zeta potential after each layer deposition on bare $CaCO_3$ microparticles. C) Zeta-potential distribution curves obtained after each layer deposition CUR-loaded $CaCO_3$ microparticles. D) Zeta-potential distribution curves obtained after each layer deposition on bare $CaCO_3$ microparticles.

Morphology of LbL coated bare and CUR loaded microparticles was examined through SEM imaging. As seen in Figure 3.14, the aggregation was at a greater extent for LbL coated CUR loaded microparticles. This was possibly due to hydrophobic CUR, enhancing the hydrophobic-hydrophobic interactions between the CUR loaded particles.

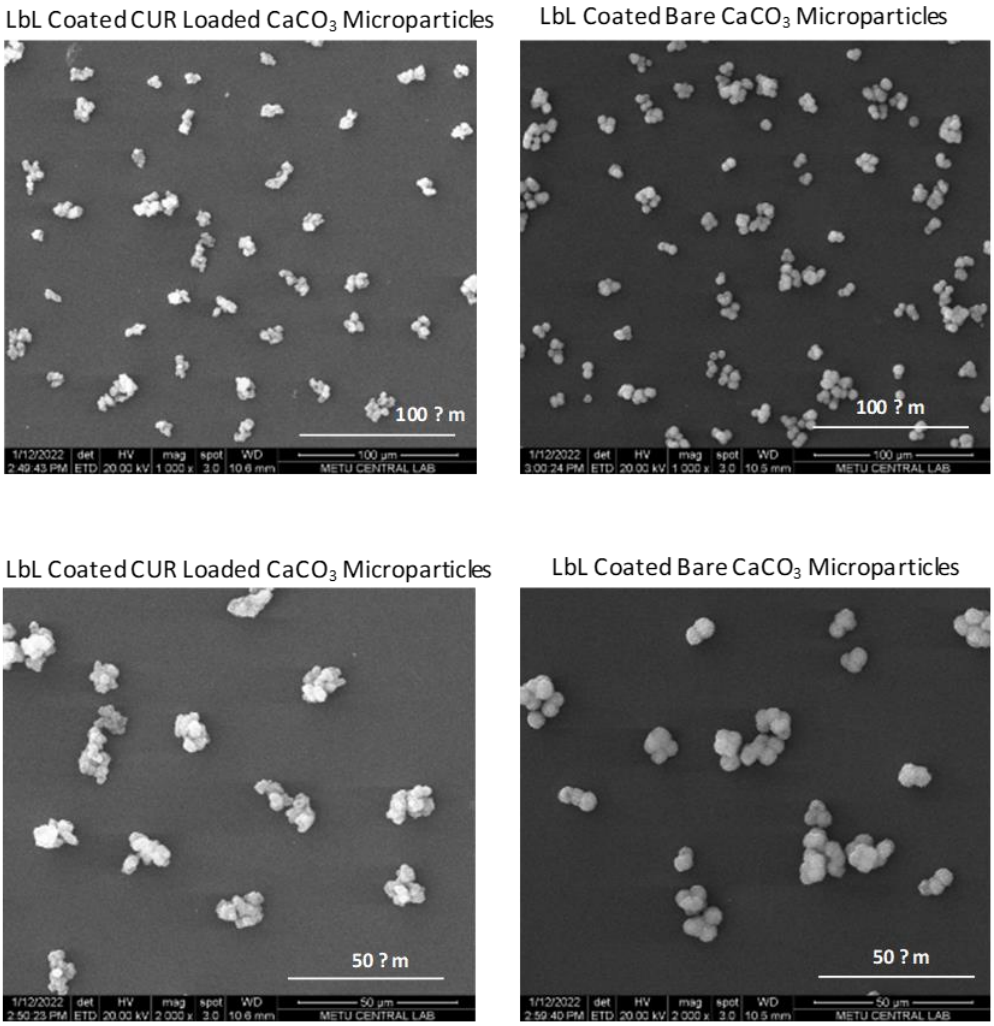

Figure 3.14. (A) SEM image of CUR-loaded $CaCO_3$ microparticles coated with 5-layer PIPOX-PEI/TA. B) SEM image of bare $CaCO_3$ microparticles coated with 5-layer PIPOX-PEI/TA.

3.10 Crosslinking of LbL coated particles

Crosslinking of both types of LbL-coated microparticles (deposited onto bare and CUR loaded $CaCO_3$ microparticles) was performed using $NaIO_4$ solution. However, it was observed that the color of LbL-coated CUR loaded microparticles changed after treatment with 10 mM $NaIO_4$ solution. To further understand the reason of the color change, 10 mg CUR loaded $CaCO_3$ microparticles were exposed to $NaIO_4$ solution at varying concentrations and shaked for 5 minutes using a vortex mixer. Then, $NaIO_4$ treated particles were dispersed into 20% v/v EtOH-PBS solution at 25 °C and the fluorescence intensity was measured. As a control, non-treated microparticles were also dispersed into EtOH-PBS mixture. Figure 3.15 contrasts the change in fluorescence intensity of CUR after $NaIO_4$ treatment. The significant decrease in fluorescence intensity of CUR upon treatment with $NaIO_4$ solution was attributed to degradation of CUR. For this reason, crosslinking was only performed to TA/PIPOX-PEI multilayer coated bare $CaCO_3$ microparticles.

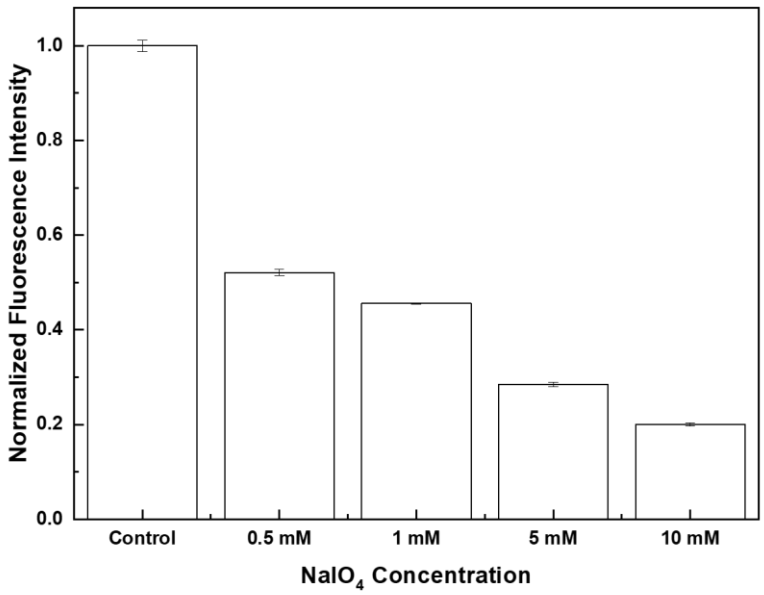

Figure 3.15. The change in fluorescence intensity of CUR after varying concentration of $NaIO_4$ treatment.

3.11 Preparation of hollow capsules

Preparation of hollow capsules was performed with non-crosslinked and crosslinked TA/PIPOX-PEI multilayer coated bare $CaCO_3$ microparticles. LbL-coated microparticles were dispersed into 0.25 M EDTA solution, followed by stirring using a vortex mixer for 15 minutes. The microparticles were precipitated and rinsed with 10 mM phosphate buffer. This cycle was repeated for 3 times to assure core dissolution. Figure 3.16A shows SEM image of hollow noncross-linked TA/PIPOX-PEI multilayer capsules. The absence of Ca in the EDX analysis of hollow LbL capsules confirm successful core dissolution.

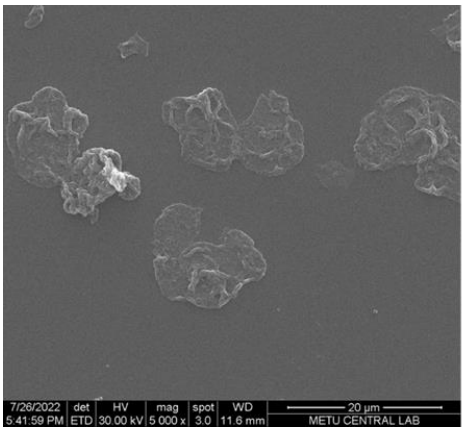
7/26/2022 det HV mag spot WD 20 µm
5:41:59 PM ETD 30.00 kV 5 000 x 3.0 11.6 mm METU CENTRAL LAB

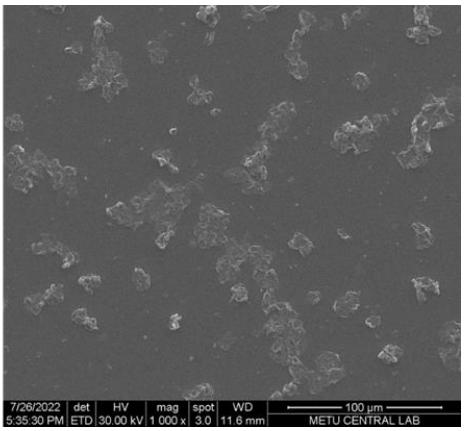
7/26/2022 det HV mag spot WD 100 µm
5:35:30 PM ETD 30.00 kV 1 000 x 3.0 11.6 mm METU CENTRAL LAB

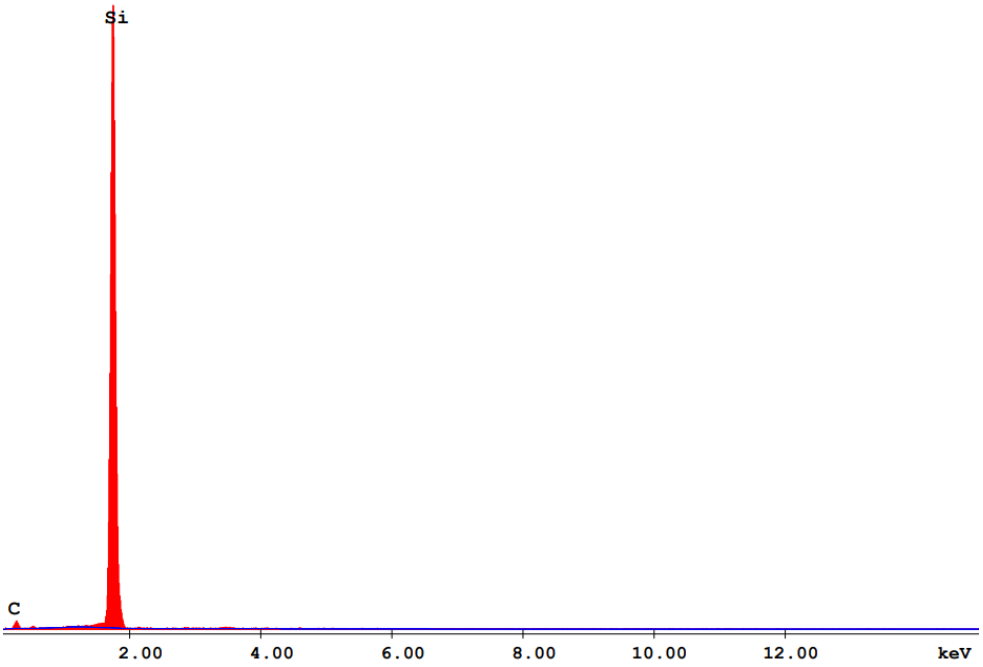
Si
C
2.00
4.00
6.00
8.00
10.00
12.00
keV

EDAX ZAF Quantification (Standardless)
Element Normalized
SEC Table : Default

Element	Wt %	At %	K-Ratio	Z	A	F
C K	34.70	55.41	0.0337	1.0323	0.0940	1.0001
SiK	65.30	44.59	0.6184	0.9821	0.9642	1.0000
Total	100.00	100.00				

Element	Net Inte.	Bkgd Inte.	Inte. Error	P/B
C K	18.52	2.47	3.99	7.50
SiK	2282.85	6.66	0.32	342.64

Figure 3.16. A) SEM image of hollow noncross-linked capsule. B) EDX analysis of hollow noncross-linked capsule.

3.12 Drug release studies

3.12.1 CUR release from LBL coated CUR loaded microparticles

CUR release was followed from TA/PIPOX-PEI coated CUR loaded $CaCO_3$ microparticles.

As explained in detail in Section 2.2.11, approximately 0.132 ± 0.002 g of $CaCO_3$ microparticles were obtained after synthesis. The amount of CUR loaded into $CaCO_3$ microparticles was quantified through fluorescence spectroscopy and the amount of CUR was found as ~ 8.2 ± 1.1 mg. CUR release from LbL coated CUR loaded $CaCO_3$ microparticles was first performed in PBS. However, CUR is a hydrophobic molecule, and the amount of release was very low in aqueous environment. Therefore, it could not be successfully quantified. To induce CUR release from microparticles, ethanol was added into PBS at 20 % in volume and CUR release was monitored under different pH and temperature conditions.

5 mg LbL modified particles were dispersed in 4 mL of 80% PBS-EtOH mixture and stirred at 100 rpm. The particles were precipitated and the amount of CUR in the supernatant was determined by following the fluorescence intensity of CUR at 525

nm nm. 4 mL of fresh 80% PBS-EtOH mixture was then added onto the precipitated LbL microparticles and CUR release was continued.

The amount of CUR in the supernatant was too high and the fluorescence intensities lied outside of the linear range in the calibration curve. Therefore, the supernatants obtained at the end of the first and third hours were first diluted with PBS-EtOH solution containing 20% vol. with 1:5 ratio. Then, this solution was rediluted with pure ethanol with 1:1 ratio, finally resulting in 60 % ethanol in the solution. CUR release was quantified using calibration curves presented in Appendix 3 and 4 The amounts of CUR released at the end of the fifth and seventh hours were relatively low compared to the first and third hours. Therefore, dilution of the release solution was not required. Since the supernatant was discarded after each measurement and fresh 20% v/v EtOH-PBS mixture was added instead, the concentration values indicated in Figure 3.17 are cumulative concentration values.

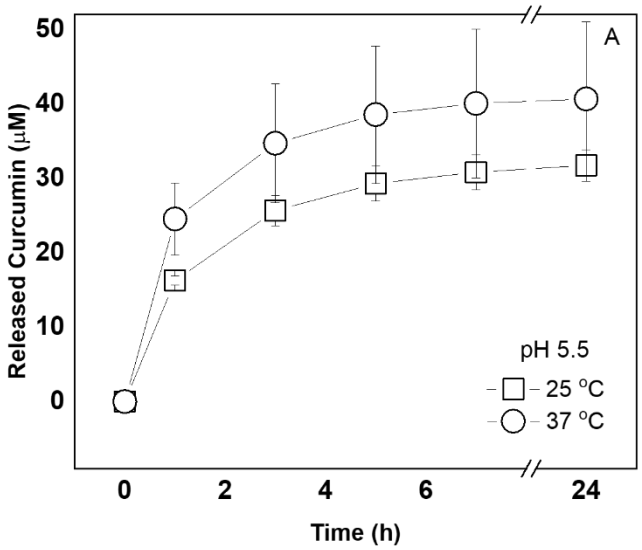

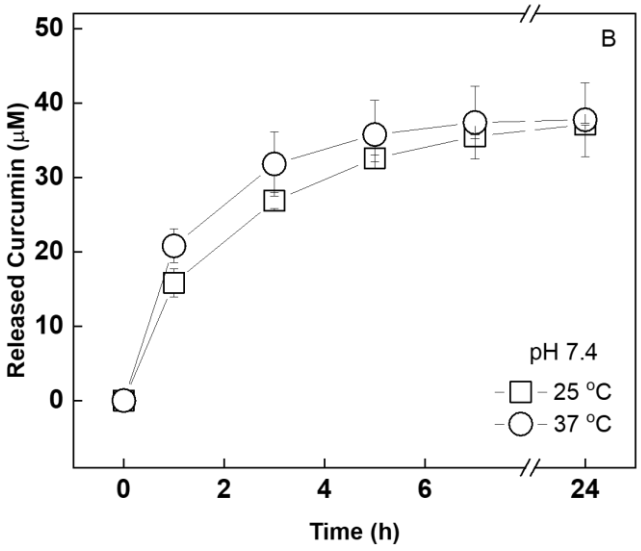
B
Released Curcumin (μM)
Time (h)
pH 7.4
25 °C
37 °C

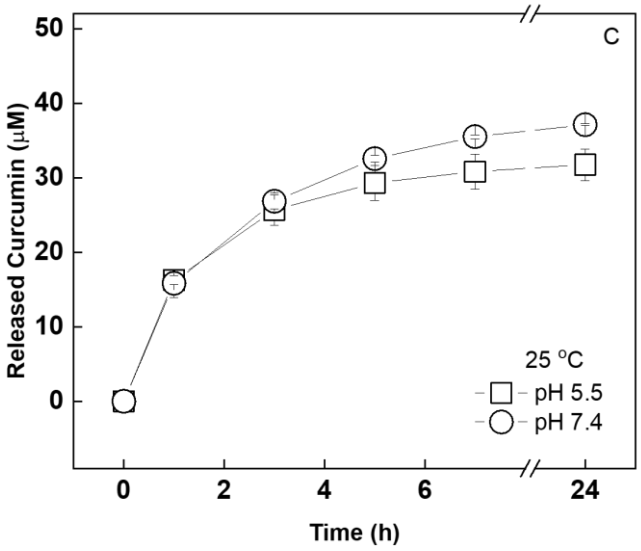
C
Released Curcumin (μM)
Time (h)
25 °C
pH 5.5
pH 7.4

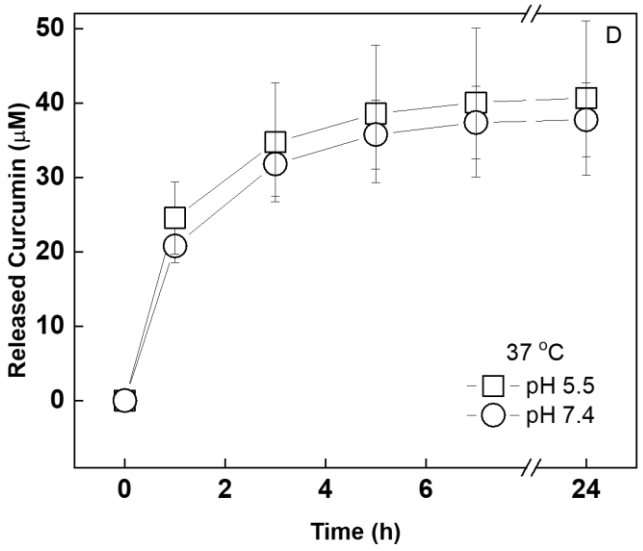

Figure 3.17. Released CUR from PIPOX-PEI/TA coated CUR loaded CaCO3 microparticles A) 25°C and 37°C pH 5.5; B) 25°C and 37°C pH 7.4; C) 37°C pH 7.4 and pH 5.5; D) 25°C pH 7.4 and pH 5.5.

Figure 3.17A and 3.17B show the effect of temperature on CUR release at pH 5.5 and pH 7.4, respectively. No significant difference in the amount of CUR release was observed between 25°C and 37 °C at both pH values. Figure 3.17C and 3.17D show the effect of pH on CUR release at 25°C and 37 °C, respectively. Similarly, no significant effect of pH on the amount of CUR release from the particles was recorded. Despite the pH and temperature responsive LbL coating, stimuli responsive release of CUR was not observed. As obvious from the large error bars especially at 37 °C, batch-to-batch variation was also remarkable. The challenges and the sources of errors during CUR release in 20% v/v EtOH-PBS mixture and quantification are summarized below:

i. The evolution of fluorescence intensity of CUR (0.001 mg/mL) in 20% v/v EtOH-PBS mixture was followed as a function of time. Before each measurement, 1 ml of pure EtOH was added to 1 ml of CUR solution placed in the cuvette. Thus, similar to the release experiments, the final % EtOH (by volume) in the mixture was 60%. As seen in Figure 3.18, a decrease in the fluorescence intensity of CUR was observed over time at pH 7.4, both at 25 °C and at 37 °C. This decrease in fluorescence intensity was more pronounced at 37 °C. This decrease was correlated with the degradation of CUR. For this reason, the quantified amount of CUR might possibly be lower than the actual released amount, especially for pH 7.4/37 °C condition. Therefore, the discussion on pH and temperature sensitive release of CUR need reassessment after cell culture studies.

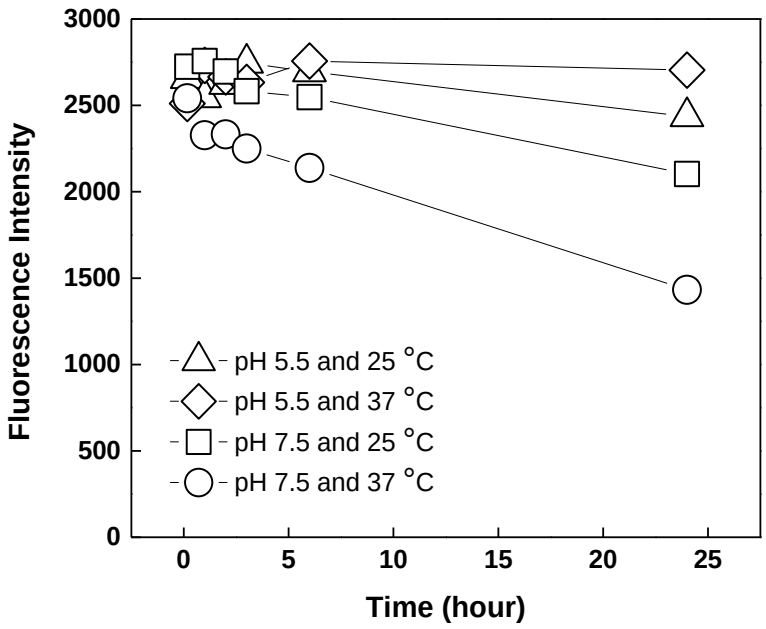

Figure 3.18. Time dependent variation of fluorescence intensity of CUR.

ii. It was also found that PIPOX-PEI/TA films lost their pH and temperature-dependent swelling properties when 20 % by volume ethanol was added into PBS. Figure 3.19 contrasts the time-dependent variation of the fraction retained at the surface of PIPOX-PEI/TA films upon exposure to either PBS or PBS solution containing 20 % vol. EtOH. The difference in the behavior of the multilayers was attributed to the shift in the critical temperature of PIPOX-PEI in the presence of ethanol. Note that, Pooch et al. reported a shift in the critical temperature of PIPOX to higher values in the presence of methanol[120].

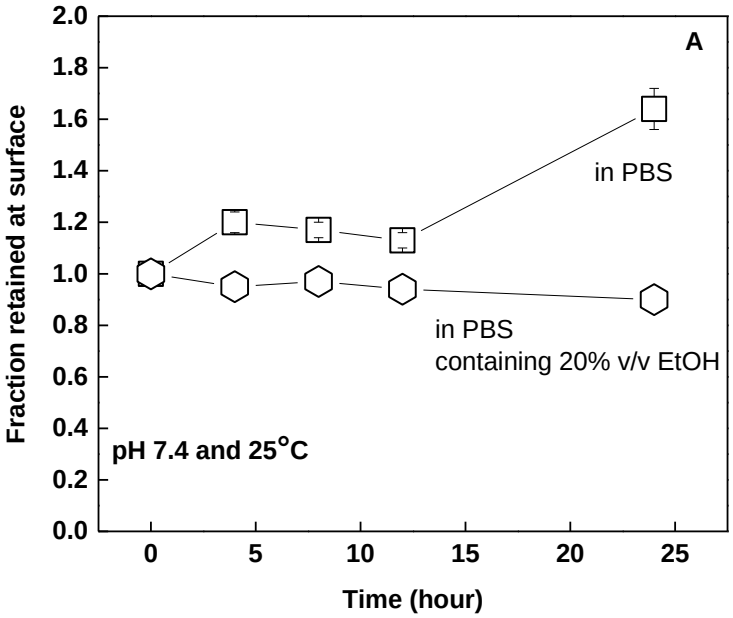

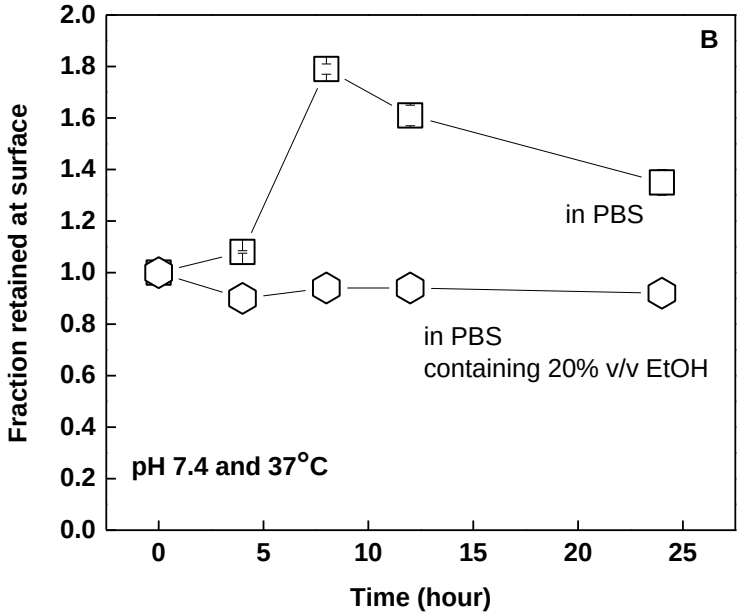
B
Fraction retained at surface
2.0
1.8
1.6
1.4
1.2
1.0
0.8
0.6
0.4
0.2
0.0
0
5
10
15
20
25
Time (hour)
in PBS
in PBS
containing 20% v/v EtOH
pH 7.4 and 37°C

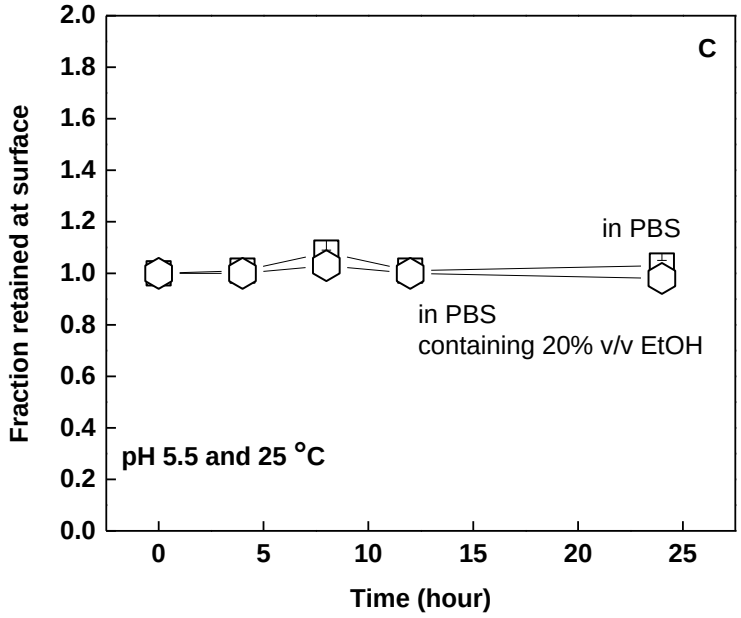
C
Fraction retained at surface
2.0
1.8
1.6
1.4
1.2
1.0
0.8
0.6
0.4
0.2
0.0
0
5
10
15
20
25
Time (hour)
in PBS
in PBS
containing 20% v/v EtOH
pH 5.5 and 25 °C

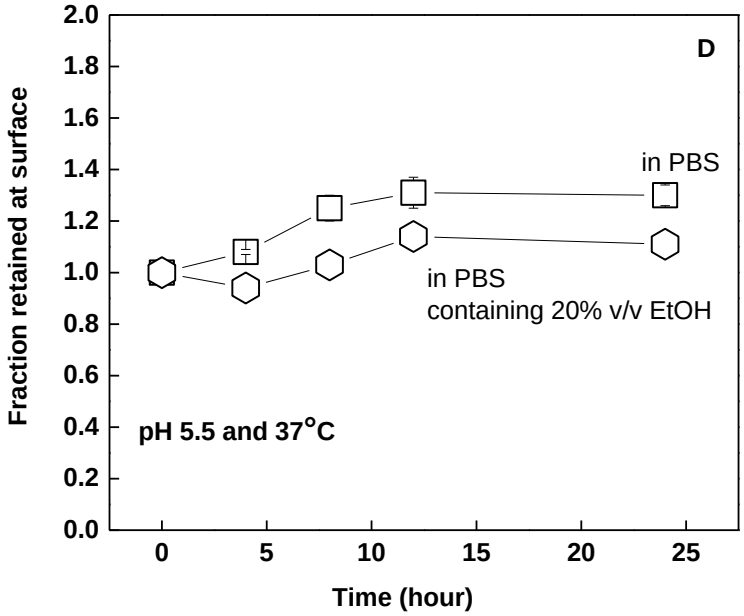

Figure 3.19. Time dependent variation of the fraction retained at the surface of ionic bonded PIPOX-PEI/TA multilayer films immersed in PBS and PBS solution containing 20% EtOH by volume A) pH 7.4/25°C; B) pH 7.4/37°C; C) pH 5.5/25°C; D) pH 5.5/37°C.

3.12.2 DOX Release from PIPOX-PEI/TA Multilayer-coated $CaCO_3$ microparticles

DOX loading into LbL-coated microparticles was performed at pH 7.4. 2 mg of LbL-coated $CaCO_3$ microparticles were dispersed in 1 mL of 0.1 mg/mL DOX solution (prepared in 10 mM phosphate buffer) and mixed using a vortex shaker for 1 hour at room temperature. The amount of DOX loaded into LbL $CaCO_3$ microparticles was calculated by first measuring the fluorescence intensity of DOX at 555 nm, then quantifying the amount of DOX in the supernatant, and finally subtracting the amount in the supernatant from the amount of DOX in the loading solution. The amount of DOX loaded into microparticles was ~0.045 ± 0.006 mg per 2 mg microparticles.

DOX release was started by dispersing 2 mg LbL-coated microparticles into 2 mL of PBS solution which was then placed on a magnetic stirrer and stirred at 100 rpm. At determined time intervals, LbL microparticles were precipitated and the amount of DOX in the supernatant was calculated by measuring the intensity at 555 nm using fluorescence spectroscopy. After each measurement, 2 mL of fresh PBS solution was added onto precipitated microparticles, and DOX release was continued. DOX was quantified using calibration curves prepared under release conditions.

Figure 3.20 shows the effects of pH and temperature on the DOX release. The amount of DOX released from LbL-coated microparticles was more at pH 5.5 both at 25 and 37 ^{o}C compared to pH 7.4 This can be explained by the protonation of the phenolic hydroxyl groups of TA ($pKa_{,1} \sim 6.5$ and $pKa_{,2} \sim 8$) at pH 5.5 which resulted in disruption of electrostatic interaction between TA and DOX and induced DOX release from multilayers. In addition, the DOX release was higher at 37 ^{o}C than 25 ^{o}C. PIPOX displays LCST-type phase behavior at ~36 ^{0}C. As discussed earlier in Section 1.1.3, when temperature was increased, PIPOX-PEI possibly transformed from extended to globular form. This conformational change might have caused formation of voids between the layers within the film, leading to enhanced DOX release.

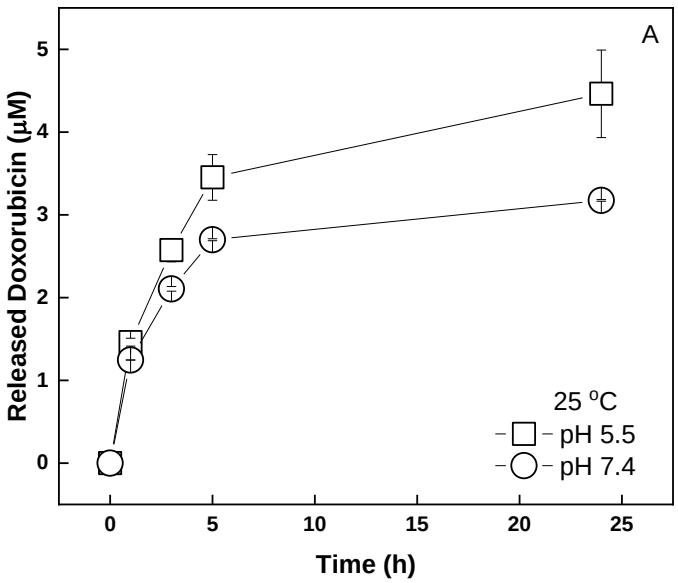
A
Released Doxorubicin (μM)
Time (h)
25 °C
pH 5.5
pH 7.4
0
1
2
3
4
5
0
5
10
15
20
25

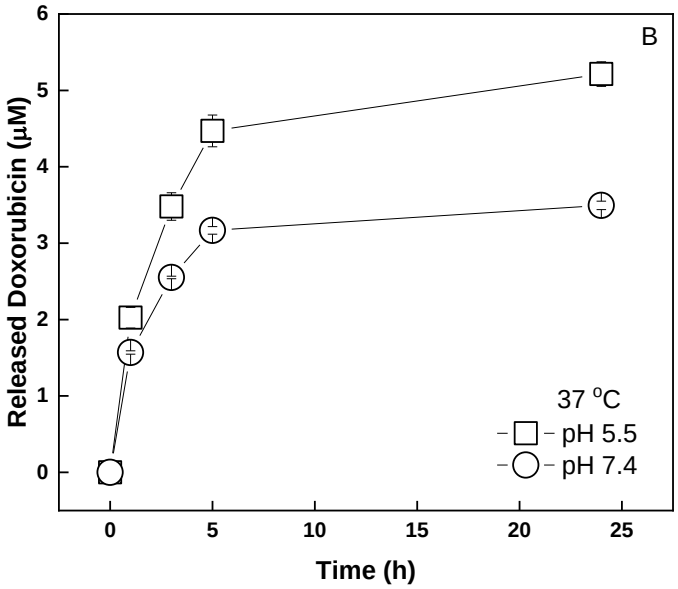
B
Released Doxorubicin (μM)
Time (h)
37 °C
pH 5.5
pH 7.4
0
1
2
3
4
5
6
0
5
10
15
20
25

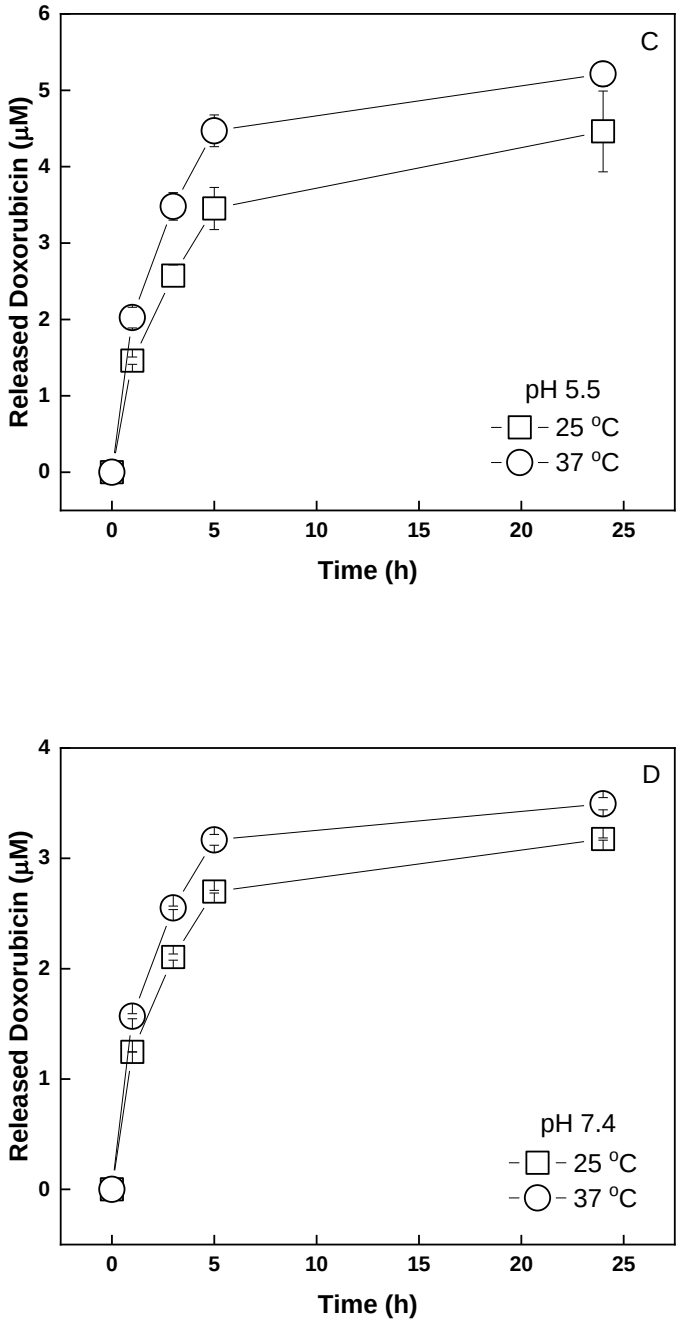

Figure 3.20. Released of the DOX from TA/PIPOX-PEI coated $CaCO_3$ microparticles in PBS at (A) 25°C pH 7.4 and pH 5.5; (B) 37°C pH 7.4 and pH 5.5; (C) 25°C and 37°C pH 5.5; (D) 25°C and 37°C pH 7.4.

3.12.3 CUR and DOX loading and release into/from hollow LbL capsules

Both non-crosslinked and crosslinked TA/PIPOX-PEI multilayer capsules were used for loading and release studies of CUR and DOX. Release studies was performed at pH 5.5 and pH 7.4 at 37°C.

3.12.4 CUR loading and release into/from hollow LbL capsules

CUR loading into crosslinked and non-crosslinked hollow capsules were performed at pH 5. Crosslinked and non-crosslinked hollow capsules were dispersed in 2 mL of 0.2 mg/mL CUR solution (prepared in 20% EtOH-10 mM phosphate buffer) and mixed using a vortex shaker for 4 hours at room temperature. The amount of CUR loaded into crosslinked and non-crosslinked hollow capsules were calculated by first measuring the fluorescence intensity of CUR at 525 nm, then quantifying the amount of CUR in the supernatant, and finally subtracting the amount in the supernatant from the amount of CUR in the loading solution. The amount of CUR loaded into non-crosslinked and crosslinked hollow capsules were similar and ~ 240 μM ± 7.5.

Crosslinked and non-crosslinked hollow capsules were dispersed in 2 mL of 80% PBS-EtOH mixture and stirred at 100 rpm. The hollow capsules were precipitated and the amount of CUR in the supernatant was determined by following the fluorescence intensity of CUR at 525 nm. After each measurement, 2 mL of fresh 80% PBS-EtOH solution was added onto precipitated hollow capsules, and CUR release was continued. CUR was quantified using calibration curves prepared under release conditions.

The amount of CUR in the supernatant was too high also and the fluorescence intensities lied outside of the linear range in the calibration curve. Therefore, the

supernatants obtained at the end of the first, third and fifth hours were first diluted with PBS-EtOH solution (containing 20% vol. ethanol) with 1:100 ratio. Then, this solution was rediluted with pure ethanol with 1:1 ratio, finally resulting in 60 % ethanol in the solution. CUR release was quantified using calibration curves presented in Appendix 3 and 4. Since the supernatant was discarded after each measurement and fresh 20% v/v EtOH-PBS mixture was added instead, the concentration values were assessed as cumulative concentration values. Unfortunately, the difference in the amount of CUR released from different samples was remarkable for both crosslinked and noncrosslinked hollow capsules. Similar problem was not observed during DOX release studies. Therefore, CUR release from crosslinked and noncrosslinked capsules was not preferred to be represented graphically. Further studies will be conducted to optimize CUR release from hollow capsules.

3.12.5 DOX loading and release into/from hollow LbL capsules

DOX loading into crosslinked and non-crosslinked hollow capsules were performed at pH 7.4. Crosslinked and non-crosslinked hollow capsules were dispersed in 2 mL of 0.1 mg/mL DOX solution (prepared in 10 mM phosphate buffer) and mixed using a vortex shaker for 1 hour at room temperature. The amount of DOX loaded into crosslinked and non-crosslinked hollow capsules were calculated by first measuring the fluorescence intensity of DOX at 555 nm, then quantifying the amount of DOX in the supernatant, and finally subtracting the amount in the supernatant from the amount of DOX in the loading solution. The amount of DOX loaded into non-crosslinked and crosslinked were ~ 73.1 µM ± 2.9 and 70.3 µM ± 3.0 mg respectively.

DOX release was started by dispersing crosslinked and non-crosslinked hollow capsules into 2 mL of PBS solution at pH 5.5 and pH 7.4 and at 37°C which was then placed on a magnetic stirrer and stirred at 100 rpm. At determined time intervals, crosslinked and non-crosslinked hollow capsules were precipitated and the amount

of DOX in the supernatant was calculated by measuring the intensity at 555 nm using fluorescence spectroscopy. After each measurement, 2 mL of fresh PBS solution was added onto precipitated hollow capsules, and DOX release was continued. DOX was quantified using calibration curves prepared under release conditions. The amount of DOX in the supernatant was too high and the fluorescence intensities lied outside of the linear range in the calibration curve. Therefore, the supernatants obtained at the end of the first and third hours were diluted with PBS solution with 1:100 ratio. DOX release was quantified using calibration curves presented in Appendix 1 and 2. Since the supernatant was discarded after each measurement and fresh PBS mixture was added instead, the concentration values indicated in Figure 3.21A are cumulative concentration values.

The amount of DOX release from noncross-linked hollow capsules was greater compared to crosslinked capsules. As discussed earlier in the context of studies performed on 2D, crosslinking multilayers resulted in loss of conformational changes and a rearrangement within the multilayers which was possibly the reason of not observing stimuli-responsive release behavior. The amount of DOX release from hollow capsules (both crosslinked and noncrosslinked) was higher compared to DOX release from TA/PIPOX-PEI multilayer coated $CaCO_3$ microparticles (non-hollow). This was possibly due to relatively large and available empty space for DOX loading in hollow LbL capsules.

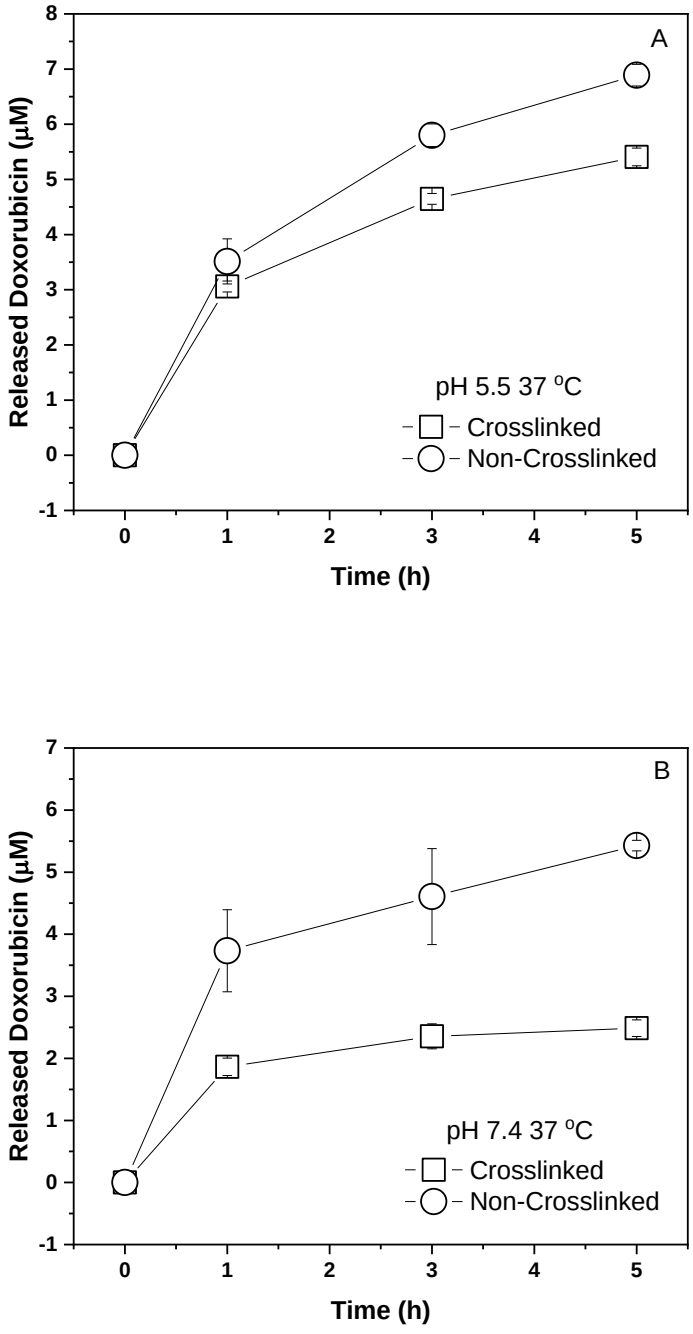

Figure 3.21. Release from non-crosslinked and crosslinked hollow LbL capsules A) DOX release at pH 5.5 at 37 °C and B) DOX release at pH 7.4 at 37 °C.

3.13 Preliminary result on the effect of synergistic effect of DOX and CUR on HCT 116 cell line

Cytotoxicity tests were only conducted with TA/PIPOX-PEI multilayer coated CUR loaded $CaCO_3$ microparticles which were then post-loaded with DOX. Experiments were conducted on HCT 116 cell line by Çağdaş Ermiş in Department of Biology in Prof.Sreeparna Banerjee's Laboratory. Cytotoxicity studies will also be continued using hollow LbL capsules. Three different samples were prepared: i) LbL-coated CUR loaded $CaCO_3$ microparticles; ii) LbL-coated bare $CaCO_3$ microparticles, postloaded with DOX; iii) LbL-coated CUR loaded $CaCO_3$ microparticles, postloaded with DOX and iv) LbL-coated bare $CaCO_3$ microparticles. As seen in Figure 3.22, only CUR loaded LbL microparticles was not effective on killing the cancer cells. Only DOX loaded LbL microparticles required 1.5 µM of DOX release to obtain 50 % decrease in survival. However, the required DOX concentration decreased to 0.2 µM when combined with 20 µM CUR release, indicating a synergistic effect. These studies are still in progress and will be further continued with hollow LbL capsules.

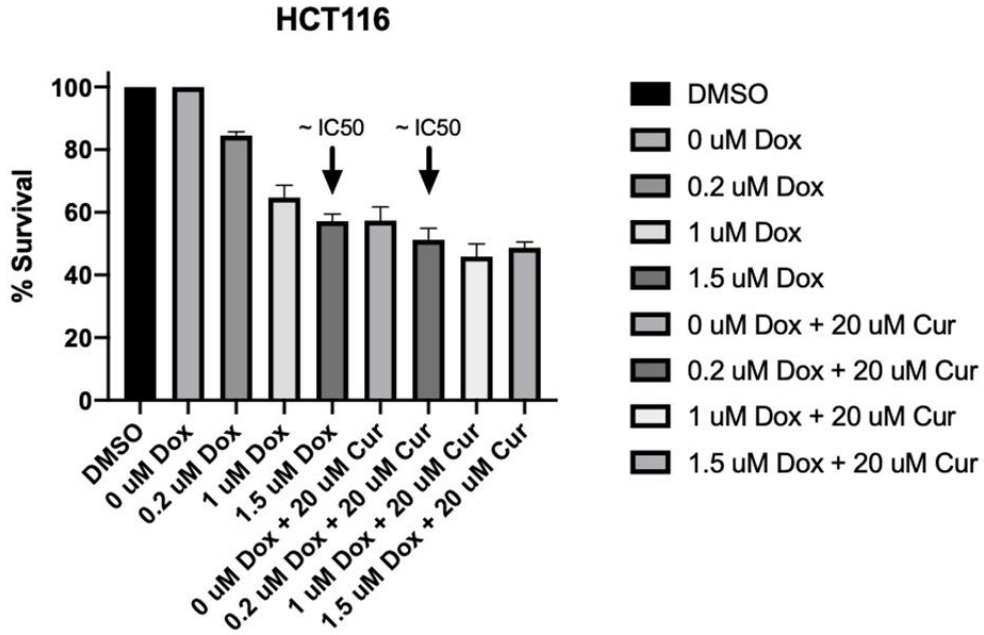

Figure 3.22. Cytotoxicity experiments on HCT 116 cell line.

CHAPTER 4

CONCLUSION

In this thesis study, temperature sensitive PIPOX was synthesized through cationic ring opening polymerization. PIPOX-PEI was then synthesized by partial hydrolysis of PIPOX at acidic medium. LbL deposition and crosslinking of temperature-responsive PIPOX-PEI and pH-responsive TA were first studied on 2D substrates. TA and PIPOX-PEI multilayers could be successfully deposited at the surface through hydrogen bonding and electrostatic interactions. Cross-linked and noncross-linked films were contrasted with respect to stability under physiologically related pH and temperature conditions. Noncross-linked multilayers displayed thickness increment upon exposure to PBS at pH 7.4 and 37°C. On the other hand, thickness increase was lower at pH 5.5 and 37°C than that at pH 7.4 and 37°C. Such a pH-dependent difference in the behavior of the multilayers was attributed to the strength of association among the layers. Hydrogen bonding interactions between PIPOX and TA was partially disrupted at pH 7.4 and possibly allowed conformational transition of PIPOX around its critical temperature and a rearrangement within the multilayers, facilitating water uptake. The association between the layers was more intense at pH 5.5, making a conformational re-arrangement within the multilayers less likely. Importantly, thickness increment upon exposure to PBS was not observed at 37°C regardless of the pH of the PBS solution when PIPOX-PEI and TA multilayers were crosslinked using $NaIO_4$. This can be explained by the covalent bonding among the layers, suppressing such a conformational transition.

The fundamental knowledge generated on 2D surfaces was then applied to deposit multilayers onto $CaCO_3$ microparticles. Two different $CaCO_3$ microparticles were synthesized through co-precipitation method, i.e. CUR loaded $CaCO_3$ microparticles (Type 1) and bare $CaCO_3$ microparticles (Type 2). TA and PIPOX-PEI multilayers could be deposited successfully onto both types of $CaCO_3$ microparticles. Type 1

was post-loaded with DOX. On the other hand, Type 2 was made hollow using EDTA solution and both CUR and DOX were post-loaded into TA/PIPOX-PEI hollow capsules. These two different particles exhibited different amount of drug uptake. DOX release from hollow LbL capsules was higher than TA/PIPOX-PEI coated $CaCO_3$ microparticles (Type 1), pointing out the importance of the empty available space in the particles. Both pH and temperature affected the amount of DOX released from LbL coated particles and hollow capsules. Importantly, DOX release from noncross-linked hollow capsules was greater than cross-linked hollow capsules. CUR release from Type 1 and Type 2 particles could not be contrasted due to challenges in quantification of CUR release arising from degradation of CUR.

Preliminary studies on cytotoxicity tests, conducted using Type 1 microparticles demonstrated synergistic effect of CUR and DOX on HCT 116 cell line. Cytotoxicity tests will be conducted using LbL hollow capsules. Considering the higher CUR and DOX release from hollow capsules, Type 2 microparticles may be more efficient for anticancer applications.

Overall, this study generated fundamental knowledge on LbL deposition and crosslinking of TA and PIPOX-PEI multilayers. The structure-property relationship in PIPOX-PEI/TA multilayers have been explored on both 2D and 3D substrates. These dual stimuli-responsive microparticles, capable of releasing multiple drugs may be promising carriers for anticancer applications.

REFERENCES

1. Glassner, M., Vergaelen, M. & Hoogenboom, R. Poly(2-oxazoline)s: A comprehensive overview of polymer structures and their physical properties. *Polymer International* vol. 67 32–45 Preprint at https://doi.org/10.1002/pi.5457 (2018).

2. Hoogenboom, R. & Schlaad, H. Bioinspired Poly(2-oxazoline)s. *Polymers* vol. 3 467–488 Preprint at https://doi.org/10.3390/polym3010467 (2011).

3. Verbraeken, B., Monnery, B. D., Lava, K. & Hoogenboom, R. The chemistry of poly(2-oxazoline)s. *European Polymer Journal* vol. 88 451–469 Preprint at https://doi.org/10.1016/j.eurpolymj.2016.11.016 (2017).

4. Luxenhofer, R. *et al.* Poly(2-oxazoline)s as polymer therapeutics. *Macromolecular Rapid Communications* vol. 33 1613–1631 Preprint at https://doi.org/10.1002/marc.201200354 (2012).

5. Guerrero-Sanchez, C., Hoogenboom, R. & Schubert, U. S. Fast and 'green' living cationic ring opening polymerization of 2-ethyl-2-oxazoline in ionic liquids under microwave irradiation. *Chemical Communications* 3797–3799 (2006) doi:10.1039/b608364a.

6. Journal of Polymer Science Part B Polymer Letters - September 1967 - Levy - Polymerization of cyclic imino ethers II .

7. Lava, K., Verbraeken, B. & Hoogenboom, R. Poly(2-oxazoline)s and click chemistry: A versatile toolbox toward multi-functional polymers. *European Polymer Journal* vol. 65 98–111 Preprint at https://doi.org/10.1016/j.eurpolymj.2015.01.014 (2015).

8. Rossegger, E., Schenk, V. & Wiesbrock, F. Design strategies for functionalized poly(2-oxazoline)s and derived materials. *Polymers* vol. 5 956–1011 Preprint at https://doi.org/10.3390/polym5030956 (2013).

9. Paulus, R. M., Becer, C. R., Hoogenboom, R. & Schubert, U. S. Acetyl halide initiator screening for the cationic ring-opening polymerization of 2-ethyl-2-oxazoline. *Macromol Chem Phys* **209**, 794–800 (2008).

10. Guerrero-Sanchez, C., Hoogenboom, R. & Schubert, U. S. Fast and 'green' living cationic ring opening polymerization of 2-ethyl-2-oxazoline in ionic liquids under microwave irradiation. *Chemical Communications* 3797–3799 (2006) doi:10.1039/b608364a.

11. Guillerm, B., Monge, S., Lapinte, V. & Robin, J. J. Novel investigations on kinetics and polymerization mechanism of oxazolines initiated by iodine. *Macromolecules* **43**, 5964–5970 (2010).

12. Guis, C. & Cheradame, H. *Synthesis of polymers containing pseudohalide groups by cationic polymerization 15. Study of the functionalizing living cationic polymerization of 2-methyl-2-oxazoline in the presence of trimethylsilylazide q*.

13. Guillerm, B., Monge, S., Lapinte, V. & Robin, J. J. How to modulate the chemical structure of polyoxazolines by appropriate functionalization. *Macromolecular Rapid Communications* vol. 33 1600–1612 Preprint at https://doi.org/10.1002/marc.201200266 (2012).

14. Kobayashi, S., Masuda, F., & Shoda, S.-ichiro. (1989). *Synthesis of Acryl- and Methacryl-Type Macromonomers and Telechelics by Utilizing Living Polymerization of 2-Oxazolines*, *22*(7).

15. Hsiue, G. H., Swamikannu, A. X. & Litts, M. H. *Synthesis and Characterization of a Multiblock Copolymer of Poly(N-Isovaleryl Ethyleneimine) and Poly(ethylene Glycol)*.

16. Weber, C., Hoogenboom, R. & Schubert, U. S. Temperature responsive bio-compatible polymers based on poly(ethylene oxide) and poly(2-oxazoline)s. *Progress in Polymer Science* vol. 37 686–714 Preprint at https://doi.org/10.1016/j.progpolymsci.2011.10.002 (2012).

17. Zhang, Q. & Hoogenboom, R. Polymers with upper critical solution temperature behavior in alcohol/water solvent mixtures. *Progress in Polymer Science* vol. 48 122–142 Preprint at https://doi.org/10.1016/j.progpolymsci.2015.02.003 (2015).

18. Lin, P., Clash, C., Pearce, E. M., Kwei, T. K. & Aponte, M. A. *Solubility and Miscibility of Poly(ethyl oxazoline)*.

19. Uyama, H., & Kobayashi, S. (1992). *Chemistry Letters*, 1643–1646.

20. Park, J. S. & Kataoka, K. Comprehensive and accurate control of thermosensitivity of poly(2-alkyl-2-oxazoline)s via well-defined gradient or random copolymerization. *Macromolecules* **40**, 3599–3609 (2007).

21. Howards second book 1-s2.0-007967009290023R-main.

22. Oleszko-Torbus, N. Recent Advances in Modifications, Properties and Applications of 2-Isopropyl-2-Oxazoline (Co)Polymers. *Polymer Reviews* vol. 62 529–548 Preprint at https://doi.org/10.1080/15583724.2021.1993252 (2022).

23. Li, T., Tang, H. & Wu, P. Molecular Evolution of Poly(2-isopropyl-2-oxazoline) Aqueous Solution during the Liquid-Liquid Phase Separation and Phase Transition Process. *Langmuir* **31**, 6870–6878 (2015).

24. Sun, B., Lin, Y., Wu, P. & Siesler, H. W. A FTIR and 2D-IR spectroscopic study on the microdynamics phase separation mechanism of the poly(N-isopropylacrylamide) aqueous solution. *Macromolecules* **41**, 1512–1520 (2008).

25. Wang, H., Li, L., Tong, Q. & Yan, M. Evaluation of photochemically immobilized poly(2-ethyl-2-oxazoline) thin films as protein-resistant surfaces. *ACS Appl Mater Interfaces* **3**, 3463–3471 (2011).

26. Tauhardt, L., Kempe, K., Gottschaldt, M. & Schubert, U. S. Poly(2-oxazoline) functionalized surfaces: From modification to application. *Chem Soc Rev* **42**, 7998–8011 (2013).

27. Lehmann, T. & Ruhe, J. *Polyethyloxazoline Monolayers for Polymer Supported Biomembrane Models*. *Macrornol. Syrnp* vol. 142 (1999).

28. Pidhatika, B. *et al.* The role of the interplay between polymer architecture and bacterial surface properties on the microbial adhesion to polyoxazoline-based ultrathin films. *Biomaterials* **31**, 9462–9472 (2010).

29. Konradi, R., Pidhatika, B., Mühlebach, A. & Textor, M. Poly-2-methyl-2-oxazoline: A peptide-like polymer for protein-repellent surfaces. *Langmuir* **24**, 613–616 (2008).

30. Waschinski, C. J. *et al.* Insights in the antibacterial action of poly(methyloxazoline)s with a biocidal end group and varying satellite groups. *Biomacromolecules* **9**, 1764–1771 (2008).

31. Konradi, R., Acikgoz, C. & Textor, M. Polyoxazolines for nonfouling surface coatings - A direct comparison to the gold standard PEG. *Macromolecular Rapid Communications* vol. 33 1663–1676 Preprint at https://doi.org/10.1002/marc.201200422 (2012).

32. Maechling-Strasser, C. *et al. Synthesis and adsorption of a poly(N-acetylethyleneimine)-polyethyleneoxide-poly (N-acetylethyleneimine) triblock-copolymer at a silica/solution interface. Influence of its preadsorption on platelet adhesion and fibrinogen adsorption*.

33. Hoogenboom, R. Poly(2-oxazoline)s: A polymer class with numerous potential applications. *Angewandte Chemie - International Edition* **48**, 7978–7994 (2009).

34. Donev, R., Koseva, N., Petrov, P., Kowalczuk, A. & Thome, J. Characterisation of different nanoparticles with a potential use for drug

delivery in neuropsychiatric disorders. *World Journal of Biological Psychiatry* **12**, 44–51 (2011).

35. Luxenhofer, R. *et al.* Structure-property relationship in cytotoxicity and cell uptake of poly(2-oxazoline) amphiphiles. in *Journal of Controlled Release* vol. 153 73–82 (2011).

36. Tong, J. *et al.* Neuronal uptake and intracellular superoxide scavenging of a fullerene (C60)-poly(2-oxazoline)s nanoformulation. *Biomaterials* **32**, 3654–3665 (2011).

37. Glassner, M., Kempe, K., Schubert, U. S., Hoogenboom, R. & Barner-Kowollik, C. One-pot synthesis of cyclopentadienyl endcapped poly(2-ethyl-2-oxazoline) and subsequent ambient temperature Diels-Alder conjugations. *Chemical Communications* **47**, 10620–10622 (2011).

38. Goddard, P., Hutchinson, L. E., Brown, J. & Brookman, L. J. *SOLUBLE POLYMERIC CARRIERS FOR DRUG DELIVERY. PART 2. PREPARATION AND IN VW0 BEHAVIOUR OF N-ACYLETHYLENIMINE COPOLYMERS*.

39. Gaertner, F. C., Luxenhofer, R., Blechert, B., Jordan, R. & Essler, M. Synthesis, biodistribution and excretion of radiolabeled poly(2-alkyl-2-oxazoline)s. *Journal of Controlled Release* **119**, 291–300 (2007).

40. Zalipsky, S., Hansen, C. B., Oaks, J. M. & Allen, T. M. *Evaluation of Blood Clearance Rates and Biodistribution of Poly(2-oxazoline)-Grafted Liposomes §*. (1996).

41. Trushina, D. B., Bukreeva, T. v, Kovalchuk, M. v & Antipina, M. N. CaCO 3 vaterite microparticles for biomedical and personal care applications. *Materials Science & Engineering C* **45**, 644–658 (2014).

42. Volodkin, D. CaCO3 templated micro-beads and -capsules for bioapplications. *Adv Colloid Interface Sci* **207**, 306–324 (2014).

43. Maleki Dizaj, S., Barzegar-Jalali, M., Zarrintan, M. H., Adibkia, K. & Lotfipour, F. Calcium carbonate nanoparticles as cancer drug delivery system. *Expert Opinion on Drug Delivery* vol. 12 1649–1660 Preprint at https://doi.org/10.1517/17425247.2015.1049530 (2015).

44. Oral, Ç. M. & Ercan, B. Influence of pH on morphology, size and polymorph of room temperature synthesized calcium carbonate particles. *Powder Technol* **339**, 781–788 (2018).

45. Ferreira, A. M., Vikulina, A. S. & Volodkin, D. CaCO3 crystals as versatile carriers for controlled delivery of antimicrobials. *Journal of Controlled Release* vol. 328 470–489 Preprint at https://doi.org/10.1016/j.jconrel.2020.08.061 (2020).

46. Ferreira, A. M., Vikulina, A. S. & Volodkin, D. CaCO3 crystals as versatile carriers for controlled delivery of antimicrobials. *Journal of Controlled Release* vol. 328 470–489 Preprint at https://doi.org/10.1016/j.jconrel.2020.08.061 (2020).

47. Boyjoo, Y., Pareek, V. K. & Liu, J. Synthesis of micro and nano-sized calcium carbonate particles and their applications. *Journal of Materials Chemistry A* vol. 2 14270–14288 Preprint at https://doi.org/10.1039/c4ta02070g (2014).

48. Chen, J. & Xiang, L. Controllable synthesis of calcium carbonate polymorphs at different temperatures ☆. *Powder Technol* **189**, 64–69 (2010).

49. Patra, J. K. *et al.* Nano based drug delivery systems: Recent developments and future prospects 10 Technology 1007 Nanotechnology 03 Chemical Sciences 0306 Physical Chemistry (incl. Structural) 03 Chemical Sciences 0303 Macromolecular and Materials Chemistry 11 Medical and Health Sciences 1115 Pharmacology and Pharmaceutical Sciences 09 Engineering 0903 Biomedical Engineering Prof Ueli Aebi, Prof Peter Gehr. *Journal of Nanobiotechnology* vol. 16 Preprint at https://doi.org/10.1186/s12951-018-0392-8 (2018).

50. Tai, C. Y. & Chen, F.-B. *Polymorphism of CaCO, Precipitated in a Constant-Composition Environment*.

51. Ogino, T., Suzuki, T. & Sawada, K. *The formation and transformation mechanism of calcium carbonate in water*. *Gaxhhrmica pt Cosmochrm~ca Acfa* vol. 51 (1987).

52. Feoktistova, N. *et al.* Controlling the Vaterite CaCO3 Crystal Pores. Design of Tailor-Made Polymer Based Microcapsules by Hard Templating. *Langmuir* **32**, 4229–4238 (2016).

53. Kitamura, M. Strategy for control of crystallization of polymorphs. *CrystEngComm* **11**, 949–964 (2009).

54. Volodkin, D. v. *et al.* One-step formulation of protein microparticles with tailored properties: Hard templating at soft conditions. *Adv Funct Mater* **22**, 1914–1922 (2012).

55. Shafiu Kamba, A., Ismail, M., Tengku Ibrahim, T. A. & Zakaria, Z. A. B. A pH-sensitive, biobased calcium carbonate aragonite nanocrystal as a novel anticancer delivery system. *Biomed Res Int* **2013**, (2013).

56. Peng, H. *et al.* Preparation of hierarchical mesoporous CaCO3 by a facile binary solvent approach as anticancer drug carrier for etoposide. *Nanoscale Res Lett* **8**, 1–11 (2013).

57. Isa, T. *et al.* Antibacterial activity of ciprofloxacin-encapsulated cockle shells calcium carbonate (Aragonite) nanoparticles and its biocompatability in macrophage J774A.1. *Int J Mol Sci* **17**, (2016).

58. Sahoo, P. C., Kausar, F., Lee, J. H. & Han, J. I. Facile fabrication of silver nanoparticle embedded CaCO3 microspheres via microalgae-templated CO2 biomineralization: Application in antimicrobial paint development. *RSC Adv* **4**, 32562–32569 (2014).

59. Ferreira, C., Pereira, A. M., Pereira, M. C., Simões, M. & Melo, L. F. Biofilm control with new microparticles with immobilized biocide. in *Heat Transfer Engineering* vol. 34 712–718 (2013).

60. Begum, G. *et al.* In Situ Strategy to Encapsulate Antibiotics in a Bioinspired CaCO3 Structure Enabling pH-Sensitive Drug Release Apt for Therapeutic and Imaging Applications. *ACS Appl Mater Interfaces* **8**, 22056–22063 (2016).

61. Ariga, K., Hill, J. P. & Ji, Q. Layer-by-layer assembly as a versatile bottom-up nanofabrication technique for exploratory research and realistic application. *Physical Chemistry Chemical Physics* **9**, 2319–2340 (2007).

62. Iler, R. K. *MULTILAYERS OF COLLOIDAL PARTICLES*. JOURNAL OF COLLOID AND INTERFACE SCIENCE* vol. 21 (1966).

63. Ber Bunsenges Phys Chem - November 1991 - Decher - Buildup of Ultrathin Multilayer Films by a Self-Assembly Process II .

64. Decher, G. & Hong, J.-D. *BUILDUP OF ULTRATHIN MULTILAYER FILMS BY A SELF-ASSEMBLY PROCESS, 1 CONSECUTIVE ADSORPTION OF ANIONIC AND CATIONIC BIPOLAR AMPHIPHILES ON CHARGED SURFACES*. *Makromol. Chem., Macromol. Symp* vol. 46 (1991).

65. Wanunu, M. *et al.* Branched coordination multilayers on gold. *J Am Chem Soc* **127**, 17877–17887 (2005).

66. *Communications to the Editor*.

67. Stockton, W. B. & Rubner, M. F. *Molecular-Level Processing of Conjugated Polymers. 4. Layer-by-Layer Manipulation of Polyaniline via Hydrogen-Bonding Interactions*. https://pubs.acs.org/sharingguidelines (1997).

68. Sukhishvili, S. A. & Granick, S. Layered, erasable, ultrathin polymer films [7]. *Journal of the American Chemical Society* vol. 122 9550–9551 Preprint at https://doi.org/10.1021/ja002410t (2000).

69. Such, G. K., Quinn, J. F., Quinn, A., Tjipto, E. & Caruso, F. Assembly of Ultrathin Polymer Multilayer Films by Click Chemistry Scheme 1. LbL Assembly of Polymer Films Using Click Chemistry. **13**, 46 (2022).

70. Chen, J. *et al.* Self-assembly ultrathin films based on diazoresins. *Langmuir* **15**, 7208–7212 (1999).

71. Ariga, K., Lvov, Y. M., Kawakami, K., Ji, Q. & Hill, J. P. Layer-by-layer self-assembled shells for drug delivery. *Advanced Drug Delivery Reviews* vol. 63 762–771 Preprint at https://doi.org/10.1016/j.addr.2011.03.016 (2011).

72. Fujii, N. *et al.* The simplest layer-by-layer assembly structure: Best paired polymer electrolytes with one charge per main chain carbon atom for multilayered thin films. *Macromolecules* **43**, 3947–3955 (2010).

73. Lvov, Y., Ariga, K., Onda, M., Ichinose, I. & Kunitake, T. *A careful examination of the adsorption step in the alternate layer-by-layer assembly of linear polyanion and polycation*. *Colloids and Surfaces A: Physicochemical and Engineering Aspects* vol. 146 (1999).

74. cl.1994.2323.

75. Lvov, Y., Ariga, K., Onda, M., Ichinose, I. & Kunitake, T. *Alternate Assembly of Ordered Multilayers of SiO 2 and Other Nanoparticles and Polyions*. https://pubs.acs.org/sharingguidelines (1997).

76. Volodkin, D. v., Petrov, A. I., Prevot, M. & Sukhorukov, G. B. Matrix Polyelectrolyte Microcapsules: New System for Macromolecule Encapsulation. *Langmuir* **20**, 3398–3406 (2004).

77. Mauser, T., Déjugnat, C., Möhwald, H. & Sukhorukov, G. B. Microcapsules made of weak polyelectrolytes: Templating and stimuli-responsive properties. *Langmuir* **22**, 5888–5893 (2006).

78. Gao, C., Donath, E., Mˆhwald, H. & Shen, J. *Spontaneous Deposition of Water-Soluble Substances into Microcapsules: Phenomenon, Mechanism, and Application**. Angew. Chem. Int. Ed* vol. 41 (2002).

79. Liu, X., Gao, C., Shen, J. & Möhwald, H. Multilayer microcapsules as anti-cancer drug delivery vehicle: Deposition, sustained release, and in vitro bioactivity. *Macromol Biosci* **5**, 1209–1219 (2005).

80. Wening, K. & Breitkreutz, J. Oral drug delivery in personalized medicine: Unmet needs and novel approaches. *International Journal of Pharmaceutics* vol. 404 1–9 Preprint at https://doi.org/10.1016/j.ijpharm.2010.11.001 (2011).

81. Russo, E. *et al.* A focus on mucoadhesive polymers and their application in buccal dosage forms. *J Drug Deliv Sci Technol* **32**, 113–125 (2016).

82. Borges, A. F., Silva, C., Coelho, J. F. J. & Simões, S. Oral films: Current status and future perspectives: I-Galenical development and quality attributes. *Journal of Controlled Release* vol. 206 1–19 Preprint at https://doi.org/10.1016/j.jconrel.2015.03.006 (2015).

83. Li, Y. T., Fang, Q., Zhang, L. I. & Tao, H. W. Spatial Asymmetry and Short-Term Suppression Underlie Direction Selectivity of Synaptic Excitation in the Mouse Visual Cortex. *Cerebral Cortex* **28**, 2059–2070 (2018).

84. Boddupalli, B. M., Mohammed, Z. N. K., Nath A., R. & Banji, D. Mucoadhesive drug delivery system: An overview. *Journal of Advanced Pharmaceutical Technology and Research* vol. 1 381–387 Preprint at https://doi.org/10.4103/0110-5558.76436 (2010).

85. Kang-Mieler, J. J., Osswald, C. R. & Mieler, W. F. Advances in ocular drug delivery: Emphasis on the posterior segment. *Expert Opinion on Drug Delivery* vol. 11 1647–1660 Preprint at https://doi.org/10.1517/17425247.2014.935338 (2014).

86. Castro, P. M. *et al.* Oral films as breakthrough tools for oral delivery of proteins/peptides. *Journal of Controlled Release* vol. 211 63–73 Preprint at https://doi.org/10.1016/j.jconrel.2015.05.258 (2015).

87. Borges, A. F., Silva, C., Coelho, J. F. J. & Simões, S. Oral films: Current status and future perspectives: I-Galenical development and quality attributes. *Journal of Controlled Release* vol. 206 1–19 Preprint at https://doi.org/10.1016/j.jconrel.2015.03.006 (2015).

88. Kumorek, M. *et al.* pH-responsive and antibacterial properties of self-assembled multilayer films based on chitosan and tannic acid. *Materials Science and Engineering C* **109**, (2020).

89. Park, S., Han, U., Choi, D. & Hong, J. Layer-by-layer assembled polymeric thin films as prospective drug delivery carriers: Design and applications. *Biomaterials Research* vol. 22 Preprint at https://doi.org/10.1186/s40824-018-0139-5 (2018).

90. Vodouhê, C. *et al.* Control of drug accessibility on functional polyelectrolyte multilayer films. *Biomaterials* **27**, 4149–4156 (2006).

91. Chuang, H. F., Smith, R. C. & Hammond, P. T. Polyelectrolyte multilayers for tunable release of antibiotics. *Biomacromolecules* **9**, 1660–1668 (2008).

92. Shukla, A., Avadhany, S. N., Fang, J. C. & Hammond, P. T. Tunable vancomycin releasing surfaces for biomedical applications. *Small* **6**, 2392–2404 (2010).

93. Han, U., Seo, Y. & Hong, J. Effect of pH on the structure and drug release profiles of layer-by-layer assembled films containing polyelectrolyte, micelles, and graphene oxide. *Sci Rep* **6**, (2016).

94. Tao, B. *et al.* BMP2-loaded titania nanotubes coating with pH-responsive multilayers for bacterial infections inhibition and osteogenic activity improvement. *Colloids Surf B Biointerfaces* **177**, 242–252 (2019).

95. Ochs, C. J., Such, G. K., Yan, Y., van Koeverden, M. P. & Caruso, F. Biodegradable click capsules with engineered drug-loaded multilayers. *ACS Nano* **4**, 1653–1663 (2010).

96. Li, Q. L. *et al.* Mesoporous silica nanoparticles coated by layer-by-layer self-assembly using cucurbit[7]uril for in vitro and in vivo anticancer drug release. *Chemistry of Materials* **26**, 6418–6431 (2014).

97. Volodkin, D. v., Petrov, A. I., Prevot, M. & Sukhorukov, G. B. Matrix Polyelectrolyte Microcapsules: New System for Macromolecule Encapsulation. *Langmuir* **20**, 3398–3406 (2004).

98. Zhao, Q., Zhang, S., Tong, W., Gao, C. & Shen, J. Polyelectrolyte microcapsules templated on poly(styrene sulfonate)-doped CaCO3 particles for loading and sustained release of daunorubicin and doxorubicin. *Eur Polym J* **42**, 3341–3351 (2006).

99. Liu, X., Gao, C., Shen, J. & Möhwald, H. Multilayer microcapsules as anti-cancer drug delivery vehicle: Deposition, sustained release, and in vitro bioactivity. *Macromol Biosci* **5**, 1209–1219 (2005).

100. Kazemi-Andalib, F., Mohammadikish, M., Divsalar, A. & Sahebi, U. Hollow microcapsule with pH-sensitive chitosan/polymer shell for in vitro delivery of curcumin and gemcitabine. *Eur Polym J* **162**, (2022).

101. Wang, P. *et al.* Poly-L-ornithine/fucoidan-coated calcium carbonate microparticles by layer-by-layer self-assembly technique for cancer theranostics. *J Mater Sci Mater Med* **29**, (2018).

102. Du, C., Shi, J., Shi, J., Zhang, L. & Cao, S. PUA/PSS multilayer coated CaCO3 microparticles as smart drug delivery vehicles. *Materials Science and Engineering C* **33**, 3745–3752 (2013).

103. He, T. *et al.* Stable pH responsive layer-by-layer assemblies of partially hydrolysed poly(2-ethyl-2-oxazoline) and poly(acrylic acid) for effective

prevention of protein, cell and bacteria surface attachment. *Colloids Surf B Biointerfaces* **161**, 269–278 (2018).

104. Li, Y., Pan, T., Ma, B., Liu, J. & Sun, J. Healable Antifouling Films Composed of Partially Hydrolyzed Poly(2-ethyl-2-oxazoline) and Poly(acrylic acid). *ACS Appl Mater Interfaces* **9**, 14429–14436 (2017).

105. da Fonseca Antunes, A. B. *et al.* Hydrogen bonded polymeric multilayer films assembled below and above the cloud point temperature. *Chemical Communications* **49**, 9663–9665 (2013).

106. Haktaniyan, M., Atilla, S., Cagli, E. & Erel-Goktepe, I. pH- and temperature-induced release of doxorubicin from multilayers of poly(2-isopropyl-2-oxazoline) and tannic acid. *Polym Int* **66**, 1851–1863 (2017).

107. Hendessi, S., Tatar Güner, P., Miko, A. & Demirel, A. L. Hydrogen bonded multilayers of poly(2-ethyl-2-oxazoline) stabilized silver nanoparticles and tannic acid. *Eur Polym J* **88**, 666–678 (2017).

108. Cagli, E., Ugur, E., Ulusan, S., Banerjee, S. & Erel-Goktepe, I. Effect of side chain variation on surface and biological properties of poly(2-alkyl-2-oxazoline) multilayers. *Eur Polym J* **114**, 452–463 (2019).

109. Akbar, M., Cagli, E. & Erel-Göktepe, I. Layer-By-Layer Modified Superparamagnetic Iron Oxide Nanoparticles with Stimuli-Responsive Drug Release Properties. *Macromol Chem Phys* **220**, (2019).

110. Mathivanan, N. *et al.* Hydrogen-Bonded Multilayer Thin Films and Capsules Based on Poly(2-n-propyl-2-oxazoline) and Tannic Acid: Investigation on Intermolecular Forces, Stability, and Permeability. *Langmuir* **35**, 14712–14724 (2019).

111. Paramasivam, G., Vergaelen, M., Ganesh, M. R., Hoogenboom, R. & Sundaramurthy, A. Hydrogen bonded capsules by layer-by-layer assembly of

tannic acid and poly(2-: N -propyl-2-oxazoline) for encapsulation and release of macromolecules. *J Mater Chem B* **5**, 8967–8974 (2017).

112. Kempe, K. *et al.* Clickable poly(2-oxazoline) architectures for the fabrication of low-fouling polymer capsules. *ACS Macro Lett* **2**, 1069–1072 (2013).

113. Kempe, K., Ng, S. L., Gunawan, S. T., Noi, K. F. & Caruso, F. Intracellularly degradable hydrogen-bonded polymer capsules. *Adv Funct Mater* **24**, 6187–6194 (2014).

114. Adams, N. & Schubert, U. S. Poly(2-oxazolines) in biological and biomedical application contexts. *Advanced Drug Delivery Reviews* vol. 59 1504–1520 Preprint at https://doi.org/10.1016/j.addr.2007.08.018 (2007).

115. Legros, C., de Pauw-Gillet, M. C., Tam, K. C., Taton, D. & Lecommandoux, S. Crystallisation-driven self-assembly of poly(2-isopropyl-2-oxazoline)-block-poly(2-methyl-2-oxazoline) above the LCST. *Soft Matter* **11**, 3354–3359 (2015).

116. Park, J. S., Akiyama, Y., Winnik, F. M. & Kataoka, K. Versatile synthesis of end-functionalized thermosensitive poly(2-isopropyl-2-oxazolines). *Macromolecules* **37**, 6786–6792 (2004).

117. Toncheva-Moncheva, N., Veleva-Kostadinova, E., Tsvetanov, C., Momekova, D. & Rangelov, S. Preparation and properties of positively charged mesoglobules based on poly(2-isopropyl-2-oxazoline) and evaluation of their potential as carriers of polynucleotides. *Polymer (Guildf)* **111**, 156–167 (2017).

118. Zhou, H. *et al.* Co-precipitation of calcium carbonate and curcumin in an ethanol medium as a novel approach for curcumin dissolution enhancement. *J Drug Deliv Sci Technol* **51**, 397–402 (2019).

119. Longo, J. *et al.* Stable Bioactive Enzyme-Containing Multilayer Films Based on Covalent Cross-Linking from Mussel-Inspired Adhesives. *Langmuir* **31**, 12447–12454 (2015).

120. Pooch, F., Teltevskij, V., Karjalainen, E., Tenhu, H. & Winnik, F. M. Poly(2-propyl-2-oxazoline)s in Aqueous Methanol: To Dissolve or not to Dissolve. *Macromolecules* (2019) doi:10.1021/acs.macromol.9b01234.

APPENDICES

A. Calibration Curve of DOX in PBS at pH 5.5

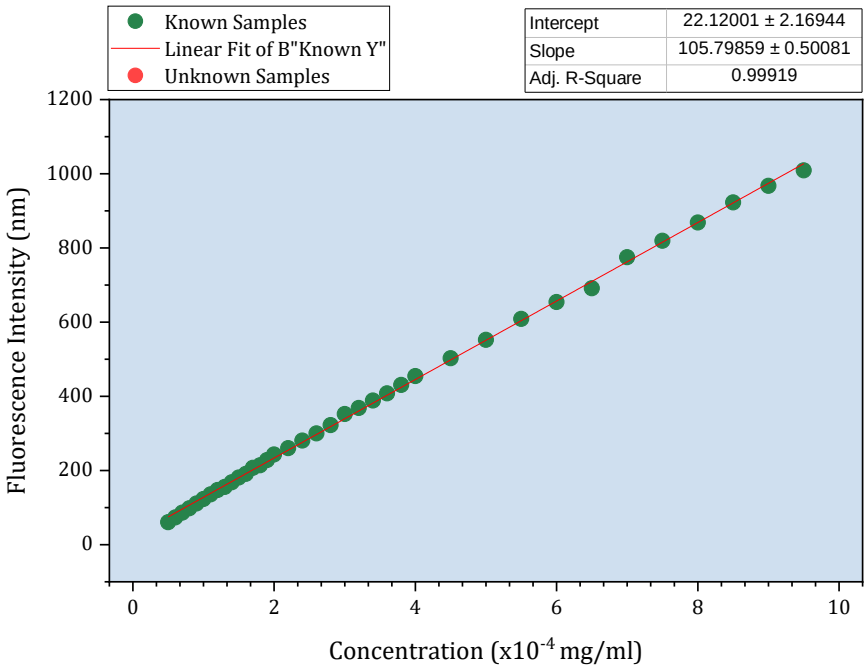

B. Calibration Curve of DOX in PBS at pH 7.4

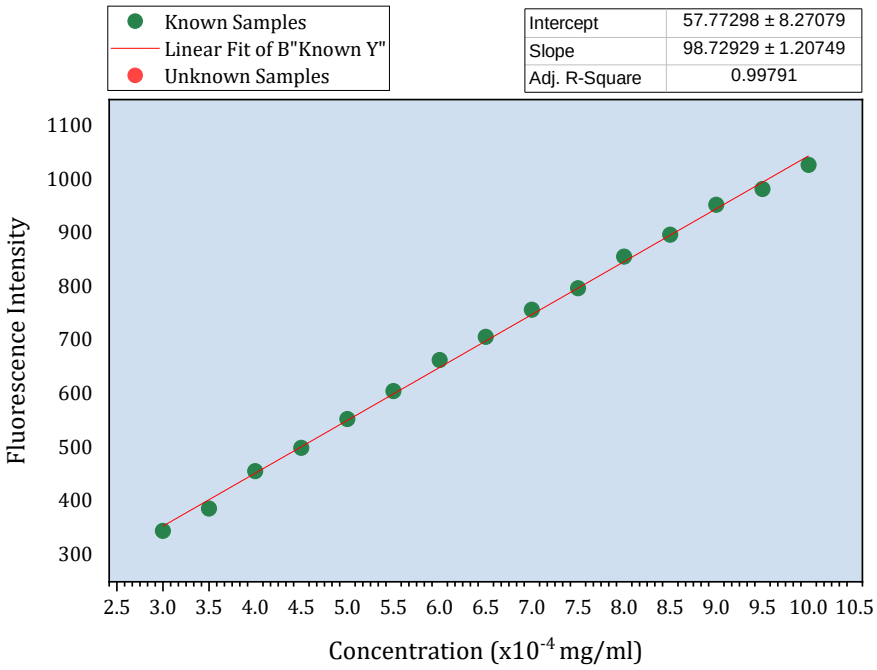

C. Calibration Curve of CUR in 60% EtOH-PBS at pH 5.5

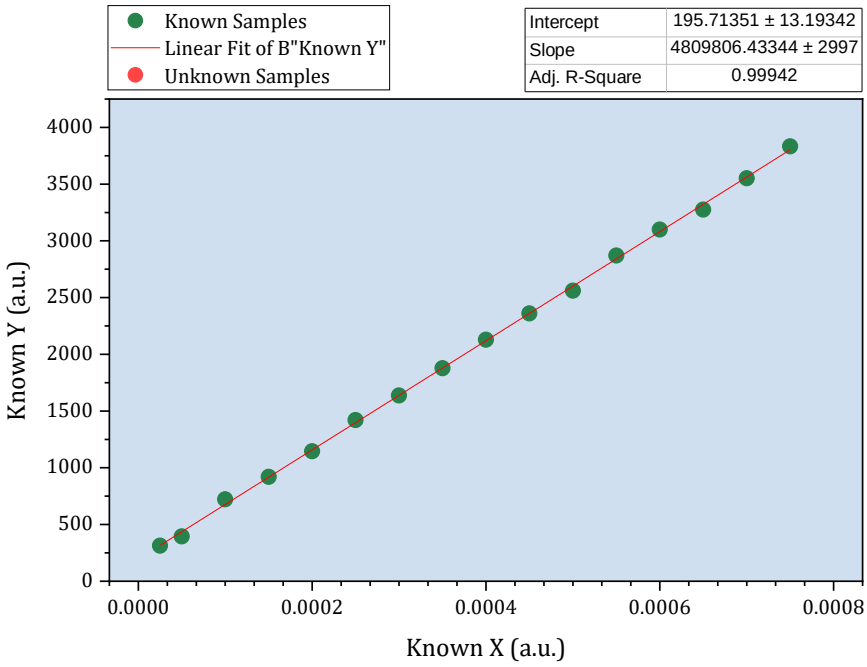

D. Calibration Curve of CUR in 60% EtOH-PBS at pH 7.4